

MASTER THESIS
Justin Tran

Indication of wet and dry periods in Germany using machine learning on meteorological and remote sensing data

Faculty of Engineering and Computer Science
Department Computer Science

Justin Tran

Indication of wet and dry periods in Germany using
machine learning on meteorological and remote
sensing data

Master thesis submitted for examination in Master´s degree
in the study course *Master of Science Informatik*
at the Department Computer Science
at the Faculty of Engineering and Computer Science
at University of Applied Science Hamburg

Supervisor: Prof. Dr. Thomas Clemen

Supervisor: Prof. Dr. Christian Lins

Submitted on: 5th September 2024

Justin Tran

Title of Thesis

Indication of wet and dry periods in Germany using machine learning on meteorological and remote sensing data

Keywords

Machine Learning, Drought, Prediction, Forecast, Detection, Geoinformatics, Meteorology, Remote Sensing

Abstract

This thesis investigates the calculation, comparison, and forecasting of the Standardized Precipitation-Evapotranspiration Index (SPEI) using diverse data sources and methods. The study recalculates SPEI values for Germany employing various potential evapotranspiration (PET) equations — FAO-56 Penman-Monteith, Thornthwaite, Priestley-Taylor, and Hargreaves — using weather station data from the German Weather Service and remote sensing data from ERA5-Land Reanalysis. Significant variations were observed in SPEI values across different PET equations, with the Thornthwaite and Hargreaves equations showing the closest alignment with the SPEIbase - created by the SPEI inventors. The remote sensing approach with the FAO-56 Penman-Monteith PET equation yielded smooth and seasonally consistent SPEI values.

The Pearson correlation between SPEI and the Soil Moisture Index (SMI) was examined, revealing negligible weak negative correlation coefficients near zero for the weather station and remote sensing SPEI, except for the remote sensing 1-, 3- and 6-month SPEI which achieved weak positive correlation coefficients near zero, meaning that no correlation was found. Also the distance correlation has been examined between the SPEI and SMI, where the 24-month remote sensing SPEI reached a distance correlation coefficient near 0.5 with the upper and total soil SMI and the 1-month SPEIbase SPEI accomplished a distance correlation coefficient above 0.5 with the upper soil SMI.

Forecasting models, including Gradient Boosting Regressor (GBR), XGBoost, Prophet, and SARIMA, were evaluated for their predictive performance. The GBR model C+L+DOY with adjusted hyperparameters, incorporating geographical coordinates, lagged SPEI values, and day of the year, achieved the lowest Root Mean Squared Error (RMSE) of 0.26234. The XGBoost model SL trained with the 1-month SPEI lagged had to lowest

RMSE of 0.106524 and the model MIMO identified a 6-month lag as optimal for forecasting accuracy with an RMSE of 0.289719. The Prophet model effectively captured long-term trends and seasonal patterns, indicating an increasing trend in SPEI values while achieving an RMSE of above 0.65. The SARIMA model with the lowest metrics values achieved Akaike Information Criterion (AIC) of 149.38 and RMSE of 0.98 showing a higher RMSE than the previous mentioned methods.

The study's findings have significant implications for drought monitoring and management, emphasizing the need for careful PET equation selection because they influence the SPEI values, the utility of remote sensing data because the results differ from the comparative dataset (SPEIbase), and the importance of lagged values in forecasting because they improved the forecast accuracy. It can be said that the 1-month SPEIbase SPEI can reflect the short-term soil moisture, whereas the 24-month remote sensing SPEI for the upper and total soil barely reached the 0.5 correlation threshold (see Section 4.1 for all requirements stated for this thesis).

Unfortunately, it could not be answered whether using weather station and remote sensing data over only weather station data provides an advantage even though the remote sensing SPEI mimicked the course of the seasons realistically. The problem was that SPEIbase only had the 1-month SPEI with a 0.5 degrees spatial resolution and that there were no other SPEI comparison datasets found.

Statistical methods can undoubtedly be considered as outperformed by the machine learning regarding forecasting. Two forecast accurate model were found: the XGBoost SL model with the 3-months lagged 1-month SPEI values achieved the lowest RMSE of all models while the MIMO model shows the second lowest RMSE of with a lag size of 6 for the 6-month SPEI. Additionally to the SPEI it outputs other environmental features like temperature, precipitation, etc. When choosing a forecast model, it has to be considered the requirements of the project in question, as each model approach has its advantages and disadvantages.

Limitations such as data availability, complexity of the nature, and regional generalizability were identified, along with recommendations for future research focusing on enhanced data integration, regional adaptation, and long-term forecasting. This research advances the understanding of drought indices and forecasting models, contributing to improved drought management strategies and informing policymakers and the scientific community.

Contents

| | |
|--|------------|
| List of Figures | ix |
| List of Tables | xix |
| Listings | xxi |
| 1 Introduction | 1 |
| 1.1 Research Problem | 2 |
| 1.2 Goals | 4 |
| 1.3 Research Hypotheses | 4 |
| 1.4 Thesis Structure | 5 |
| 2 Related Work | 8 |
| 2.1 Drought Indices | 8 |
| 2.1.1 Standardized Precipitation Evapotranspiration Index (SPEI) | 8 |
| 2.1.2 Soil Moisture Index (SMI) | 11 |
| 2.2 Predicting Wet and Drought Periods | 13 |
| 2.2.1 Assessment and Prediction of Meteorological Drought using Machine Learning | 13 |
| 2.2.2 Drought Forecasting using Stochastic Models | 13 |
| 2.2.3 Drought Monitoring and Prediction System (GIDMaPS) | 14 |
| 2.2.4 Machine Learning in Drought Prediction | 15 |
| 2.2.5 Deep Learning Models for Drought Prediction | 15 |
| 2.2.6 Hybrid Random Forest Model for SPEI Forecasting | 16 |
| 2.2.7 Drought Forecast in the Guanzhong Area, China | 16 |
| 2.2.8 Hybrid ARIMA-LSTM model for SPEI forecasting | 17 |
| 2.2.9 SPEI Forecasting using an Informer Model | 17 |

| | | |
|----------|--|-----------|
| 3 | Methods | 18 |
| 3.1 | Satellite Data Hub | 18 |
| 3.1.1 | DEWS' Data Collection | 21 |
| 3.1.2 | Application of DEWS DH | 21 |
| 3.2 | Selection of the Drought Index | 23 |
| 3.3 | Selection of the PET equations | 23 |
| 3.4 | Data Collection | 23 |
| 3.4.1 | Weather Station Data | 25 |
| 3.4.2 | Remote Sensing Data | 25 |
| 3.4.3 | Soil Moisture Index (SMI) | 26 |
| 3.5 | Data Preprocessing | 27 |
| 3.5.1 | Weather Station Data | 27 |
| 3.5.2 | Remote Sensing Data | 28 |
| 3.6 | Calculations | 29 |
| 3.6.1 | Potential Evapotranspiration (PET) | 29 |
| 3.6.2 | Difference | 33 |
| 3.6.3 | SPEI | 34 |
| 3.6.4 | Correlation | 34 |
| 3.7 | Prediction | 37 |
| 3.7.1 | Gradient Boosting Regressor | 37 |
| 3.7.2 | XGBoost | 38 |
| 3.7.3 | Prophet | 39 |
| 3.7.4 | SARIMA | 40 |
| 4 | Experimental Setup | 43 |
| 4.1 | Requirements | 43 |
| 4.1.1 | SPEI Accuracy | 43 |
| 4.1.2 | Correlation with SMI | 44 |
| 4.1.3 | Prediction Accuracy | 44 |
| 4.2 | SPEI Calculation | 44 |
| 4.2.1 | Data Preprocessing | 45 |
| 4.2.2 | Calculation | 47 |
| 4.2.3 | Evaluation | 50 |
| 4.3 | Correlation with SMI | 51 |
| 4.4 | Prediction Models | 52 |
| 4.4.1 | Gradient Boosting Regressor | 52 |

| | | |
|----------|-------------------------------------|------------|
| 4.4.2 | XGBoost | 58 |
| 4.4.3 | Prophet | 61 |
| 4.4.4 | SARIMA | 62 |
| 5 | Results | 65 |
| 5.1 | SPEI Calculations | 65 |
| 5.1.1 | Weather Stations Data | 65 |
| 5.1.2 | Remote Sensing Data | 76 |
| 5.1.3 | Result Comparison | 81 |
| 5.2 | Comparison with SMI | 83 |
| 5.2.1 | Upper soil | 83 |
| 5.2.2 | Total soil | 93 |
| 5.3 | Prediction | 105 |
| 5.3.1 | Gradient Boosting Regressor | 105 |
| 5.3.2 | XGBoost | 113 |
| 5.3.3 | Prophet | 123 |
| 5.3.4 | SARIMA | 126 |
| 6 | Discussion | 128 |
| 6.1 | Interpretation of Results | 128 |
| 6.1.1 | SPEI Calculation | 128 |
| 6.1.2 | Correlation with SMI | 129 |
| 6.1.3 | Gradient Boosting Regressor (GBR) | 130 |
| 6.1.4 | XGBoost | 131 |
| 6.1.5 | Prophet | 132 |
| 6.1.6 | SARIMA | 132 |
| 6.2 | Forecasts | 133 |
| 6.3 | Implications for Drought Monitoring | 134 |
| 6.4 | Limitations | 134 |
| 6.5 | Recommendations for Future Research | 136 |
| 7 | Conclusion | 138 |
| 7.1 | Summary of Key Findings | 138 |
| 7.1.1 | SPEI Calculations | 138 |
| 7.1.2 | SMI Correlation | 139 |
| 7.1.3 | Prediction Methods | 139 |
| 7.1.4 | Requirements | 140 |

| | |
|------------------------------------|------------|
| 7.2 Final Remarks | 141 |
| Bibliography | 143 |
| Declaration of Autorship | 151 |

List of Figures

| | | |
|-----|--|----|
| 1.1 | Dry periods in Germany in Jan 2021, Sep 2022, and Jul 2023 (<i>left to right</i>) (Helmholtz Zentrum für Umweltforschung, 2024) | 1 |
| 1.2 | Map of all weather stations by the German Weather Service distributed throughout Germany (Deutscher Wetterdienst, 2024d) | 3 |
| 2.1 | 1-month SPEI map for Middle Europe in August 2022 captured from the SPEI Global Drought Monitor (Vicente-Serrano et al., 2024) in a browser | 10 |
| 2.2 | Drought conditions of Germany (August 2022) represented by the SMI (Samaniego et al., 2013). The Helmholtz Center for Environmental Research (UFZ) uses a high-resolution hydrological model (mHM) to calculate the drought index. Drought maps of Germany can be seen at the Drought Monitor Germany of the Helmholtz Zentrum für Umweltforschung (2024). | 12 |
| 3.1 | DEWS DH’s satellite data details page whose images were taken on the 17th of April 2024 from a region near Uhlenhorst (Schwarzenbek) in Germany. The information had been received by a request to the Sentinel Hub API. | 19 |
| 3.2 | Comparison of RGB and NDVI images of a region near Uhlenhorst (Schwarzenbek) in Germany from the 17th April 2024. | 20 |
| 3.3 | Planned pipeline of the process for storing, calculating indices, and detecting droughts using satellite images. Planned additions in light red. Existing features in other colors. | 22 |

LIST OF FIGURES

| | | |
|-----|---|----|
| 4.1 | SPEI color bar from blue (SPEI 2.0/wet) to green (SPEI 0.0/normal) to red (SPEI -2.0/dry). | 48 |
| 4.2 | 1-month weather station SPEI map for January 2022 of Germany using the FAO-56 Penman-Monteith PET equation | 49 |
| 4.3 | 1-month remote sensing SPEI map for January 2022 of Germany using the FAO-56 Penman-Monteith PET equation | 50 |
| 4.4 | Simple Gradient Boosting Regressor tree model with 100 estimators, a learning rate of 0.1, a max depth of 3, and a random state of 42. The features x_0 to x_4 represent latitude, longitude, SPEI of the previous month, SPEI of two months ago, and SPEI of three months ago (<i>in this order</i>). | 53 |
| 4.5 | Section of the tree of the Gradient Boosting Regressor model with the lowest RMSE value 0.0 (see Table 5.4) out of all tested model configurations. The features C, L, and DOY were used. For a detailed view see the model in the GitHub repository in <code>data_comparison/gbt_output</code> (Tran, 2024b). | 56 |
| 5.1 | SPEI value distribution in percentage separated by PET equation for Germany represented as bars which mirror the SPEI categories from Extreme Wet ($2.0 \leq x$) to Extreme Drought ($x \leq -2.0$). Each bar shows the percentage quantity of the total quantity of the SPEI values. The values of the PET equations FAO-56 Penman-Monteith (FAO56PM), Thornthwaite (TW), Priestley-Taylor (PT), and Hargreaves (HG) are shown. The SPEIbase (SPEI DB) (Beguería, 2010) is included to have comparison values. The y-axis represents the percentage quantity of the total quantity by SPEI category and the x-axis shows the different PET equation methods. | 66 |
| 5.2 | SPEI value distribution in percentage separated by SPEI categories for Germany represented as bars which mirror the SPEI categories' quantity of the specific SPEI equation from Extreme Drought (<i>left</i>) to Extreme Wet (<i>right</i>). Each bar shows the percentage quantity of the total quantity of the SPEI values of the specific PET equation used. | 68 |
| 5.3 | Comparison of the PET equation method's maximum monthly 1-month SPEI values using weather stations data for the year 2022 in Germany compared to the SPEI DB result (<i>purple</i>). | 70 |

| | | |
|-----|---|----|
| 5.4 | Comparison of the PET equation method’s mean monthly 1-month SPEI values using only weather station data for the year 2022 in Germany compared to the SPEI DB result (<i>purple</i>). All calculated datasets have a mean 1-month SPEI of around 0 while the SPEI DB’s values vary from -2.0 to 0.8. | 71 |
| 5.5 | Comparison of the PET equation method’s minimum monthly 1-month SPEI values using only weather station data for the year 2022 in Germany compared to the SPEI DB result (<i>violet</i>). | 72 |
| 5.6 | SPEI value maps of Germany in January 2022 calculated using data from German weather stations by Deutscher Wetterdienst (2024c). The Thornthwaite (upper left), FAO-56 Penman-Monteith (lower left) and Priestley-Taylor PET equation (lower right) are visually compared to the SPEI Global Databases values (upper right). | 74 |
| 5.7 | 1-month SPEI value distribution comparison in percentage between the SPEIbase (Beguería, 2010) (SPEI DB) and the remote sensing SPEI (SPEI RS) for the year 2022. | 76 |
| 5.8 | Comparison of the max. 1-month SPEI values using remote sensing data for the year 2022 in Germany compared to the SPEIbase (Beguería, 2010). The remote sensing SPEI (<i>blue</i>) starts in January 2022 at 2.1, falls month by month to 0.75 in June 2022, and then rises to 2.2 in December 2022. The values for the SPEIbase are not smooth and rise and fall from month to month having the maximum at 2.8 and the minimum at -1.3. | 77 |
| 5.9 | Comparison of the mean 1-month SPEI values using remote sensing data for the year 2022 in Germany compared to the SPEIbase (Beguería, 2010). The remote sensing SPEI (<i>blue</i>) starts in January 2022 at 1.1, drops to -0.7 in June 2022, and then rises to 1.25 in December 2022. On the other hand the values of the SPEIbase (<i>purple</i>) have no pattern as the values rise and fall except for April to August where the values are relatively close to the remote sensing SPEI. The mean difference between the values is ≈ 0.9058 | 78 |

| | | |
|------|---|----|
| 5.10 | Comparison of the min. 1-month SPEI values using remote sensing data for the year 2022 in Germany compared to the SPEIbase (Beguería, 2010). The remote sensing SPEI (<i>blue</i>) has SPEI values from 0.2 to 0.9 in the autumn to spring months while in the summer the SPEI drops to -6. For the SPEIbase (<i>purple</i>) the SPEI values range between -2.9 and 0.1 and have no actual pattern. | 80 |
| 5.11 | SPEI differences between the results of the weather station SPEI, the remote sensing SPEI, and the SPEIbase represented as maps for August 2020 in Germany. The difference between the remote sensing SPEI and SPEIbase is the least while the difference between the weather station and remote sensing SPEI is the most. | 81 |
| 5.12 | Pearson correlation between interpolated SMI of the upper soil (up to 25cm deep) and the 1-month SPEI in the date range 1st January 2015 to 31st December 2018 represented by a scatter plot. The Pearson correlation coefficient is ≈ -0.1179 | 83 |
| 5.13 | Distance correlation: 1-month Weather Station SPEI and SMI (upper soil) for the period January 2012 to December 2012 at latitude 53.6 and longitude 10.2 in Germany. The distance correlation coefficient is 0.2158. | 84 |
| 5.14 | Time series of 1-month weather station SPEI (<i>blue</i>) and SMI (upper soil) (<i>orange</i>). The SMI of the upper soil ranges between 0 and 1.9 while the SPEI ranges from -1.4 to 1.1. Overall the graphs do not have a similar course except for the period March 2017 to July 2017. | 85 |
| 5.15 | Pearson correlation between 1-month Remote Sensing SPEI and SMI (upper soil) | 87 |
| 5.16 | Pearson correlation between 3-month Remote Sensing SPEI and SMI (upper soil) | 87 |
| 5.17 | Pearson correlation between 6-month Remote Sensing SPEI and SMI (upper soil) | 87 |
| 5.18 | Pearson correlation between 9-month Remote Sensing SPEI and SMI (upper soil) | 87 |

LIST OF FIGURES

| | |
|--|----|
| 5.19 Pearson correlation between 12-month Remote Sensing SPEI and SMI (upper soil) | 87 |
| 5.20 Pearson correlation between 24-month Remote Sensing SPEI and SMI (upper soil) | 87 |
| 5.21 Pearson correlation analysis between the n-month Remote Sensing SPEI and the SMI for the upper soil at different time scales (1, 3, 6, 9, 12, 24) at the location with latitude 53.6 and longitude 10.2, from January 2015 to December 2018. | 87 |
| 5.22 Distance correlation: 1-month Remote Sensing SPEI and SMI (upper soil) | 89 |
| 5.23 Distance correlation: 3-month Remote Sensing SPEI and SMI (upper soil) | 89 |
| 5.24 Distance correlation: 6-month Remote Sensing SPEI and SMI (upper soil) | 89 |
| 5.25 Distance correlation: 9-month Remote Sensing SPEI and SMI (upper soil) | 89 |
| 5.26 Distance correlation: 12-month Remote Sensing SPEI and SMI (upper soil) | 89 |
| 5.27 Distance correlation: 24-month Remote Sensing SPEI and SMI (upper soil) | 89 |
| 5.28 Distance correlation analysis between the n-month Remote Sensing SPEI and the SMI for the upper soil at different time scales (1, 3, 6, 9, 12, 24) at the location with latitude 53.6 and longitude 10.2, from January 2015 to December 2018. | 89 |
| 5.29 1-month Remote Sensing SPEI vs. SMI (upper soil) | 90 |
| 5.30 3-month Remote Sensing SPEI vs. SMI (upper soil) | 90 |
| 5.31 6-month Remote Sensing SPEI vs. SMI (upper soil) | 90 |
| 5.32 9-month Remote Sensing SPEI vs. SMI (upper soil) | 90 |
| 5.33 12-month Remote Sensing SPEI vs. SMI (upper soil) | 90 |
| 5.34 24-month Remote Sensing SPEI vs. SMI (upper soil) | 90 |
| 5.35 Visual comparison between the n-month remote sensing SPEI and the SMI for the upper soil at different time scales (1, 3, 6, 9, 12, 24) at the location with latitude 53.6 and longitude 10.2, from January 2015 to December 2018. | 90 |

LIST OF FIGURES

5.36 Pearson correlation between the monthly interpolated SMI (upper soil) and the 1-month SPEI from SPEIbase for the period from January 2015 to December 2018 with a correlation coefficient of 0.00244977 91

5.37 Distance correlation: 1-month SPEIbase SPEI and SMI (upper soil) from January 2015 to December 2018 at latitude 53.6 and longitude 10.2. The distance correlation coefficient is 0.56983618. 92

5.38 Time series of 1-month SPEIbase SPEI (*blue*) and SMI (upper soil) (*orange*) from January 2015 to December 2018 at latitude 53.6 and latitude 10.2. 93

5.39 Pearson correlation: 1-month Weather Station SPEI and SMI (total soil) from January 2015 to December 2018 at latitude 53.6 and latitude 10.2. The Pearson correlation coefficient is -0.09828705 94

5.40 Distance correlation: 1-month Weather Station SPEI and SMI (total soil) from January 2015 to December 2018 at latitude 53.6 and latitude 10.2. The distance correlation is 0.1584. 95

5.41 Comparison: 1-month Weather Station SPEI and SMI (total soil) 96

5.42 Pearson correlation between 1-month Remote Sensing SPEI and SMI (total soil) 97

5.43 Pearson correlation between 3-month Remote Sensing SPEI and SMI (total soil) 97

5.44 Pearson correlation between 6-month Remote Sensing SPEI and SMI (total soil) 97

5.45 Pearson correlation between 9-month Remote Sensing SPEI and SMI (total soil) 97

5.46 Pearson correlation between 12-month Remote Sensing SPEI and SMI (total soil) 97

5.47 Pearson correlation between 24-month Remote Sensing SPEI and SMI (total soil) 97

LIST OF FIGURES

5.48 Pearson correlation analysis between the n-month Remote Sensing SPEI and the SMI for the total soil at different time scales (1, 3, 6, 9, 12, 24) at the location with latitude 53.6 and longitude 10.2, from January 2015 to December 2018. 97

5.49 Distance correlation: 1-month Remote Sensing SPEI and SMI (upper soil) 99

5.50 Distance correlation: 3-month Remote Sensing SPEI and SMI (upper soil) 99

5.51 Distance correlation: 6-month Remote Sensing SPEI and SMI (upper soil) 99

5.52 Distance correlation: 9-month Remote Sensing SPEI and SMI (upper soil) 99

5.53 Distance correlation: 12-month Remote Sensing SPEI and SMI (upper soil) 99

5.54 Distance correlation: 24-month Remote Sensing SPEI and SMI (upper soil) 99

5.55 Distance correlation analysis between the n-month Remote Sensing SPEI and the SMI for the upper soil at different time scales (1, 3, 6, 9, 12, 24) at the location with latitude 53.6 and longitude 10.2, from January 2015 to December 2018. 99

5.56 1-month Remote Sensing SPEI vs. SMI (total soil) 101

5.57 3-month Remote Sensing SPEI vs. SMI (total soil) 101

5.58 6-month Remote Sensing SPEI vs. SMI (total soil) 101

5.59 9-month Remote Sensing SPEI vs. SMI (total soil) 101

5.60 12-month Remote Sensing SPEI vs. SMI (total soil) 101

5.61 24-month Remote Sensing SPEI vs. SMI (total soil) 101

5.62 Time series comparison between n-month Remote Sensing SPEI and SMI for total soil at different time scales (1, 3, 6, 9, 12, 24) at the location with latitude 53.6 and longitude 10.2, from January 2015 to December 2018. . . 101

5.63 Pearson correlation between the monthly SMI (total soil) and the 1-month SPEI from SPEIbase for the period from January 2015 to December 2018 with a correlation coefficient of 0.00960535. 102

5.64 Distance correlation: 1-month SPEIbase SPEI and SMI (upper soil) for the period from January 2015 to December 2018 with a correlation coefficient of 0.46145403. 103

5.65 Time series of 1-month SPEIbase SPEI (*blue*) and SMI (total) (*orange*) from January 2015 to December 2018 at latitude 53.6 and latitude 10.2. . 104

5.66 Percentage of predicted SPEI values by dataset variant using the Gradient Boosting Regressor. The variants include the features: coordinates, the day of the year (DOY), and a lag (SPEI values of three previous months). The models have been trained and tested with features from 2000-01 to 2015-01 for the region of Germany. After that, the values were predicted for the period 2015-02 to 2020-12. 108

5.67 Variance between observed and predicted SPEI values from January 2015 to December 2020 in Germany. The maximum difference between the observed and predicted SPEI value is shown in blue, the observed SPEI value which leads to the maximum difference is shown in orange, and the predicted SPEI value which leads to the maximum difference is shown in green. Also, the minimum difference between the observed and predicted SPEI value is shown in red while the observed SPEI value which leads to the minimum difference is shown in violet, the predicted SPEI value which leads to the minimum difference is shown in brown, and last but not least the mean difference between the observed and predicted SPEI value is shown in pink. The models have been trained and tested with features from 2000-01 to 2015-01 for the region of Germany. After that, the values were predicted for the period 2015-02 to 2020-12. 109

5.68 Comparison of Gradient Boosting Regressor box plots of predicted SPEI value for the period 2015-01 to 2020-12 for the region Germany. 112

5.69 Observed (*blue*) and predicted 1-month SPEI values (*orange*) in comparison for Germany on the test dataset. The observed and predicted values share a common course with some expectations as around time index 20 to 25 and 34 to 39. 114

5.70 Actual vs. predicted 1-month (lag size: 1) 116

5.71 Actual vs. predicted 1-month (lag size: 2) 116

5.72 Actual vs. predicted 1-month (lag size: 3) 116

5.73 Actual vs. predicted 1-month (lag size: 4) 116

5.74 Actual vs. predicted 1-month (lag size: 5) 116

5.75 Actual vs. predicted 1-month (lag size: 6) 116

5.76 Comparison of the actual and predicted 1-month SPEI values for the lag sizes from 1 to 6 for the coordinates latitude 53.6 and longitude 10.2 in Germany for the period from January 1980 to June 2024. The lag size of 6 offers the lowest mean difference between the actual and predicted SPEI values, while the lowest minimum difference and the highest maximum difference are achieved by the lag size of 3. 116

5.77 1-month SPEI 119

5.78 3-month SPEI 119

5.79 6-month SPEI 119

5.80 9-month SPEI 119

5.81 12-month SPEI 119

5.82 24-month SPEI 119

5.83 Comparison between actual and predicted n-month SPEI values where n is 1, 3, 6, 9, 12 or 24. The train and test dataset contains SPEI values for the period January 1980 to June 2024 for the coordinates latitude 53.6 and longitude 10.2 in Germany. The model with the lowest MAE and RMSE is shown per n-month SPEI. 119

5.84 Prophet’s 1-month SPEI forecast graph (blue) from January 1980 to September 2032 for the coordinates latitude 53.6 and longitude 10.2 (Northern Germany). The black markers show the actual monthly 1-month SPEI values and the red line shows the rising trend which goes from -0.06 (1980) to 0.1 (2032). The blue graph shows the forecast which tends to have a seasonal pattern. 123

| | | |
|------|--|-----|
| 5.85 | Trend and yearly pattern of the Prophet forecast for the period from January 1980 to September 2032 for the coordinates latitude 53.6 and longitude 10.2 (Northern Germany. The top figure shows the trend which will rise from 1980 to 2030 from around -0.06 to 0.1. Below the yearly pattern of the SPEI is shown which rises in the summer months and falls in autumn to spring. | 124 |
| 5.86 | Performance metrics MAE and RMSE of Prophet model which forecasts the 1-month SPEI for the period from January 1980 to September 2032 for the coordinates latitude 53.6 and longitude 10.2 (Northern Germany). | 125 |
| 5.87 | Comparison of the best performing SARIMA models based on AIC, RMSE, and mean difference between the observed and forecasted 1-month SPEI values. The models have been tested with various training and forecast periods for the location (53.75, 10.25) which is located in Bargteheide/Elmenhorst in Germany. | 126 |

List of Tables

| | | |
|-----|--|-----|
| 5.1 | SPEI value ranges and corresponding conditions from extreme drought (top) to extremely wet (bottom) | 67 |
| 5.2 | Difference between the PET equation methods and the SPEI DB. Each PET equation method's total quantity per SPEI category is compared to the SPEI DB's total quantity and the difference is shown here. The right column shows the total difference between the specific PET equation method and the SPEI DB's total quantity percentage. The SPEI categories are abbreviated where D. means drought and W. means wet. For further information see Table 5.1. | 69 |
| 5.3 | Root Mean Squared Error (RMSE) of different GBR models sorted from highest (top) to lowest RMSE (bottom). The C+DOY model has the highest RMSE, whereas the C+L+DOY model has the lowest. This configuration is set to the same as in Figure 4.4. | 105 |
| 5.4 | Top 5 lowest RMSE values from lowest (top) to highest (bottom). This table shows the numbers of estimators, learning rate, max depth, and model variants for the top 5 Gradient Boosting Regressor models with the lowest RMSE value. The model variant C+L+DOY, which expects the features of geographical coordinates, the SPEI value of the last three months, and the day of the year, is represented in all 5 places and achieves the lowest RMSE with 0.26234. | 106 |

5.5 Top 5 highest RMSE values from highest (top) to lowest (bottom). This table shows the numbers of estimators, learning rate, and max depth for the top 5 Gradient Boosting Regressor models with the highest RMSE value. The model variant C+DOY, which expects geographical coordinates and the day of the year, has achieved the highest RMSE value out of all model variants with an RMSE of 1.234052. 107

5.6 Metric, variable, and lag size combinations with the lowest metric value for the metrics mentioned. The lag size of 6 appears three times for the MAE, four times for the RMSE, and the metrics min., max., and mean difference the lag size of 6 occurs the most, too. 117

5.7 Top 6 Lowest MAE for SPEI_n. SPEI_6 has achieved the lowest MAE with 0.241539 whereas the SPEI_1 reached the highest MAE with 0.653570. 120

5.8 Top 6 Lowest RMSE for SPEI_n. SPEI_6 has achieved the lowest RMSE with 0.289719 whereas the SPEI_1 reached the highest MAE with 0.825903. 120

5.9 Lowest Metric Values for SPEI_n. The lowest min. and mean difference is achieved by SPEI_1 and the lowest max. the difference, MAE, and RMSE by the SPEI_6. 120

5.10 Lowest MAE for the predicted variables *pev*, *ssr*, *str*, *t2m*, *tp*, u_{10} and v_{10} (lowest value at the top, then ascending downwards). The two occurring combinations of hyperparameters for the number of estimators, learning rate, and max depth are 50, 0.1 or 0.2, 3. 121

5.11 Lowest RMSE for the predicted variables *pev*, *ssr*, *str*, *t2m*, *tp*, u_{10} and v_{10} (lowest value at the top, then ascending downwards). The two occurring combinations of hyperparameters for the number of estimators, learning rate, and max depth are 50 or 200, 0.1 or 0.2, 3. 121

Listings

| | | |
|-----|--|----|
| 4.1 | Header of an ASCII file by the Deutscher Wetterdienst (2024a) representing the max. air temperature of Germany | 45 |
|-----|--|----|

1 Introduction

The summer months in Germany experience persistent dry spells, which become more severe yearly. Not only animals but also humans are directly affected by low water levels and crop failures (BmfBuF, 2022). In Germany, the alternation between wet, regular, and dry periods has profound effects on various sectors, including agriculture, forestry, and urban water management (Künzel et al., 2021)(Oberhäuser, 2018). To develop and apply measures against droughts, it is important to know when droughts have occurred and when they will occur in the future. As can be seen in Figure 1.1, droughts can occur at different times with different intensities depending on the location which makes this topic complex.

The probability of more frequent, severe, and long-term droughts in the future rose over the last years due to the massive release of emissions (Ault, 2020). To prevent and prepare for such drought events the information on when and how severe a drought will be is important for the decision-makers and the individual person itself.

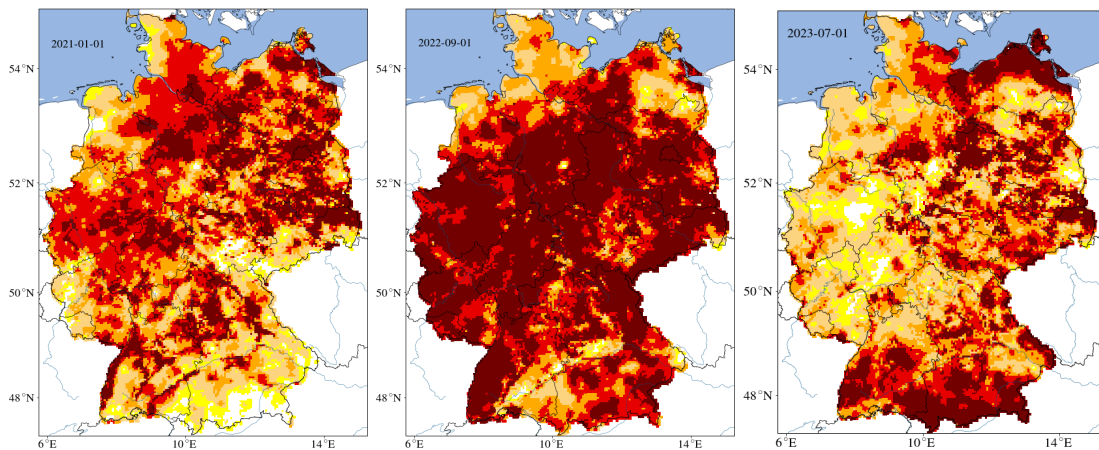


Figure 1.1: Dry periods in Germany in Jan 2021, Sep 2022, and Jul 2023 (*left to right*) (Helmholtz Zentrum für Umweltforschung, 2024)

Advancements in machine learning have revolutionized the ability to analyze and predict data patterns by learning from large datasets and improving prediction accuracy over time (European Centre for Medium-Range Weather Forecasts, 2023a). Using these methods to predict dry and wet periods can be powerful when combined with the right data. The combination of remote sensing and meteorological data provides a comprehensive and accurate approach to weather forecasting, particularly in identifying and predicting dry and wet areas (Mitra, 2023). This data is crucial for creating accurate prediction models.

One index used in assessing climate variability is the Standardized Precipitation-Evapotranspiration Index (SPEI) (Vicente-Serrano et al., 2010), which measures drought severity based on precipitation and potential evapotranspiration. A benefit is that the index can also identify wet areas. By integrating SPEI with machine learning models, researchers can enhance the precision of identifying and predicting periods of drought and excessive rainfall.

The combination of machine learning techniques, remote sensing, and meteorological data enables more accurate and timely predictions, which are essential for developing effective adaptation and mitigation strategies (Li et al., 2020). In this study developed approach helps in better understanding the dynamics of climate variability and aids in the decision-making processes for sectors dependent on weather conditions, such as agriculture and water resource management.

This study will examine how to calculate the SPEI for Germany using weather station and remote sensing data and if it differs from the official SPEIbase created by the SPEI inventors Beguería (2010). It will also find out whether a correlation between the SPEI and SMI exists as well as which prediction method and which type of data leads to a reliable and accurate prediction of dry and wet periods using the SPEI.

1.1 Research Problem

Weather stations only cover the area where they have been set up. For Germany, the weather stations available can be seen in Figure 1.2. The areas between the weather stations will be calculated using spatial interpolation. Spatial interpolation is used to estimate points with unknown values using points with known values.

Especially for locations such as oceans, deserts, and mountainous areas, it is challenging to install and maintain weather stations. Remote sensing data provides data for regions with sparse to no observation (Hao et al., 2018). With the combination of remote sensing and weather stations, the remote sensing data could improve each other's accuracy of the estimated data (Mitra, 2023).

When predicting wet and dry periods linear models and historical data may not fully capture the nonlinear variable climatic conditions affected by natural and anthropogenic factors (Hao et al., 2018). Machine learning could outperform statistical methods accuracy but still challenges exist from the complexity of climate conditions (Nandgude et al., 2023)(Hao et al., 2018).



Figure 1.2: Map of all weather stations by the German Weather Service distributed throughout Germany (Deutscher Wetterdienst, 2024d)

On the other hand, some related work (like (Shang et al., 2023), (Xu et al., 2022) or (Mehr et al., 2022)) that has been examined that they built predictive models that work like a more complicated formula. Here, the parameters (like precipitation or temperature) that are normally passed into a formula are passed to the drought prediction model, and the model "predicts" the value. The values for the month in the future need to be known for this calculation. To do this, more prediction models would have to be created to predict

the respective parameters. The predicted parameters would then have to be transferred to the drought prediction model.

Other approaches (like (Li et al., 2020)) are based on passing supposedly dependent parameters, such as the Normalized Difference Vegetation Index (NDVI), into a drought prediction model and thus calculating a drought index. Here too, it would be necessary to know the respective parameters for the future month and create further prediction models for the parameters.

This problem will be solved by this study which will recreate the SPEI for Germany and create models that need values from the past to predict the values in the future.

1.2 Goals

This thesis' primary goal is to find and develop a reliable method for detecting and predicting wet and dry periods using the SPEI. This research will explore and evaluate existing machine learning and statistical approaches in the literature, aiming to find the most accurate approaches, improve upon them, and create a simple but more effective solution.

The procedure is to compare different prediction methods and find the method with the highest accuracy. An additional objective is to improve the most reliable and accurate methodology to more accurately identify and predict the occurrence of these periods, contributing to a better understanding and management of climatic variability.

1.3 Research Hypotheses

Based on the goals of this thesis the following hypotheses were formulated:

1. **The method used to calculate potential evapotranspiration (PET) influences the values of the Standardized Precipitation-Evapotranspiration Index (SPEI).**

Given that PET is a component in determining water balance, any variation in its calculation could lead to significant differences in the assessment of drought conditions. This hypothesis aims to investigate how sensitive the SPEI is to the

choice of PET calculation method and to determine which method provides the most reliable results.

2. **Applying machine learning algorithms improves the accuracy of the indication of wet and dry phases in comparison to traditional statistical methods.**

Machine learning algorithms can learn from large datasets and uncover patterns that may not be immediately apparent. This hypothesis is grounded in the premise that machine learning techniques can enhance the precision of detecting and predicting wet and dry periods.

3. **The combination of multiple data sources (e.g., remote sensing, weather stations, etc.) leads to more accurate results in drought detection and prediction than using only weather station data.**

Drought conditions are influenced by various factors that can be captured by different types of data sources. While weather station data provides valuable localized information, remote sensing data offers broader spatial coverage and additional insights into surface conditions. By combining these diverse data sources, this hypothesis posits that a more comprehensive and accurate understanding of drought conditions can be achieved, leading to improved detection and prediction.

4. **Adding lagged features of a variable from previous months increases the prediction accuracy of the to-be-predicted variable.**

By incorporating lagged features (past values of the variable of interest) into the prediction models, it is hypothesized that the model's ability to predict future values will be enhanced. This approach recognizes the importance of temporal patterns in climatic data and aims to leverage them to improve prediction accuracy.

1.4 Thesis Structure

This thesis comprises chapters, each addressing a distinct aspect of the research. The chapters are organized as follows:

Chapter 1: Introduction

This chapter sets the stage for the thesis by introducing the research problem. It also outlines the research hypotheses and provides a summary of the thesis structure.

Chapter 2: Related Work

Here, a review of relevant literature and previous studies related to drought indices and prediction models is presented.

Chapter 3: Data and Methods

This chapter details the data sources, the methods used for data collection, and the processing techniques. It also elaborates on the SPEI calculations, correlation coefficient calculations, and the various models and methods applied for analysis and prediction.

Chapter 4: Experimental Setup

How the experimental setup was designed and carried out to calculate SPEI values using remote sensing and weather station data. Also how the calculation of the correlation with the SMI and the prediction models have been accomplished, is described in this chapter.

Chapter 5: Results

The findings of the research are presented in this chapter. It includes the results of SPEI calculations, correlation coefficients, data comparisons, and the evaluation of different prediction models.

Chapter 6: Discussion

This chapter interprets the results and discusses their implications for drought monitoring. It also highlights the limitations of the study and offers recommendations for future research.

Chapter 7: Conclusion

All key findings of the study are summarized in this last chapter.

2 Related Work

The following chapter reviews the advancements and applications of various predictive models and technologies in the context of dry and wet period forecasts. This includes an exploration of remote sensing, satellite imagery data, drought indices, and prediction methods.

The selection of papers is based on topicality, relevance, and the number of citations per year.

2.1 Drought Indices

Drought indices like the Standardized Precipitation-Evapotranspiration Index (SPEI) (Vicente-Serrano et al., 2010) and the Soil Moisture Index (SMI) (Samaniego et al., 2013) are used for monitoring drought conditions. SPEI integrates precipitation and potential evapotranspiration, while SMI focuses on soil moisture levels, providing insights into drought impacts.

2.1.1 Standardized Precipitation Evapotranspiration Index (SPEI)

In April 2010 Vicente-Serrano et al. (2010) created a multiscalar drought index that is sensitive to global warming called the Standardized Precipitation Evapotranspiration Index (SPEI). The SPEI is an index for drought assessment that integrates temperature and precipitation data. By calculating the water balance, which is the difference between the precipitation sum and the potential evapotranspiration (PET), the accumulation of water deficit or surplus across various time scales can be identified. This process is followed by fitting these values to a log-logistic probability distribution to standardize the index, allowing for consistent comparisons over time and space. The SPEI's methodology not only resembles the approach of the Standardized Precipitation Index (SPI) in its

mathematical foundation but also enhances it by incorporating the role of temperature variations. This incorporation is essential for understanding drought dynamics, particularly in the context of global warming, where temperature influences evapotranspiration rates.

For simplicity Vicente-Serrano et al. (2010) used the Thornthwaite equation (Thornthwaite, 1948) to estimate the potential evapotranspiration (PET). This equation only requires the mean air temperature and the latitude of the location while other PET equations need a few more parameters. When compared with the self-calibrated Palmer Drought Severity Index (sc-PDSI) and the Standardized Precipitation Index (SPI) across different global observatories, the SPEI was particularly effective in identifying increases in drought severity linked to higher water demand due to evapotranspiration under global warming conditions. The outcome of Vicente-Serrano et al. (2010)'s work was that the SPEI is a valuable tool for the assessment of droughts and their severity, capable of reflecting the impact of temperature on drought assessments and providing a multiscalar perspective essential for comprehensive drought analysis and monitoring.

At their website spei.csic.es Vicente-Serrano et al. (2010) offer a SPEI Global Drought Monitor which uses the Thornthwaite method to estimate the PET. Figure 2.1 shows an example of a drought map from the SPEI Global Drought Monitor. Also, a SPEI dataset, called SPEIbase (Beguería, 2010) is published which is based on the meteorological dataset CRU TS (Climatic Research Unit gridded Time Series) (Climatic Research Unit and NCAS, 2024). However, for the downloadable dataset, the FAO-56 Penman-Monteith equation is used for the estimation of the PET. Vicente-Serrano et al. (2010) say: "*The Penman-Monteith method is considered a superior method, so the SPEIbase is recommended for most uses including long-term climatological analysis.*". Contrary to the statement, the dataset only provides the 1-month SPEI.

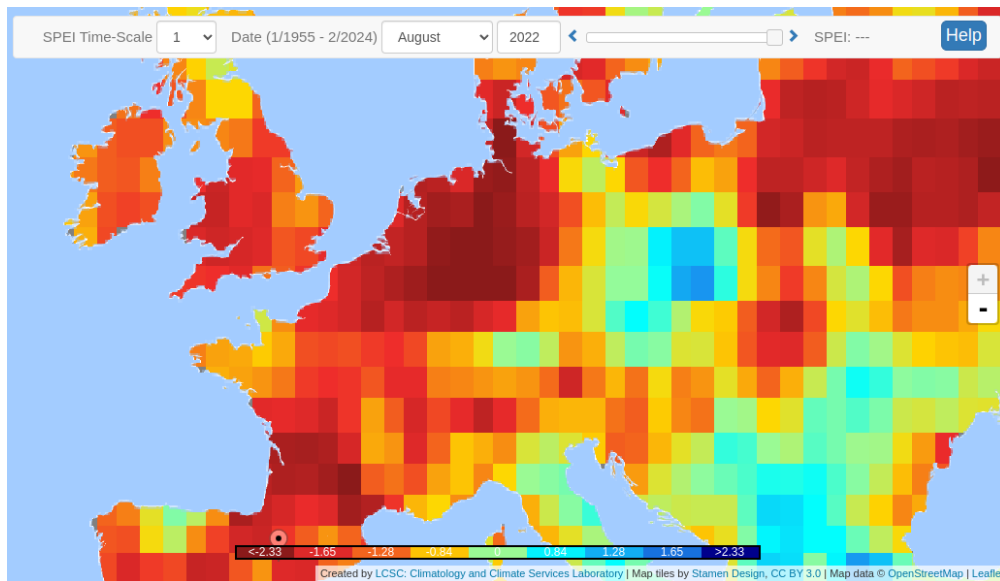


Figure 2.1: 1-month SPEI map for Middle Europe in August 2022 captured from the SPEI Global Drought Monitor (Vicente-Serrano et al., 2024) in a browser

SPEI in Europe

Dukat et al. (2022) focused on examining the trends in drought occurrence and severity across mid-latitude European locations from 1951 to 2015 using the SPI and SPEI. For the SPEI calculation, the PET was calculated using the Thornthwaite equation (Thornthwaite, 1948) like the founders of the SPEI Beguería et al. (Vicente-Serrano et al., 2010) did. The research aimed to analyze how droughts have changed over time in Europe, given the backdrop of climate change and its expected impact on increasing the frequency, duration, and intensity of drought events.

The results showed a general absence of a statistically significant trend in the increase in the occurrence of dry months. However, there was an observed increase in the severity of droughts during summer months, especially noted with the SPEI over a 6-month scale for all investigated stations. This indicates that under the conditions of global warming, droughts are becoming more severe due to higher water demand for evapotranspiration. The study highlighted the years with the highest number of dry months since the 1970s that occurred in the last five years of the analysis period (2010-2015). In the study, no comparison with the actual observed conditions is shown.

2.1.2 Soil Moisture Index (SMI)

Samaniego et al. (2013) developed the Soil Moisture Index (SMI), a hydrological indicator designed to quantify soil moisture by representing monthly soil water content as quantiles at each grid cell. Derived from high-resolution land surface hydrology simulations using a process-based hydrological model, the SMI effectively captures spatial and temporal variability in soil moisture.

Experiments to develop and validate the SMI were conducted across all major river basins in Germany, ensuring its robustness and applicability in different hydrological and climatic contexts. The SMI provides a precise measure of soil moisture, closely aligning with agricultural productivity metrics like total grain yield.

The SMI is calculated by first simulating daily soil moisture levels using the hydrological model. These daily values are then aggregated into monthly data. For each grid cell, the monthly soil moisture values are ranked and converted into quantiles, which reflect the probability of observing a particular soil moisture level. This quantile-based approach allows the SMI to consistently compare soil moisture conditions across different regions and time periods, identifying anomalies such as droughts.

German Drought Monitor

Samaniego et al. (2010) developed a high-resolution hydrological model, mHM, at the Helmholtz Center for Environmental Research (UFZ). This model is utilized by the UFZ, the Copernicus Climate Change Service System ULYSSES, and the World Meteorological Organization (2022) for various applications, including drought condition assessments in Germany. To use the mHM model, data from approximately 2500 weather stations managed by the German Weather Service are quality-checked and interpolated onto a 4 km grid using an external drift kriging method, with geographical elevation serving as an additional variable. The mHM hydrological model simulates several hydrological variables, such as soil moisture. By comparing simulated soil moisture values with their long-term expected values, the Soil Moisture Index (SMI) (Samaniego et al., 2013) is calculated to identify drought conditions. An example of drought maps of Germany can be seen at the website of the Helmholtz Zentrum für Umweltforschung (2024) and in Figure 2.2.

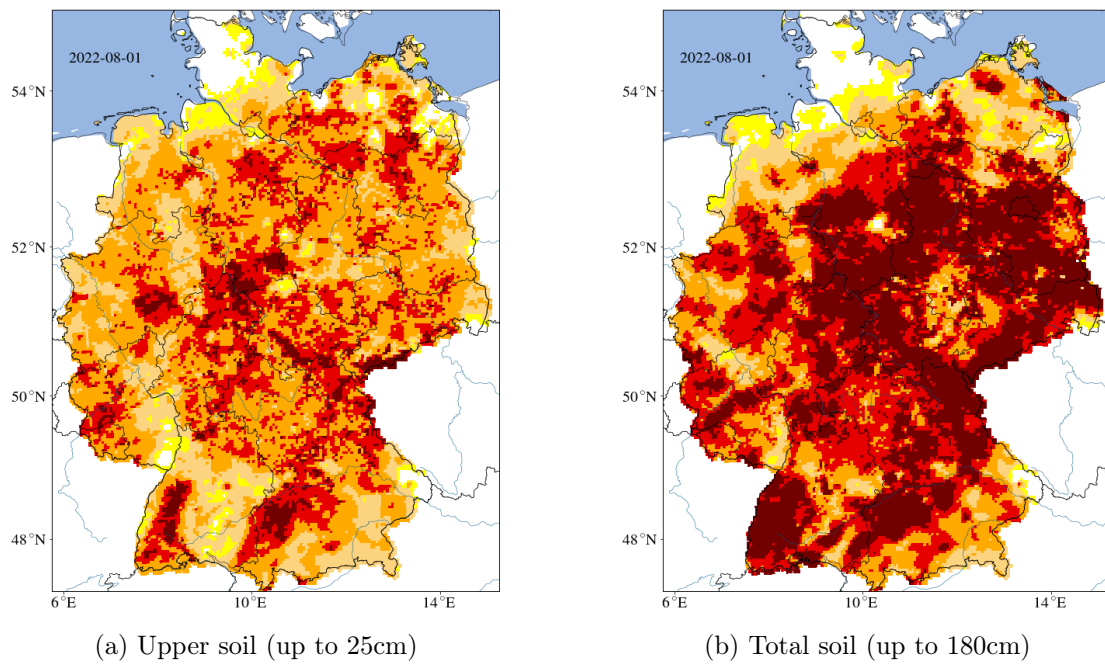


Figure 2.2: Drought conditions of Germany (August 2022) represented by the SMI (Samaniego et al., 2013). The Helmholtz Center for Environmental Research (UFZ) uses a high-resolution hydrological model (mHM) to calculate the drought index. Drought maps of Germany can be seen at the Drought Monitor Germany of the Helmholtz Zentrum für Umweltforschung (2024).

2.2 Predicting Wet and Drought Periods

Studies about predicting wet and drought periods using different methods. While re-searching the significant majority of the studies was related to droughts.

2.2.1 Assessment and Prediction of Meteorological Drought using Machine Learning

The study on drought forecasting in Morocco's Upper Drâa Basin by En-Nagre et al. (2024) utilized data from 13 weather stations collected between 1980 and 2019, focusing on temperature and precipitation. Two drought indices, the Standardized Precipitation Index (SPI) and the Standardized Precipitation Evapotranspiration Index (SPEI), were used to assess droughts over varying timescales (1, 3, 9, and 12 months). Statistical analyses, including the Mann-Kendall test and Sen's Slope estimator, were applied to identify trends.

To predict droughts, four machine learning algorithms - Random Forest (RF), Voting Regressor (VR), AdaBoost, and K-Nearest Neighbors (KNN) - were evaluated. These models were tested on SPEI-3 and SPEI-12 indices. The Random Forest algorithm showed the best performance, achieving Nash-Sutcliffe Efficiency (NSE) values ranging from 0.91 to 0.97 and Coefficient of Determination (R^2) values between 0.81 and 0.93 for predicting SPEI-3. The other models, particularly VR and AdaBoost, also performed well, with NSE and R^2 values slightly lower than RF. KNN, however, had more variability in its accuracy, with NSE values ranging from 0.44 to 0.84.

Specifically, 84% of the weather stations showed non-significant negative trends in the short-term SPEI-1 index, with only one station (M'semrir) displaying a significant negative trend. For longer-term indices like SPEI-9 and SPEI-12, 76% of stations also showed non-significant negative trends. However, no station demonstrated a significant positive trend towards wetter conditions.

2.2.2 Drought Forecasting using Stochastic Models

Stochastic methods for drought forecasting are used in the work of Mishra and Desai (2005). The SPI (Standardized Precipitation Index) for different timescales from 3 to 24 months are calculated for the period from 1965 to 2001 in the Kansabati River basin.

The method used for drought forecasting in this study is based on linear stochastic models, specifically ARIMA (Autoregressive Integrated Moving Average) and SARIMA (Seasonal ARIMA) models. These models were selected due to their ability to model time series data that exhibit both trend and seasonality. The SPI is used as the drought index, and the models are developed through a process involving identification, estimation, and diagnostic checks. The best-fitting models are selected based on criteria such as the Akaike Information Criterion (AIC) and Schwarz Bayesian Criterion (SBC).

The forecasting accuracy was evaluated by comparing observed and predicted SPI values. For instance, the SARIMA model for SPI 12 achieved a correlation of 0.925 for a 1-month lead time and 0.730 for a 3-month lead time. Similarly, the SPI 24 model had a correlation of 0.906 for a 1-month lead time and 0.714 for a 3-month lead time.

Statistical tests, including Z-tests for means and F-tests for variances, showed no significant differences between observed and predicted data. For example, the SPI 12 model had an observed mean of 0.7307 and a predicted mean of 0.7102, with the variances also showing a close match. Overall, the models provided accurate drought forecasts, particularly for higher SPI timescales, with reliable predictions up to three months in advance.

2.2.3 Drought Monitoring and Prediction System (GIDMaPS)

The Global Integrated Drought Monitoring and Prediction System (GIDMaPS) has been created by Hao et al. (2014) to provide drought information based on multiple drought indicators. Precipitation and soil moisture data from remote sensing observations including the Modern-Era Retrospective Analysis for Research and Applications, North American Land Data Assimilation System, Global Land Data Assimilation System, and the Global Drought Climate Data Record are integrated into the GIDMaPS.

SPI (Standardized Precipitation Index), SSI (Standardized Soil Moisture Index), and MSDI (Multivariate Standardized Drought Index) are used as indicators of meteorological and agricultural droughts. The concept of the Ensemble Streamflow Prediction (ESP) is used for the prediction, which is a long-term hydrologic forecast method (Alfieri et al., 2014). The ESP operates on the assumption that historical data from any location can represent potential future scenarios.

The prediction component of GIDMaPS enhances persistence-based drought forecasting by incorporating a multi-index framework that utilizes various variables. It offers short-term predictions using both univariate (SPI, SSI) and multivariate (MSDI) drought indicators. The GIDMaPS predicted several major droughts like the 2010 Amazon Basin drought, the 2010-2011 East Africa drought, and the 2011-2012 United States drought.

2.2.4 Machine Learning in Drought Prediction

Dikshit et al. (2022) show in their scientometric analysis that the most used indices for drought prediction and forecasting purposes are the Standardized Precipitation Evaporation Index (SPEI) and the Standardized Precipitation Index (SPI). Support Vector Machine (SVM) and Artificial Neural Networks (ANN) are among the most used methods for drought prediction.

Decision Trees, often in combination with RFs, are mentioned as classical machine learning models used in drought prediction. While they are recognized for their ability to handle complex datasets and provide interpretable results, the analysis suggests that they are ranked lower in comparison to more advanced methods like SVM and ANN due to issues like overfitting when trees become too deep.

2.2.5 Deep Learning Models for Drought Prediction

Gyaneshwar et al. (2023) present a contemporary review on deep learning models for drought prediction in their work. The key contributions include the identification of effective deep learning models like Deep Neural Networks (DNN), Convolutional Neural Networks (CNN), Recurrent Neural Networks (RNN), and hybrid models.

It will be suggested that the suitability of a model depends on the specific characteristics of the data and the requirements of the prediction task. For example, CNNs are particularly effective when dealing with spatial data, such as satellite images, due to their ability to capture spatial hierarchies through convolutional layers. RNNs, especially LSTMs (Long Short-Term Memory Networks), are highlighted for their ability to manage time series data, capturing temporal dependencies effectively, which is crucial for tasks that require understanding sequences, such as drought predictions over time.

Moreover, the paper emphasizes the importance of data preprocessing, model architecture selection, and the inclusion of domain-specific knowledge to optimize model performance.

2.2.6 Hybrid Random Forest Model for SPEI Forecasting

The study by Mehr et al. (2022) introduced a hybrid model combining Random Forest with Genetic Algorithms to enhance the accuracy of SPEI forecasting. Conducted at two meteorology stations in Ankara, Turkey, the research compared the performance of Genetic Algorithms against traditional Random Forest and other machine learning models like (Bat-)Extreme Learning Machine.

The results demonstrated that Genetic Algorithms outperformed other models, achieving up to 40% improvement in forecasting accuracy for SPEI with a 3- and 6-month scale. This study highlights the potential of integrating Genetic Algorithms with machine learning models to predict drought indices with higher precision.

2.2.7 Drought Forecast in the Guanzhong Area, China

Another study focused on the Guanzhong Area of China (Li et al., 2020), where researchers combined meteorological data with remote sensing products such as NDVI (Normalized Difference Vegetation Index), LTD (Land Temperature Daytime), and LTN (Land Temperature Nighttime) to predict the SPEI of a 1-month scale. The remote sensing data has been captured by PERSIANN-CRD and MODIS satellites. The researchers modified the Penman-Monteith model by integrating leaf area index (LAI) and albedo data (fraction of light that is reflected) derived from remote sensing

Li et al. (2020) compared 19 different machine learning models in total. Using a Random Forest model and remote sensing data the model predicted more accurate results than using meteorological data. Aswell the study also found out that applying a combination of remote sensing and meteorological data on a SVM model leads to a more accurate forecast model performance than using meteorological or remote sensing data only.

2.2.8 Hybrid ARIMA-LSTM model for SPEI forecasting

Xu et al. (2022) forecast the SPEI in China using six drought forecast models, namely, ARIMA, support vector regression (SVR), LSTM, ARIMA-SVR, least square-SVR (LS-SVR), and ARIMA-LSTM for the predicting of the SPEI. When comparing the results using the Nash-Sutcliffe efficiency (NSE) the results show that all three hybrid models (ARIMA-SVR, LS-SVR, and ARIMA-LSTM) had higher prediction accuracy than the single model, for a given lead time, at different scales.

The NSEs of the hybrid models for the predicted SPEI1 are 0.043, 0.168, and 0.368 (ARIMA-SVR, LS-SVR, ARIMA-LSTM) and the NSEs of SPEI24 are 0.781, 0.543, and 0.93 (ARIMA-SVR, LS-SVR, ARIMA-LSTM). Overall the hybrid models achieved higher accuracies for longer forecast periods and lower accuracies for shorter forecast periods. Expect the accuracy for the 1-month SPEI which is higher than for the 2-month SPEI.

2.2.9 SPEI Forecasting using an Informer Model

This paper by Shang et al. (2023) summarizes the application of the Informer model for Standardized Precipitation Evapotranspiration Index (SPEI) forecasting. The study compares the Informer model's performance against ARIMA and LSTM across multiple timescales.

The results demonstrate a high forecast accuracy, particularly for long-term forecasts. Data from the Yellow River Basin is utilized and the performance of the Informer model is compared with ARIMA and LSTM models on multiple timescales, including 1-, 3-, 6-, and 24-month periods. The Informer model demonstrated superior performance across all timescales. On the 24-month timescale, it achieved Nash-Sutcliffe Efficiency (NSE) values of 0.968, 0.974, 0.972, and 0.986 for four meteorological stations. These values indicate a high level of precision in forecasting the SPEI.

3 Methods

A detailed explanation of how the research was conducted and what materials (data, software, ...) were used during the process of this thesis to prove the hypotheses (List 4) and fulfill the requirements (Section 4.1).

3.1 Satellite Data Hub

Remote sensing images can be used to calculate drought indices, which is why the planned procedure had been to build a satellite image datahub that calculates files and images showing drought indices.

Since Python is a common programming language in the geospatial industry and the support for extensions is large (Robinson et al., 2024) the choice had been made to build a web application using a Python framework. This has the advantage of creating a web application where the backend can be executed directly on the same host where the front end is hosted. No file transferring, remote procedure, API calls, or similar will be needed.

One of the most popular web frameworks in Python is Django (CoMelissant, 2024) which had been used for the satellite data hub. Using a popular web framework can give the advantage of a large community that has already posted solutions to known or common problems in online forums.

For the database a PostGIS database was used which extends the capabilities of the PostgreSQL relational database by adding support for storing, indexing, and querying geospatial data (PostGIS PSC/OSGeo, 2023). This has the advantage that third-party software like QGIS (QGIS, 2024) can access the database and work with the files and information.

Out of this planning the Drought Early Warning Systems's DataHub (*short: DEWS DH*) (Tran, 2024a) had been made to import satellite data images from archives downloaded from e.g. Copernicus Browser (Copernicus, 2024a) or to request satellite data images from the Sentinel Hub API (Sinergise Solutions d.o.o., 2024). The main goal had been to have a structured overview of the satellite data where time-related or location-related files are found as well as a database to connect with other software (*e.g. QGIS*).

The screenshot displays the DEWS DH interface. At the top left is the DEWS logo. Navigation links for 'Dashboard' and 'Sat Data' are visible, along with 'Admin' and 'Logout' buttons. The main heading is 'SatData: 'Sentinel Hub Request 010cae35-e6c9-49ec-a05d-5fe961f9e9ec''. Below this is a 'Back to overview' button. The 'SatData Details' section is divided into two columns. The left column contains metadata: ID (010cae35-e6c9-49ec-a05d-5fe961f9e9ec), Name (Sentinel Hub Request 010cae35-e6c9-49ec-a05d-5fe961f9e9ec), User (dews), Mission (Sentinel-2b), Product Type (UNKNOWN), Time Travel (with a link to TimeTravel<b99aa176-0f06-41db-963e-1dca877ebb43>), Creation Time (April 17, 2024, 6:46 a.m.), and Processing Status (Done). The right column features a 'Thumbnail' of a satellite image with a download icon, and a 'Map' showing the location near Uhlenhorst with a blue bounding box and a 500m scale bar. At the bottom, the 'Extracted Path' is shown as /dews/media/sentinel_hub/99956c171c2e4b4e81c7db695878e782, with a 'Delete' button.

Figure 3.1: DEWS DH's satellite data details page whose images were taken on the 17th of April 2024 from a region near Uhlenhorst (Schwarzenbek) in Germany. The information had been received by a request to the Sentinel Hub API.

Users of the DEWS DH get their user account to store, delete, and modify their own uploaded and requested satellite data. When uploading an already locally existing satellite data archive or requesting satellite data from the Sentinel Hub API via the web application, the DEWS DH processes the information in the background.

The following information and more will be automatically extracted after the upload/request process:

- Satellite mission
- Product type
- Product start/stop time
- etc.

By looking into the often included description files this information will be filled into a satellite data object. Users can look at a details page to find the information they need. On this page, the user can modify or remove the satellite data and see other satellite data entries that have the same location but different capture times (*see Figure 3.1*).



(a) A RGB image of a region near Uhlenhorst (Schwarzenbek) in Germany from the 17th April 2024. The bands 2, 3, and 4 had been used to calculate and generate the RGB image using the DEWS DH. (b) A NDVI image of a region near Uhlenhorst (Schwarzenbek) in Germany from the 17th April 2024. Bands 4 and 8 were used to calculate and generate the NDVI image using the DEWS DH.

Figure 3.2: Comparison of RGB and NDVI images of a region near Uhlenhorst (Schwarzenbek) in Germany from the 17th April 2024.

The most time-consuming part of the upload/request process is the calculation of the indices. When uploading an archive depending on the available bands all possible indices will be calculated. On the other hand, when requesting satellite data via the Sentinel Hub API the user can choose which bands are needed and which indices should be calculated. For example the NDVI is calculated by using the bands of near-infrared (*band 8*) and red (*band 4*) or a RGB image is calculated by using the bands blue (*band 2*), green (*band 3*) and red (*band 4*)(see *Figure 3.2*).

This indices calculation and image generation process is time-consuming because TIFF files, especially those containing high-resolution satellite imagery, can be very large. Loading these files into memory takes significant time and resources. After the loading mathematical operations need to be executed for each pixel of the image, which can be computationally intensive as well.

3.1.1 DEWS' Data Collection

All satellite data of the types Sentinel-1A, -1B, -2A, -2B, -3A and -3B are supported. They can be downloaded on the user's local device via the Copernicus Browser (Copernicus, 2024a) or the Sentinel Hub API request option in the DEWS DH web application.

A detailed overview of which satellite data sources are supported can be found in the GitHub repository's README.md file (Tran, 2024a).

3.1.2 Application of DEWS DH

For further research, the DEWS DH should have been used to generate drought indices like the NDVI, SPEI, SMI, etc. With this data predictions should be made to predict drought conditions. The GIDMaPS by Hao et al. (2014), which has already predicted several major droughts like the 2010 Amazon Basin drought, has been an inspiration for the implementation of this system. The planned pipeline of the process for storing, calculating indices, and detecting droughts using satellite images is shown in *Figure 3.3*.

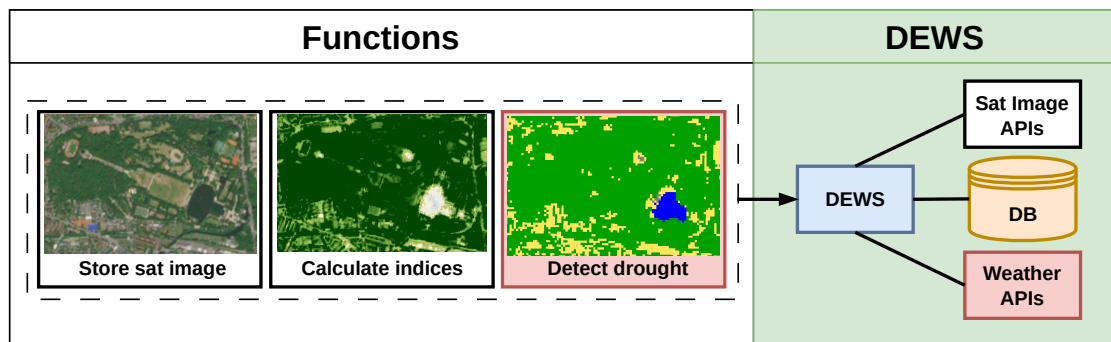


Figure 3.3: Planned pipeline of the process for storing, calculating indices, and detecting droughts using satellite images. Planned additions in light red. Existing features in other colors.

A downside for the usage of the DEWS DH for this purpose is that a large number of satellite images are required, which would have spanned several decades, to make reliable predictions. Likewise, satellite images consume a large amount of disk space, so the further development of the DEWS DH has been discontinued.

Another argument against the use of the DEWS DH in this context is that compressed drought index datasets like the SPEIbase by Vicente-Serrano et al. (2010) already exist which will be used as a comparison dataset for the evaluation of this thesis' results.

3.2 Selection of the Drought Index

The SPEI (Standardized Precipitation Evapotranspiration Index) is chosen as the drought index for this study due to its widespread adoption and proven efficacy in drought analysis across various geographical regions. Its capability to consider both precipitation and evapotranspiration makes it a comprehensive tool for assessing drought conditions. Additionally, the SPEI indicates whether an area is dry or wet. Numerous related works, such as those by Dukat et al. (2022), Dikshit et al. (2022), Mehr et al. (2022), and Li et al. (2020), have demonstrated the effectiveness of SPEI in accurately identifying drought periods. These studies highlight SPEI's reliability in capturing the temporal and spatial variability of drought, making it a robust index for drought monitoring and prediction. The integration of SPEI into this research is further justified by its ability to be tailored to different timescales, allowing for the analysis of short-term to long-term drought impacts.

3.3 Selection of the PET equations

Thornwaite PET equation by Charles W. Thornthwaite (Thornthwaite, 1948) is used for the SPEI Global Drought Monitor (Vicente-Serrano et al., 2024), which had been created by the inventors of the SPEI, Vicente-Serrano et al. (2010), and the equation requires the fewest datasets out of all found PET equations.

The second PET equation is the FAO-56 Penman-Monteith (Allen, 1998) PET equation because the inventors of the SPEI (Vicente-Serrano et al., 2010) created an official SPEI dataset called SPEIbase (Beguería, 2010), which uses the FAO-56 Penman-Monteith method as Vicente-Serrano et al. (2010) say: "*The Penman-Monteith method is considered a superior method [...].*".

Likewise, the Priestley-Taylor (Priestley and Taylor, 1972) and Hargreaves (Hargreaves and Allen, 2003) were found during the research and they were added for comparison.

3.4 Data Collection

Based on hypothesis number three (see List 4) weather station and remote sensing data are needed for the experiment of this thesis. Since most remote sensing datasets are

already a combination of multiple data sources, care had to be taken to ensure that the remote sensing dataset to be used meets this requirement. Another requirement was that the datasets had their values monthly averaged and that they should at least contain the region of Germany in the range of the latitude bound from 47.0 to 55.0 and the longitude bound from 5.5 to 15.0.

Due to the use of the Thornwaite PET equation by Charles W. Thornthwaite, the following datasets were needed:

- T_{mean} : Mean temperature at 2m height ($^{\circ}C$)
- P : Precipitation sum (m)

The FAO-56 Penman-Monteith equation Allen (1998) needs the following parameters:

- Δ_v : Slope of saturation vapor pressure curve at air temperature ($Pa K^{-1}$)
- R_n : Net irradiance ($MJ/m^{-2}/day^{-1}$)
- G : Ground heat flux ($MJ/m^{-2}/day^{-1}$)
- T_{mean} : Mean temperature at 2m height (K)
- u_2 : Wind speed at 2m height (m/s)
- δe : Vapor pressure deficit (kPa)

Since the Priestley-Taylor and Hargreaves PET equations are also to be tested and compared with all PET equations, further additional features were consulted:

- T_{min} : Minimum temperature at 2m height (K)
- T_{max} : Maximum temperature at 2m height (K)

For the temperature data, the unit doesn't need to be $^{\circ}C$ or K because the values can be converted in the other unit and vice versa.

3.4.1 Weather Station Data

The German Weather Service's (DWD) weather stations data from the Climate Data Center (Deutscher Wetterdienst, 2024a) by the DWD is the most suitable because the area under investigation is Germany, the DWD is a higher federal authority within the portfolio of the Federal Ministry for Digital, the values are monthly averaged and the datasets are publicly available.

In minute, hourly, daily, monthly, and annual intervals the values of air pressure, air temperature, wind velocity, and many more are measured. For example, for precipitation around 2000 currently activated stations are available. Measuring the air temperature happens in the around 400 climate stations that are currently active. Many more stations and values are supported which can be read about in the CDC's README file (Deutscher Wetterdienst, 2020).

For the chosen PET equations Thornthwaite, FAO-56 Penman-Monteith, Priestley-Taylor, and Hargreaves the following monthly datasets were downloaded:

- Mean, min. and max. Temperature ($^{\circ}C$)
- Total Precipitation (m)
- Global Radiation ($MJ/m^{-2}/day^{-1}$)

Datasets that are needed but were not found at the CDC (e.g. net irradiance) had to be calculated or estimated using formulae (see Section 4.2).

3.4.2 Remote Sensing Data

Monthly averaged ERA5-Land Reanalysis (Hersbach et al., 2020) data served as the primary source for remote sensing data because it met the requirement that it is a combination of remote sensing, weather station, aircraft data, etc. This dataset included several crucial meteorological and surface variables necessary for drought prediction. The data encompassed the following monthly datasets:

- u_{10} : 10m u-component of wind (m/s), which represents the eastward wind component (west to east) at a 10-meter height. It helps understanding wind patterns and their effects on evapotranspiration and moisture transport.

- v_{10} : 10m v-component of wind (m/s), which represents the northward wind component (south to north) at a 10-meter height. Similar to u_{10} , it helps in analyzing wind patterns and their impact on moisture dynamics.
- lai_{lv} : Leaf area index (low vegetation) (m^2/m^2), which represents the leaf area per unit ground area for low-lying vegetation.
- lai_{hv} : Leaf area index (high vegetation) (m^2/m^2), which represents the leaf area per unit ground area for taller vegetation such as trees.
- t_{2m} : Temperature at 2m height (K), a key variable influencing evapotranspiration rates and energy balance in the surface-atmosphere interface.
- pev : Potential evaporation (m), which measures the amount of evaporation that would occur if sufficient water were available. It reflects atmospheric demand for moisture and influences drought conditions.
- ssr : Surface net solar radiation (J/m^2), indicating the total solar energy received by the surface, impacting surface heating and evaporation processes.
- str : Surface net thermal radiation (J/m^2), referring to the balance of thermal energy at the surface, affecting the energy available for evapotranspiration.
- tp : Total precipitation (m), which measures the amount of rainfall, a primary input for assessing water availability and drought conditions.

The downloaded datasets are netCDF files (.nc) containing the mentioned parameters, which are used for calculating the SPEI. Also some parameters like the lai_{lv} or lai_{hv} are used to calculate parameters needed for the PET equations.

3.4.3 Soil Moisture Index (SMI)

The Soil Moisture Index (SMI) (Samaniego et al., 2013) is used by the German Drought Monitor (Helmholtz Zentrum für Umweltforschung, 2024) and it is a drought index, too. The higher the correlation coefficient, the stronger the correlation is and the more likely it is to show that the results of the SPEI reflect the SMI and thus enable the correct identification of droughts and wets. The correlation between the SPEI and SMI can be used as an evaluation metric for the following reasons:

- **Incorporation of Evapotranspiration:** Both SMI and SPEI consider the effects of evapotranspiration. While SPEI explicitly includes it in its calculation, SMI indirectly reflects evapotranspiration through its impact on soil moisture levels (Hunt et al., 2009)(Vicente-Serrano et al., 2010).
- **Standardization:** Both indices are standardized, meaning they provide comparable values across different climatic regions and time scales (Hunt et al., 2009)(Vicente-Serrano et al., 2010).
- **Sensitivity to Climatic Variability:** SMI, like SPEI, is sensitive to changes in climatic variables, making it suitable for monitoring and comparing the impacts of climate variability and change on moisture status (Hunt et al., 2009)(Vicente-Serrano et al., 2010).
- **Drought Indices:** Both indices are considered to detect drought periods (Helmholtz Zentrum für Umweltforschung, 2024)(Vicente-Serrano et al., 2010).

The datasets from Helmholtz Zentrum für Umweltforschung (2024) contain the upper soil SMI which represents the SMI up to 25cm deep and the total soil SMI which represents the SMI up to 180cm deep. Also, the SMI is used as an evaluation metric for the SPEI calculation to check whether a correlation exists or not.

3.5 Data Preprocessing

This section describes how the weather station and remote sensing data have been pre-processed by their provider. The data is free and publicly available for download on the specific website.

3.5.1 Weather Station Data

The German Weather Service (DWD) operates a comprehensive data processing system to handle weather station data from around the world. This system ensures the efficient and secure transport, storage, and processing of large volumes of meteorological data.

The data flow within DWD involves several stages from the reception of raw data to the final product distribution:

1. **Data Reception:** Weather data (e.g., temperature, wind speed, satellite images) is continuously received by the Deutsche Meteorologische Rechenzentrum (DMRZ) from various sources worldwide, including ground stations, ships, and aircraft (Deutscher Wetterdienst, 2024f)(Deutscher Wetterdienst, 2024b).
2. **Decoding:** The received data is in standardized formats known as weather codes. These codes are decoded by specialized programs to convert them into formats suitable for further processing (Deutscher Wetterdienst, 2024h).
3. **Data Storage:** The decoded data is stored in central data storage systems. The relational climate database, a subset of the main data storage, allows for extensive querying and serves as the basis for climatological analyses (Deutscher Wetterdienst, 2024e).
4. **Product Creation and Distribution:** Forecast fields and other meteorological data are processed to create various products for different users. These products are distributed through multiple channels such as FTP (Deutscher Wetterdienst, 2024g).
5. **Archiving:** Data is periodically archived in a tape library system. While forecast data has a limited archival period, observational data and analyses are stored permanently (Deutscher Wetterdienst, 2024e).

3.5.2 Remote Sensing Data

Once acquired, the ERA5-Land data (Muñoz Sabater et al., 2021) undergoes several preprocessing steps to prepare it for analysis and usage:

- **In-situ Measurement:** The ERA5-Land reanalysis is based on a variety of observational data sources, including satellite remote sensing, in-situ measurements, and ground-based observations. Key satellite missions that contribute to ERA5-Land include the satellite missions Modis, Sentinel-1/2, and more.
- **Data Assimilation:** A data assimilation system is used to integrate the diverse observational data into a consistent global model. The system, known as the Integrated Forecasting System (IFS), operates sequentially, continuously updating the model state with the latest available observations. This process helps to correct the model's trajectory and ensures that the reanalysis output is as close as possible

to the observed state of the Earth system at each time step (European Centre for Medium-Range Weather Forecasts, 2023b).

- **Land Surface Model:** ERA5-Land employs a specialized land surface model within the IFS framework. This model, known as HTESSEL (Hydrology Tiled ECMWF Scheme for Surface Exchanges over Land), simulates various land surface processes, including soil moisture dynamics, snow cover, vegetation growth, and energy fluxes between the land surface and the atmosphere. HTESSEL's high-resolution grid ($0.1^\circ \times 0.1^\circ$) allows for detailed representation of surface heterogeneity and local land-atmosphere interactions (Balsamo et al., 2009).
- **Reanalysis Production:** Data assimilation is performed for each time step, generating global fields of land surface variables. These fields are then archived and made available in standardized formats, such as GRIB (General Regularly-distributed Information in Binary) and NetCDF (Network Common Data Form). The output data includes variables such as soil moisture, land surface temperature, snow depth, and evapotranspiration.
- **Quality Control and Validation:** After the reanalysis data is produced, it undergoes rigorous quality control and validation procedures. This includes comparisons with independent observations, inter-comparisons with other reanalysis datasets, and consistency checks over time and space. These procedures ensure the reliability and accuracy of the ERA5-Land dataset for scientific research and operational use (European Centre for Medium-Range Weather Forecasts, 2024).

3.6 Calculations

This section is about how the PET, water balance (difference), SPEI, and correlation with the SMI are calculated in general.

3.6.1 Potential Evapotranspiration (PET)

The Potential Evapotranspiration (PET), which is the amount of water that would evaporate and transpire from a given area if sufficient water were available, can be calculated using one of the following PET equations.

Thornthwaite's PET Equation

Thornthwaite's equation, introduced by Charles Warren Thornthwaite (1948), is used for estimating the potential evapotranspiration (PET). It requires the mean monthly temperature in degrees Celsius (T), the average day length in hours for the month (L), the number of days in the month (N), and the heat index (I) which depends on the 12 monthly mean temperatures. Thornthwaite's approach allowed for more accessible and widespread application, making it particularly useful for regions with limited meteorological data (Thornthwaite, 1948).

The general form of the Thornthwaite equation is:

$$PET = 16 \left(\frac{L}{12} \right) \cdot \left(\frac{N}{30} \right) \cdot \left(\frac{10 \cdot T_d}{I} \right)^\alpha$$

where:

- PET is the potential evapotranspiration in millimeters per month,
- T_m is the mean monthly temperature in degrees Celsius,
- L is the average day length in hours for the month,
- N is the number of days in the month,
- I is a heat index that depends on the annual mean temperature, and
- a is an empirically derived exponent that is a function of I .

The heat index I is calculated as the sum of the 12 previous monthly indices, each derived from the mean monthly temperature:

$$I = \sum_{i=1}^{12} \left(\frac{T_i}{5} \right)^{1.514}$$

where T_i is the mean monthly temperature for month i .

The exponent a is an empirically derived exponent, which is computed using the heat index I :

$$a = 6.75 \times 10^{-7} I^3 - 7.71 \times 10^{-5} I^2 + 1.792 \times 10^{-2} I + 0.49239$$

In regions where only temperature data are available the Thornthwaite equation is primarily used. However, it has limitations, particularly in its assumption that temperature alone can adequately represent all the factors affecting evapotranspiration. The Thornthwaite equation tends to be less accurate in arid and tropical regions where factors like humidity, wind speed, and solar radiation play significant roles (Aschonitis et al., 2022).

FAO-56 Penman-Monteith's PET Equation

A total of 13 parameters is required by the original Penman-Monteith equation. To simplify this equation, the Food and Agriculture Organization (FAO) proposed the FAO-56 Penman-Monteith equation in 1998 (Allen, 1998). This simplified version reduces the number of required parameters from 13 to 8, making it more practical for various applications. The general form of the FAO-56 Penman-Monteith equation is:

$$ET_o = \frac{0.408 \cdot \Delta \cdot (R_n - G) + \frac{900}{T} \cdot \gamma \cdot u_2 \cdot \delta e}{\Delta + \gamma(1 + 0.34 \cdot u_2)}$$

where:

1. Δ_v is the slope of saturation vapor pressure curve at air temperature ($PA K^{-1}$)
2. R_n is the net irradiance ($MJ/m^{-2}/day^{-1}$),
3. G is the ground heat flux ($MJ/m^{-2}/day^{-1}$),
4. T is the air temperature at 2m height (K),
5. u_2 is the wind speed at 2m height (m/s),
6. δe is the vapor pressure deficit (kPa), and
7. γ is the psychrometric constant ($\gamma \simeq 66 Pa K^{-1}$).

The FAO-56 Penman-Monteith equation is widely used because it provides a reliable estimate of PET by incorporating critical meteorological factors. This equation is particularly beneficial for agricultural planning, irrigation management, and hydrological studies. For example, the founders of the SPEI (Vicente-Serrano et al., 2010) use the FAO 56 Penman-Monteith equation for the estimation of the PET since SPEIbase's version 2.0 (Beguería, 2010).

Priestley-Taylor's PET Equation

Priestley-Taylor's equation to estimate the PET relies on empirical results and is even simpler than the FAO 56 Penman-Monteith equation because it requires fewer data inputs, primarily solar radiation, and temperature. The general form of the Priestley-Taylor equation is:

$$ET_0 = \alpha \cdot (R_n - G) \cdot \frac{\Delta}{\Delta + \gamma}$$

where:

1. α is the empirical coefficient,
2. Δ is the slope of the saturation vapor pressure curve at air temperature,
3. γ is the psychrometric constant ($\gamma \simeq 66 \text{ Pa K}^{-1}$),
4. R_n is the net irradiance ($\text{MJ/m}^{-2}/\text{day}^{-1}$), and
5. G is the ground heat flux ($\text{MJ/m}^{-2}/\text{day}^{-1}$).

The Priestley-Taylor PET equation (Priestley and Taylor, 1972) works by combining energy available for evaporation (given by net radiation R_n) with the capacity of the air to hold water vapor (influenced by the current temperature through Δ) and the properties of the air (via γ). The empirical coefficient α is used to adjust the ratio between the energy term and the vapor pressure term, accounting for the fact that not all available energy is used for evapotranspiration due to factors like surface resistance. The value $\alpha = 1.26$ is suggested by Priestley and Taylor for the estimation which corresponds to a saturated surface, or wet conditions. Specifically, lower values of the dryness coefficient should be used in humid regions while higher values should be used in arid regions (Priestley and Taylor, 1972).

Hargreaves' PET Equation

The Hargreaves PET equation (Hargreaves and Allen, 2003) is a simplified method for estimating potential evapotranspiration (PET) and is particularly useful in areas where limited meteorological data are available. The equation is expressed as:

$$ET_0 = 0.0023 \cdot R_A \cdot (T_{max} - T_{min})^{0.5} \cdot (T_{mean} + 17.8)$$

where:

1. R_A is the mean monthly extra-terrestrial radiation ($MJ m^{-2} day^{-1}$), which is a function of latitude and day of the year.
2. T_{max} is the maximum daily air temperature ($^{\circ}C$).
3. T_{min} is the minimum daily air temperature ($^{\circ}C$).
4. T_{mean} is the mean daily air temperature ($^{\circ}C$).

The Hargreaves equation has an advantage over the FAO-56 Penman-Monteith equation in that it requires less data, relying primarily on temperature and radiation data, which are often more available than other meteorological variables. This makes it particularly useful for preliminary assessments and in regions where data collection infrastructure is limited.

On the other hand, it is less accurate and reliable than the FAO-56 Penman-Monteith equation, especially in varying climatic conditions, as it primarily relies on temperature data alone (Ndulue and Ranjan, 2021).

3.6.2 Difference

The first step in calculating the SPEI is to compute the difference (D) between precipitation (P) and potential evapotranspiration (PET). This difference (D) is calculated as follows:

$$D = P - PET$$

The difference (D) represents the water balance and the sign indicates whether there is a surplus (wet)(positive value) or deficit of water (dry)(negative value).

3.6.3 SPEI

The difference (D) will be fitted to the log-logistic distribution. The log-logistic distribution is chosen because it can effectively model the skewed nature of hydro-meteorological variables and it is used by Vicente-Serrano et al. (2010) as well. The probability density function (PDF) of the log-logistic distribution is given by:

$$f(x; \alpha, \beta) = \frac{(\beta/\alpha)(x/\alpha)^{\beta-1}}{(1 + (x/\alpha)^\beta)^2}$$

where α and β are the scale and shape parameters, respectively.

The fitted parameters are used to compute the cumulative distribution function (CDF). The CDF represents the probability that a random variable takes a value less than or equal to a particular value. The CDF values are then converted to z-scores using the inverse standard normal distribution. Z-scores indicate how many standard deviations an element is from the mean of the distribution:

$$z = \Phi^{-1}(CDF)$$

where Φ^{-1} is the inverse of the standard normal CDF . The z-scores indicate how many standard deviations the observed D is from the mean of the distribution. They represent the desired SPEI values as well.

3.6.4 Correlation

To identify if a correlation between two variables exists the Pearson and distance correlation coefficient are used.

Pearson Correlation Coefficient

The Pearson correlation coefficient is a statistical measure used to quantify the strength and direction of the linear relationship between two continuous variables (Blyth, 1994). The Pearson correlation coefficient, denoted as r , ranges from -1 to 1, where:

- $r = 1$ implies a perfect positive linear relationship,
- $r = -1$ implies a perfect negative linear relationship, and

- $r = 0$ implies no linear relationship.

Mathematically, the Pearson correlation coefficient between two variables X and Y is calculated using the formula:

$$r = \frac{\sum_{i=1}^n (X_i - \bar{X})(Y_i - \bar{Y})}{\sqrt{\sum_{i=1}^n (X_i - \bar{X})^2} \sqrt{\sum_{i=1}^n (Y_i - \bar{Y})^2}}$$

Here, X_i and Y_i are the individual data points, \bar{X} and \bar{Y} are the mean values of X and Y , respectively, and n is the number of data points. The numerator of the formula represents the covariance between X and Y , while the denominator is the product of their standard deviations. This normalization by the standard deviations ensures that the coefficient is dimensionless and lies within the range of -1 to 1.

Distance Correlation

Distance correlation by Székely et al. (2007) is a measure of dependence between two random variables or two sets of random variables. Unlike Pearson's correlation coefficient, which only captures linear relationships, distance correlation can detect both linear and non-linear associations between variables.

The distance correlation between two random vectors X and Y in \mathbb{R}^p and \mathbb{R}^q , respectively, is defined based on the idea of distance covariance. The distance covariance is a measure of the joint variability of two random vectors based on the distances between pairs of observations. For two independent random vectors, the distance covariance is zero, but the converse is not necessarily true.

To compute the distance correlation, we first calculate the pairwise Euclidean distances among all observations in both random vectors X and Y . We then center these distances by subtracting the mean of the corresponding row and column and adding the overall mean. The centered distance matrices for X and Y are then used to calculate the distance covariance. The distance correlation is obtained by normalizing the distance covariance by the square root of the product of the distance variances of X and Y .

Formally, the distance covariance between X and Y is given by:

$$\text{dCov}^2(X, Y) = \frac{1}{n^2} \sum_{i,j=1}^n A_{ij} B_{ij},$$

where A_{ij} and B_{ij} are the elements of the centered distance matrices for X and Y , respectively. The distance variance is computed similarly as:

$$\text{dVar}^2(X) = \frac{1}{n^2} \sum_{i,j=1}^n A_{ij}^2,$$

and the distance correlation is:

$$\text{dCor}(X, Y) = \frac{\text{dCov}(X, Y)}{\sqrt{\text{dVar}(X) \cdot \text{dVar}(Y)}}.$$

Distance correlation ranges from 0 to 1, where 0 indicates no dependence and 1 indicates complete dependence.

Line of best fit

For the Pearson and distance correlation the line of best fit, or linear regression line, can be used to visualize the correlation. It represents the relationship between two variables with a straight line. It is used when the relationship is linear, meaning changes in one variable correspond proportionally to changes in another. The formula for the line of best fit is $y = mx + b$, where m is the slope (indicating the rate of change) and b is the y-intercept (the value of y when $x = 0$). This line minimizes the sum of the squared differences between the observed data points and the line, providing the best linear approximation of the relationship. The experiments it is intended to find out whether there is a linear relationship between SPEI and SMI and, if not, whether it is possibly non-linear. The non-linear relationship can be determined using the following polynomial fit.

Polynomial fit

Likewise, the polynomial fit can be used for both correlation coefficients. A polynomial fit models the relationship between two variables using a polynomial equation, which can capture non-linear patterns. A degree 2 polynomial fit, or quadratic fit, is described by the equation $y = ax^2 + bx + c$, where a , b , and c are coefficients. The term ax^2 introduces curvature, allowing the fit to model parabolic relationships where changes in y are not constant concerning changes in x . This method is useful when the data shows a curved

trend that a straight line cannot accurately represent which could be the case for SPEI and SMI.

3.7 Prediction

This section is about how the selected prediction method of wet and dry works.

3.7.1 Gradient Boosting Regressor

The Gradient Boosting Regressor (GBR) is a machine learning algorithm designed for regression tasks (Prettenhofer and Louppe, 2014).

The GBR works by building an ensemble of weak prediction models, typically decision trees, in a sequential manner. Each new model attempts to correct the errors made by the previous models. The process begins with the initialization of a simple model, often a decision tree with limited depth, which makes an initial prediction.

Subsequent models are trained on the residual errors of the combined ensemble of previous models. This iterative process continues, with each new model focusing on the errors made by the ensemble so far. By iteratively reducing the residual errors, the Gradient Boosting algorithm minimizes the overall prediction error.

Mathematically, at each step m , a new model $h_m(x)$ is added to the existing ensemble $F_{m-1}(x)$ to produce an updated ensemble $F_m(x)$. The new model is chosen to minimize a specific loss function $L(y, F_{m-1}(x) + h_m(x))$, where y represents the true values and x represents the input features. The ensemble model is updated as follows:

$$F_m(x) = F_{m-1}(x) + \nu \cdot h_m(x)$$

Here, ν is a learning rate parameter that controls the contribution of each new model.

This boosting approach leads to a predictive model that provides accurate results compared to single models, especially in cases where the relationship between features and the target variable is complex and nonlinear.

3.7.2 XGBoost

XGBoost (eXtreme Gradient Boosting) is an optimized distributed gradient boosting library designed to be highly efficient, flexible, and portable. It implements machine learning algorithms under the Gradient Boosting framework (Chen and Guestrin, 2016).

XGBoost builds an additive model in a forward stage-wise manner. Let the dataset be $\{(x_i, y_i)\}_{i=1}^n$, where x_i are the features and y_i are the target values. The model at stage t can be expressed as:

$$\hat{y}_i^{(t)} = \sum_{k=1}^t f_k(x_i), \quad (3.1)$$

where f_k is a function from the function space \mathcal{F} . Typically, \mathcal{F} consists of regression trees (Chen and Guestrin, 2016).

The objective function to be minimized is defined as:

$$\mathcal{L}^{(t)} = \sum_{i=1}^n l(y_i, \hat{y}_i^{(t)}) + \sum_{k=1}^t \Omega(f_k), \quad (3.2)$$

where l is a differentiable convex loss function that measures the difference between the prediction \hat{y}_i and the target y_i , and Ω is a regularization term that penalizes the complexity of the model:

$$\Omega(f) = \gamma T + \frac{1}{2} \lambda \sum_{j=1}^T w_j^2, \quad (3.3)$$

with T being the number of leaves in the tree, w_j the score on each leaf, γ and λ are regularization parameters (Chen and Guestrin, 2016).

XGBoost incorporates several advanced features that enhance its performance and scalability (Chen and Guestrin, 2016):

- **Regularization:** To prevent overfitting, XGBoost includes $L1$ (Lasso) and $L2$ (Ridge) regularization terms.

- **Parallelization:** It exploits the sparsity of the input data and supports parallel tree construction, leading to faster computation.
- **Handling Missing Values:** XGBoost handles missing values internally by learning which path to take in a tree based on the presence of a missing value.
- **Tree Pruning:** The algorithm uses a depth-first approach for tree pruning, avoiding the creation of branches that do not reduce the loss function.
- **Column Block:** For better cache performance, XGBoost stores the data in a compressed column block format.

3.7.3 Prophet

Prophet is a forecasting procedure implemented in R and Python, developed by Meta's Core Data Science team. It is designed to handle time series data that may have missing values and shifts in the trend, also it is robust to outliers. Prophet provides a straightforward and flexible framework that allows users to make accurate forecasts without extensive knowledge of time series models (Taylor and Letham, 2018).

The Prophet model decomposes a time series $y(t)$ into three main components: trend $g(t)$, seasonality $s(t)$, and holidays $h(t)$:

$$y(t) = g(t) + s(t) + h(t) + \epsilon_t, \quad (3.4)$$

where ϵ_t represents the error term that captures any residual variability not explained by the model.

The trend component $g(t)$ models non-periodic changes in the value of the time series. Prophet supports two types of trend models:

- **Piecewise Linear Trend:** Suitable for time series with sharp changes.
- **Logistic Growth Trend:** Suitable for time series that saturate at a certain level.

For this study, the piecewise linear trend is used with which the model is defined as:

$$g(t) = (k + a(t)^\top \delta)t + (m + a(t)^\top \gamma), \quad (3.5)$$

where k is the growth rate, m is the offset parameter, $a(t)$ is an indicator function representing trend change points, and δ and γ are rate and offset adjustments at change points.

The seasonality component $s(t)$ captures periodic changes. Prophet models seasonality using a Fourier series:

$$s(t) = \sum_{n=1}^N \left[a_n \cos\left(\frac{2\pi nt}{P}\right) + b_n \sin\left(\frac{2\pi nt}{P}\right) \right], \quad (3.6)$$

where P is the period of the seasonality (e.g., 365.25 for yearly seasonality), and N determines the number of Fourier terms.

Prophet includes several key features that make it a robust and flexible forecasting tool:

- **Automatic Change Point Detection:** Prophet automatically detects points in the time series where the trend changes significantly.
- **Flexible Seasonality:** Users can specify multiple seasonalities of different periods (e.g. daily, weekly, yearly).
- **Holiday Effects:** Custom holiday effects can be included in the model, which we do not do in this study.
- **Handling Missing Data and Outliers:** Prophet is robust to missing data and outliers, making it suitable for real-world applications.

3.7.4 SARIMA

The SARIMA model (Seasonal Autoregressive Integrated Moving Average), denoted as $\text{SARIMA}(p,d,q)(P,D,Q)_s$, is an extension of the ARIMA (Autoregressive Integrated Moving Average) model designed to handle seasonal effects in time series data. The model includes parameters for both non-seasonal and seasonal components, making it suitable for time series with repeating patterns or seasonal cycles (Dabral and Murry, 2017).

The SARIMA model is denoted as $\text{SARIMA}(p,d,q)(P,D,Q)_s$ where:

- **p:** Non-seasonal autoregressive order which is the number of lag observations. In this thesis' case, it is the previous month's SPEI values.

- **d**: Non-seasonal differencing order which is the number of times a raw observation is differenced.
- **q**: Non-seasonal moving average order which is the size of the moving average window.
- **P**: Seasonal autoregressive order which is the same as p but for seasonal periods.
- **D**: Seasonal differencing order which is the same as d but for seasonal periods.
- **Q**: Seasonal moving average order which is the same as q but for seasonal periods.
- **s**: Length of the seasonal cycle which is the number of observations per cycle (e.g., 12 for monthly data with annual seasonality).

The SARIMA model incorporates both non-seasonal and seasonal components into the ARIMA framework. The general form of the SARIMA model can be expressed as:

$$\Phi_P(B^s)\phi_p(B)(1-B)^d(1-B^s)^D y_t = \Theta_Q(B^s)\theta_q(B)\epsilon_t, \quad (3.7)$$

where:

- $\phi_p(B)$ and $\Phi_P(B^s)$ are the non-seasonal and seasonal autoregressive polynomials of orders p and P respectively.
- $\theta_q(B)$ and $\Theta_Q(B^s)$ are the non-seasonal and seasonal moving average polynomials of orders q and Q respectively.
- $(1-B)^d$ and $(1-B^s)^D$ are the non-seasonal and seasonal differencing operators.
- B is the backshift operator, $B^k y_t = y_{t-k}$.
- ϵ_t is white noise error term.

The non-seasonal autoregressive polynomial $\phi_p(B)$ is defined as:

$$\phi_p(B) = 1 - \phi_1 B - \phi_2 B^2 - \dots - \phi_p B^p, \quad (3.8)$$

and the seasonal autoregressive polynomial $\Phi_P(B^s)$ is defined as:

$$\Phi_P(B^s) = 1 - \Phi_1 B^s - \Phi_2 B^{2s} - \dots - \Phi_P B^{Ps}. \quad (3.9)$$

Similarly, the non-seasonal moving average polynomial $\theta_q(B)$ is:

$$\theta_q(B) = 1 + \theta_1 B + \theta_2 B^2 + \dots + \theta_q B^q, \quad (3.10)$$

and the seasonal moving average polynomial $\Theta_Q(B^s)$ is:

$$\Theta_Q(B^s) = 1 + \Theta_1 B^s + \Theta_2 B^{2s} + \dots + \Theta_Q B^{Qs}. \quad (3.11)$$

The SARIMA model's ability to model both seasonal and non-seasonal components makes it highly flexible and effective for various types of time series data. Key features of the SARIMA model include:

- **Seasonal Decomposition:** The model explicitly accounts for seasonality, making it suitable for data with repeating seasonal patterns.
- **Differencing:** Both seasonal and non-seasonal differencing can be applied to achieve stationarity.
- **Flexibility:** By adjusting the orders of AR, MA, and differencing terms, the model can be tailored to fit a wide range of time series behaviors.
- **Forecasting:** SARIMA is used for forecasting in various domains, providing predictions by capturing complex seasonal structures.

4 Experimental Setup

The experimental setup was designed to calculate the SPEI using weather station and remote sensing data. After that, the performance of various models in predicting wet and dry periods was evaluated using the SPEI. The experiments involved calculating and evaluating the SPEI, training and testing multiple models, and comparing their outputs against the comparison dataset SPEIbase (Beguería, 2010). Requirements for the specific experiments were stated to evaluate the final results and verify the hypotheses.

4.1 Requirements

In this section, the key requirements for evaluating the accuracy and relevance of the Standardized Precipitation Evapotranspiration Index (SPEI) derived from weather station data and remote sensing methods are outlined, and compared to the SPEIbase. As well as the requirements for predicting the SPEI. These enumerated requirements are crucial for ensuring the reliability and consistency of SPEI values, and the accuracy of the SPEI predictions.

4.1.1 SPEI Accuracy

The SPEI values derived from weather station data and remote sensing should deviate on average by **less than 0.3 SPEI** from the results obtained from the SPEIbase. This requirement is established to ensure that the derived SPEI values are consistent with the benchmark data provided by the SPEIbase (Beguería, 2010). According to Vicente-Serrano et al. (2010), the accuracy of SPEI calculations is vital for understanding climate variability and drought impacts, making this threshold necessary for credible results.

4.1.2 Correlation with SMI

The correlation between the SPEI derived from weather station data and the Soil Moisture Index (SMI), including both upper and total soil moisture, should be **above 0.5**. The same requirement applies to the correlation between the SPEI derived from remote sensing data and the SMI. A correlation coefficient above 0.5 is considered to represent a meaningful positive correlation for both the distance and Pearson correlation coefficient, indicating that changes in SPEI are appropriately reflected in soil moisture conditions.

4.1.3 Prediction Accuracy

For prediction purposes, an RMSE of **maximum 0.3** is considered acceptable for the prediction of the SPEI values. This tolerance is based on the understanding that the RMSE is in the desired unit and a deviation of up to 0.3 only changes the classification of the SPEI value by one category, which is generally negligible in practice. For example, a shift from 0.7 to 1.0 would move the classification from Normal to Moderate Drought (see Table 5.1), a change that does not significantly alter the overall interpretation of the data. This requirement ensures that the prediction model remains usable even with minor inaccuracies.

4.2 SPEI Calculation

For the calculation of the SPEI the weather station data by Deutscher Wetterdienst (2020) and the remote sensing datasets by Copernicus (2024b) were used based on the required data by the chosen PET equations Thornthwaite, FAO-56 Penman-Monteith, Priestley-Taylor and Hargreaves. The first hypothesis that states that the selected PET equation influences the values of the SPEI is examined here. As well as the third hypothesis also says that the combination of weather station and remote sensing data increases the accuracy of the SPEI values calculated in comparison to using weather station data only (see hypotheses in List 4).

4.2.1 Data Preprocessing

By using preprocessing data can be cleaned, transformed, and structured. This makes it more suitable for model training or analysis. For example, missing values are removed or the representation of a value is transformed.

Weather Station Data

To adjust the data for the needs of this study the data has been preprocessed on the consumer side again. Since the weather station data by the DWD's CDC (Deutscher Wetterdienst, 2024a) are ASCII files all cell values were loaded into a Numpy ndarray. Cells with no data are assigned with -999 (see Listing 4.1) these values have been replaced with NaN. The temperature data has been converted from $^{\circ}C$ to K by adding 273.15 and the values have been added to the dataset. This had to be done because the Thornthwaite PET equation needs the temperature in $^{\circ}C$, while the other PET equations need the temperature in K .

Additionally, the position of the cells has been flipped vertically because the orientation of the raw file did not represent the map of Germany correctly. This whole process has been used on all the precipitation, temperature, and radiation datasets by the Deutscher Wetterdienst (2020). The subregion had not to be extracted because the datasets represent Germany already.

```
1 NCOLS 654
2 NROWS 866
3 XLLCORNER 3280414.711633467
4 YLLCORNER 5237500.62890625
5 CELLSIZE 1000
6 NODATA_VALUE -999
```

Listing 4.1: Header of an ASCII file by the Deutscher Wetterdienst (2024a) representing the max. air temperature of Germany

Remote Sensing Data

On the download page of ERA5-Land (Hersbach et al., 2020), the subregion to be extracted has been specified which is the latitude bound from 47.0 to 55.0 and the longitude bound from 5.5 to 15.0. These latitude and longitude bounds represent the region of Germany.

To facilitate data manipulation and analysis within the Pandas framework, the netCDF files were loaded using XArray and then converted to CSV format. This conversion ensured compatibility with Pandas, a widely used data analysis library in Python (Gupta and Bagchi, 2024).

After importing the data into a Pandas DataFrame, the following steps were undertaken to derive additional variables essential for drought prediction:

- u_2 : The wind speed at 2m height (u_2) has been calculated by combining the u_{10} and v_{10} components.
- T : The temperature at 2m height (t_{2m}) has been converted from degrees Kelvin to Celsius (T).
- es : Using the Magnus-Tetens formula, the saturation vapor pressure (es) has been calculated.
- ea : An approximation involving the leaf area indexes (lai_{hv})(lai_{lv}) has been used to compute the actual vapor pressure (ea).
- R_n : The net radiation (R_n) has been derived as the average of surface net solar radiation (ssr) and surface net thermal radiation (str), and converted from Joules per square meter (J/m^2) to Megajoules per square meter MJ/m^2 .
- Δ_v : The slope of the vapor pressure curve (Δ_v) has been calculated.
- vpd : The vapor pressure deficit (vpd) has been determined as the difference between the saturation vapor pressure (es) and the actual vapor pressure (ea).

In the end, the below listed variables were included in the dataset:

- u_{10} : 10m u-component of wind (m/s),
- v_{10} : 10m v-component of wind (m/s),

- t_{2m} : Temperature at 2m height (K),
- lai_{hv} : Leaf area index (high vegetation) (m^2/m^2),
- lai_{lv} : Leaf area index (low vegetation) (m^2/m^2),
- pev : Potential evaporation (m),
- $shlf$: Surface latent heat flux (J/m^2),
- ssr : Surface net solar radiation (J/m^2),
- str : Surface net thermal radiation (J/m^2),
- sp : Surface air pressure (Pa),
- e : Evaporation (*mo of water equivalent*),
- tp : Total precipitation (m),
- u_2 : Wind speed at 2m height,
- T : Temperature at 2m height ($^{\circ}C$),
- es : Saturation vapor pressure (kPa),
- ea : Actual vapor pressure (kPa),
- R_n : Net radiation (MJ/m^2),
- Δ_v : Slope of the vapor pressure curve and
- vpd : Vapor pressure deficit (kPa).

4.2.2 Calculation

After the data preprocessing the weather station and remote sensing SPEI were calculated. The calculations have been repeated five times each to ensure the values remain the same each run.

Weather Station SPEI

The calculation of the weather station SPEI for the range from January 1980 to December 2022 (*515 months*) includes several steps, beginning with the calculation of the Potential Evapotranspiration (PET). Thornthwaite, FAO-56 Penman-Monteith, Priestley-Taylor, and Hargreaves PET equation. After that, the difference (D) has been calculated by subtracting the PET from the precipitation sum (P).

First, the difference data D is flattened into a one-dimensional array to facilitate subsequent computations. Then, any NaN (Not a Number) or infinite values in the difference data (D) are removed to avoid computational errors.

Next, the cleaned D data is fitted to a log-logistic distribution. Using the fitted parameters, the cumulative distribution function (CDF) is computed.

An array of NaNs is initialized with the same shape as the original D data. This array will eventually hold the SPEI values. A mask is created to identify the positions of finite (non-NaN, non-infinite) values in the original data array. The SPEI dataset is flattened to match the structure of the different data for ease of assignment. The finite mask is applied to assign the calculated z-scores to the corresponding positions in the SPEI array. Finally, the SPEI values are reshaped to match the original shape of the D data, resulting in the final SPEI dataset.

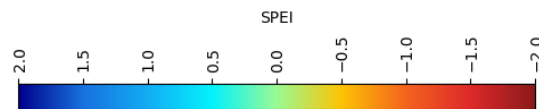


Figure 4.1: SPEI color bar from blue (SPEI 2.0/wet) to green (SPEI 0.0/normal) to red (SPEI -2.0/dry).

To plot the SPEI, a color map is generated using Matplotlib to represent the SPEI values, which typically range from extreme drought (negative values) to extreme wet conditions (positive values). This color map has the same colors as the SPEI Global Drought Monitor (Vicente-Serrano et al., 2024) is used for the plots (see Figure 4.1). The shape of Germany is overlaid on the map to provide geographical context. The x and y axes are adjusted according to the latitude and longitude coordinates to ensure accurate geographical representation. For the timescales 1, 3, 6, 9, and 12 the SPEI

calculation has been repeated. For each month a n-month SPEI map plot has been created. An example can be seen in Figure 4.2.

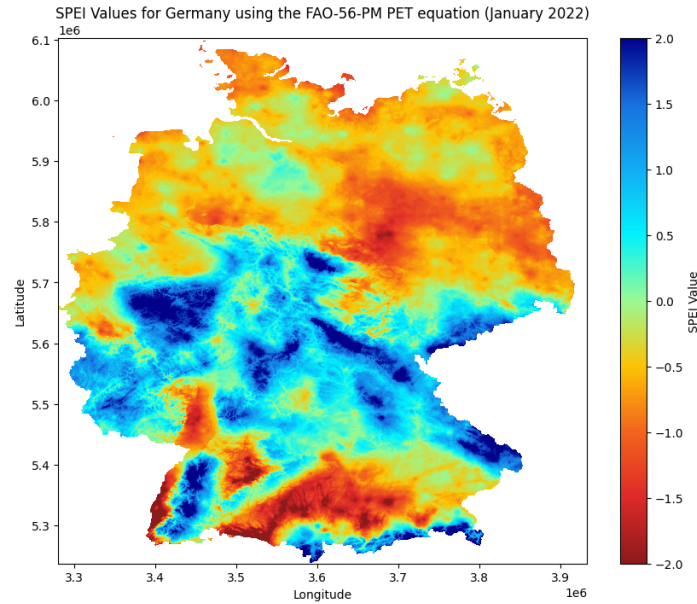


Figure 4.2: 1-month weather station SPEI map for January 2022 of Germany using the FAO-56 Penman-Monteith PET equation

Because several data sources, like the ERA5-Land (Hersbach et al., 2020) or SPEIbase (Beguería, 2010), had the file format NetCDF the SPEI results were saved as ASCII and netCDF files for a higher compatibility for future researches.

Remote Sensing SPEI

Also for the remote sensing SPEI, the range from January 1980 to December 2022 (515 months) has been chosen. The FAO-56 Penman-Monteith (FAO56PM) PET equation is used because the value progression for the weather station SPEI was relatively similar to the SPEIbase (SPEI DB) like in the Figures 5.3 and 5.5. As related work, like (Vicente-Serrano et al., 2010) or (Allen, 1998), and the results of the weather station SPEI have shown that the FAO-56 Penman-Monteith is a suitable and widely used PET equation.

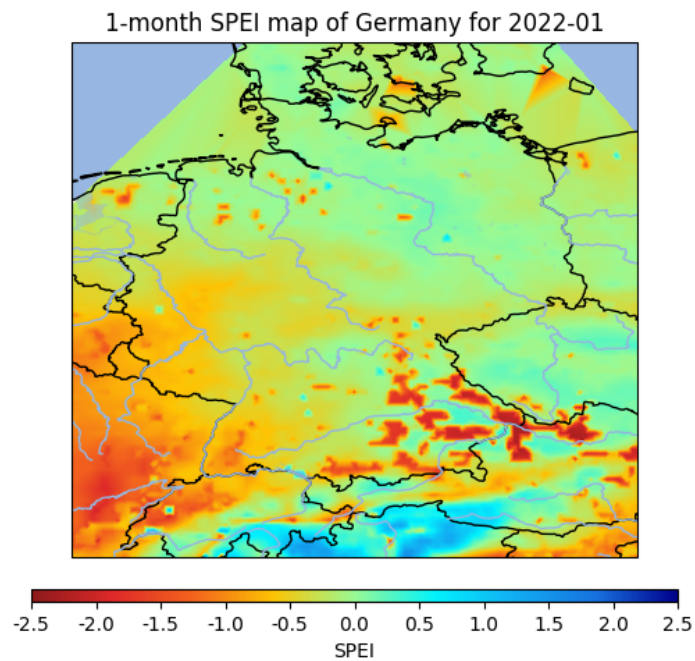


Figure 4.3: 1-month remote sensing SPEI map for January 2022 of Germany using the FAO-56 Penman-Monteith PET equation

Based on the data preprocessing step the 1-, 3-, 6-, 9-, 12-, and 24-month SPEI has been calculated using the FAO-56 Penman Monteith. After that, the map plots were created using Matplotlib where an example can be seen in Figure 4.3.

4.2.3 Evaluation

Evaluation is required to be able to assess whether the data created is correct and to what extent it differs from the comparison dataset. For the SPEI, the comparison dataset SPEIbase (Beguería, 2010) was used, which was created by the inventors of the SPEI, Vicente-Serrano et al. (2010), and is freely available for download.

Weather Station Data

Min, Mean, Max

As a comparison value the min, mean, and max values of each monthly SPEI result of a specific year are taken to be compared to each other. The smaller the differences of the SPEI between the SPEIbase (Beguería, 2010) and the result is, the higher the chance that it correctly represents the SPEI.

SMI

First, the specific SPEI dataset and the SMI upper soil dataset by Helmholtz Zentrum für Umweltforschung (2024) are interpolated to match the coordinates of both datasets. Then the Pandas framework is used to identify a correlation between the values of the two datasets. The same procedure is repeated for the SMI total soil dataset by Helmholtz Zentrum für Umweltforschung (2024). Finally, plots are created to visually understand the correlation coefficient and the regression line.

Remote Sensing Data

The same evaluation methods as for the weather station SPEI are used for the remote sensing SPEI.

4.3 Correlation with SMI

To check if a correlation between the SPEI values and the SMI exists, a distance and Pearson correlation is calculated between the weather station or remote sensing SPEI and the SMI of the upper or total soil.

First, the SMI dataset with the upper soil is taken which represents the SMI up to 25 cm deep. Last but not least the SMI dataset with the total soil is taken which represents the SMI up to 180 cm deep. Both datasets, which are also used for the German Drought Monitor, were downloaded from the Helmholtz Zentrum für Umweltforschung (2024). An interpolation has been carried out to align the nearest coordinates of the SPEI and SMI datasets.

The calculation of the Pearson correlation itself has been done with the Pandas framework which computes the pairwise correlation of columns, excluding null values, and returns

the Pearson correlation coefficient. For the distance correlation the Python library *dcorr* has been used, which the data frames have been passed to. The library was also used to generate the line of best fit and polynomial fit of degree 2.

To have a comparison value, it has been checked whether there is any distance or Pearson correlation between the interpolated SMI of the upper and total soil and the SPEIbase's SPEI values using the same procedure as described.

4.4 Prediction Models

To examine the second hypothesis, which claims that machine learning algorithms improve the indication of wet and dry phases in comparison to traditional statistical methods, both machine learning and statistical methods are used to predict the SPEI. Last but not least the fourth hypothesis, which states that adding lagged features improves the to-be-predicted variable, is investigated by adding the lagged features to the methods. See an enumeration of the hypothesis at List 4.

For the prediction the remote sensing SPEI has been chosen and four prediction approaches have been selected for this experiment: Gradient Boosting Regressor (GBR), XGBoost, Prophet, and SARIMA. The configuration of the models has been adjusted sequentially to determine the most appropriate configuration for each method, which had the lowest error value in predicting the remote sensing SPEI value. To reduce the complexity the coordinates where the SPEI had to be predicted are latitude 53.6 and longitude 10.2 in 22145 Stapelfeld, Germany because these coordinates were available in the datasets and near the thesis author's home. All approaches have been applied ten times to ensure to get the model's most accurate results possible. The results of the run with the best evaluation metrics have been described in the Results section.

4.4.1 Gradient Boosting Regressor

The GBR model has been implemented with a focus on optimizing hyperparameters such as the number of estimators, learning rate, and tree depth. The model was trained on data from January 2000 to January 2015 and tested on data from February 2015 to December 2020, with cross-validation and evaluation metrics used to ensure robustness.

For the prediction latitude 53.6 and longitude 10.2 in 22145 Stapelfeld, Germany are used.

Implementation

Initial models

For a better understanding, an initial model has been created as an example for explanation which can be seen in Figure 4.4. In the course of the thesis, the configuration will be adjusted to achieve an accurate model.

For the initial model, the number of estimators has been set to 100, which means the model will build 100 sequential trees. The learning rate is 0.1, controlling the contribution of each tree to the final model, and balancing the trade-off between model accuracy and overfitting. The maximum depth of each tree is limited to 3, ensuring that the model remains relatively simple and less prone to overfitting by not capturing too much noise from the training data. Finally, the random state is set to 42, ensuring reproducibility of results by initializing the random number generator to a fixed state. This specific configuration aims to create a robust initial model that generalizes well to new data.

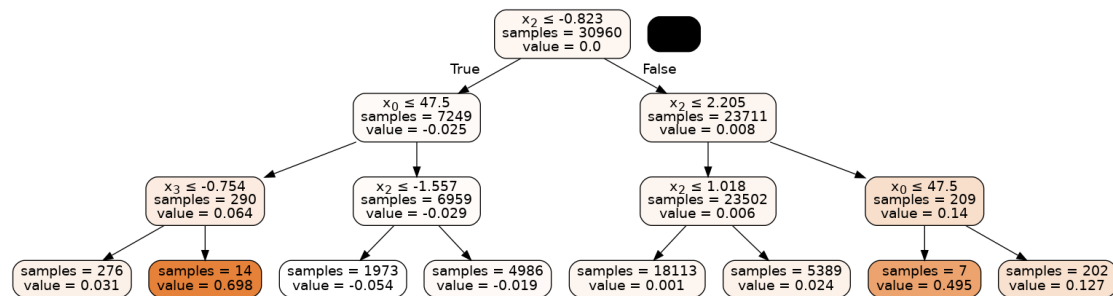


Figure 4.4: Simple Gradient Boosting Regressor tree model with 100 estimators, a learning rate of 0.1, a max depth of 3, and a random state of 42. The features x_0 to x_4 represent latitude, longitude, SPEI of the previous month, SPEI of two months ago, and SPEI of three months ago (*in this order*).

In Figure 4.4 the decision tree from the Gradient Boosting Regressor is shown which is used to predict the Standardized Precipitation-Evapotranspiration Index (SPEI) based on several features: latitude (lat), longitude (lon), SPEI values of the three previous months, and the day of the year. Here is an assignment of each feature name to the actual feature.

- x_0 - Latitude
- x_1 - Longitude
- x_2 - SPEI of previous month
- x_3 - SPEI of two months ago
- x_4 - SPEI of three months ago

At the root of the tree, the decision is made based on the SPEI value of the previous month (x_2), with a threshold of -0.823 . If this value is less than or equal to -0.823 , the tree follows the left branch; otherwise, it follows the right branch.

For the left branch, another decision is made based on the day of the year (x_0), with a threshold of 47.5 . If the day of the year is less than or equal to 47.5 , the tree further splits on the SPEI value of two months ago (x_3), with a threshold of -1.557 . This branch continues to split based on various thresholds of the SPEI values and other features, ultimately leading to terminal nodes that provide specific predicted SPEI values.

On the right branch, starting from the root, the tree immediately makes another decision based on the SPEI value of the previous month (x_2), with a threshold of 2.205 . This branch follows a similar pattern of splits based on the features until it reaches terminal nodes.

The tree's structure captures the relationship between these features and the target SPEI value, using the splits to progressively narrow down the prediction based on the provided input features. The intermediate nodes represent the decision points, while the terminal nodes provide the final SPEI value prediction based on the conditions met along the path from the root to the leaf.

In the Results section results are displayed where the following configuration settings of the Gradient Boosting Regressor have been adjusted:

- Number of estimators
- Learning rate
- Maximum depth of the tree

Five different models were trained using the configuration from the initial model with varying sets of features: geographical coordinates (C), the day of the year (DOY), and the lagged SPEI values of the three previous months (L).

Configuration mix

To ensure a comprehensive evaluation of the model's performance across different configurations, a combination of the following configurations has been tested:

- **Parameter:** Number of estimators (`n_estimators`)
 - **Values:** 25, 50, 75, 100, 150, 200, 250, 300
 - **Justification:** The number of estimators represents the number of boosting stages to be run. A lower number of estimators may lead to underfitting, while a higher number can cause overfitting. By selecting values ranging from 25 to 300, the aim is to capture the model's behavior from underfitting to potential overfitting, thus identifying an optimal range for this parameter.

- **Parameter:** Learning Rate (`learning_rate`)
 - **Values:** 0.01, 0.05, 0.1, 0.2, 0.3, 0.5, 0.75, 1.0
 - **Justification:** The learning rate controls the contribution of each tree to the final model. Lower learning rates require more boosting stages to achieve similar model accuracy, while higher learning rates can lead to faster convergence but may risk overfitting. The chosen range from 0.01 to 1.0 allows us to observe the effects of both very conservative and more aggressive learning rates on the model's performance.

- **Parameter:** Max tree depth (`max_depth`)
 - **Values:** 3, 4, 5, 6, 7, 8, 9, 10, 11, 12
 - **Justification:** The max depth defines the maximum depth of each tree. This parameter helps control the complexity of the model. Shallow trees (lower depths) may not capture the underlying data patterns well which leads to underfitting, whereas deeper trees may model the noise in the data which can lead to overfitting. By selecting depths from 3 to 12, a wide range of model complexities is ensured.

These values were chosen to balance the trade-off between underfitting and overfitting, allowing for a thorough investigation of the model’s performance across various settings. This systematic should help in identifying the most effective configuration for achieving high predictive accuracy.

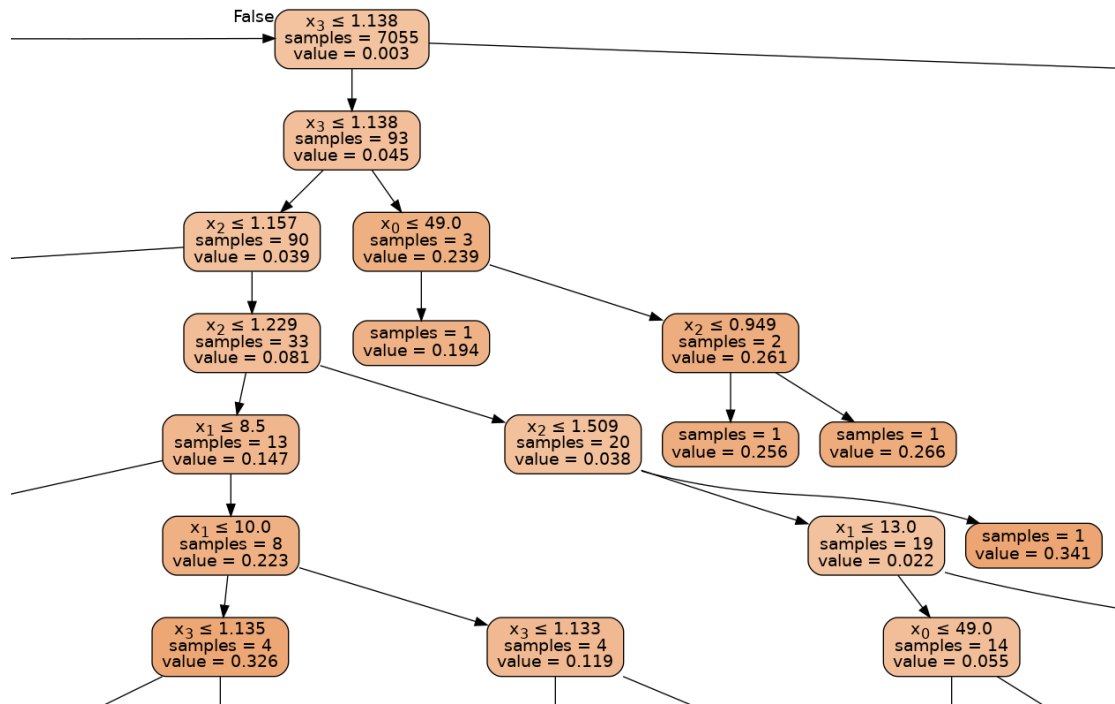


Figure 4.5: Section of the tree of the Gradient Boosting Regressor model with the lowest RMSE value 0.0 (see Table 5.4) out of all tested model configurations. The features C, L, and DOY were used. For a detailed view see the model in the GitHub repository in `data_comparison/gbt_output` (Tran, 2024b).

Figure 4.5 shows a section of a Gradient Boosting Regressor model’s tree with 50 estimators, a learning rate of 0.3 and a max depth of 9 with the C+L+DOY dataset variant. Here is the mapping of the feature variables to the feature name:

- x_0 - Latitude
- x_1 - Longitude
- x_2 - SPEI of previous month
- x_3 - SPEI of two months ago

- x_4 - SPEI of three months ago
- x_5 - Day of year

For example, starting from the root node the feature x_3 is checked if it is lower or equal to 1.13. If true, the tree is followed to the left, and if false, the tree is followed on the right side. The right side is shown in Figure 4.5 where the feature x_3 is checked if it is lower or equal to 1.138, and the tree is followed again depending on the input.

Evaluation

To rigorously evaluate the predicted SPEI, the dataset is split into training and testing sets. This split allows for an unbiased assessment of the model's performance. The training set consists of past data, which the Gradient Boosting Regressor uses to learn the underlying patterns and relationships in the data. By training on historical data, the model builds an understanding of how various factors influence SPEI. As well, the testing set comprises a different set of past data which has not been used during the training phase. This testing set is used to evaluate the model's predictive performance. By testing historical data with known outcomes, the predicted SPEI values can directly be compared with the observed values.

Root Mean Squared Error

The RMSE is used because it is in the same units as the SPEI, making it easier to understand the magnitude of prediction errors directly in the context of the index values. This interpretability is crucial when communicating results to stakeholders or making practical decisions based on the prediction. The SKLearn library is used to calculate the RMSE.

Difference to observed SPEI

The predicted SPEI values are compared to the observed SPEI values. Min., max., and mean difference between the observed and predicted SPEI values are a part of the evaluation because one can directly see the deviation and accuracy of the used GBR model. Lower values mean a higher accuracy and a lower deviation between the two compared values.

4.4.2 XGBoost

For the XGBoost models, the SPEI values from January 1980 to June 2024 for the location in Germany have been used for training and testing. Two models were created: one with the lagged SPEI only (SL) and another with all lagged features with multi-input and multi-output (MIMO). These models were designed to capture temporal dependencies in the data, with multiple lagged features passed into the model to enhance prediction accuracy. The location for the prediction is at latitude 53.6 and longitude 10.2 in 22145 Stapelfeld, Germany.

Implementation

Two models are to be created: SPEI lagged (SL) and multi-in multi-out (MIMO).

SPEI Lag

For the SL model, the lagged feature SPEI is created for the three 1-month SPEI. Every n-month SPEI has its model to validate which configuration of the hyperparameters has the lowest errors. In the end, the following monthly features were in the dataset which was passed to the models for training:

- *month*: The month of the year (1-12), represents the period of the data.
- *latitude*: The geographic latitude of the location where the data is recorded.
- *longitude*: The geographic longitude of the location where the data is recorded.
- *u₁₀*: The eastward component of the 10-meter wind speed.
- *v₁₀*: The northward component of the 10-meter wind speed.
- *t_{2m}*: The 2-meter air temperature.
- *pev*: Potential evaporation, indicating the amount of evaporation that would occur if a sufficient water source were available.
- *ssr*: Surface solar radiation, representing the total amount of solar radiation reaching the surface.
- *str*: Surface thermal radiation, indicating the thermal radiation emitted by the surface.

- *tp*: Total precipitation.
- *SPEI_1*: The Standardized Precipitation-Evapotranspiration Index (SPEI) for 1 month, representing drought conditions.
- *SPEI_1_lag_1*: The 1-month SPEI lagged by 1 month.
- *SPEI_1_lag_2*: The 1-month SPEI lagged by 2 months.
- *SPEI_1_lag_3*: The 1-month SPEI lagged by 3 months.

For the SL model the feature *SPEI_n* had to be predicted with the input of the following monthly features:

- *u10*: Eastward component of the 10-meter wind speed,
- *v10*: Northward component of the 10-meter wind speed,
- *t2m*: Temperature at 2m height,
- *pev*: Potential evaporation,
- *ssr*: Surface solar radiation,
- *str*: Surface thermal radiation,
- *tp*: Total precipitation
- *SPEI_1_lag_1*: 1-month SPEI lagged by 1 month
- *SPEI_1_lag_2*: 1-month SPEI lagged by 2 months, and,
- *SPEI_1_lag_3*: 1-month SPEI lagged by 3 months.

With the SL model, the user has to input the three previous 1-month SPEI values from the past and the other features could, for example, be determined by other calculations or predictions and thus the SPEI could be found. The problem of not knowing certain feature values in advance and therefore having to estimate or predict them should be solved with the second model MIMO which is presented in the next section.

Multi-in Multi-out

The second model MIMO contains these monthly features:

- *month*: The month of the year (1-12), represents the period of the data.

- *latitude*: The geographic latitude of the location where the data is recorded.
- *longitude*: The geographic longitude of the location where the data is recorded.
- *u₁₀*: The eastward component of the 10-meter wind speed.
- *u_{10_lag_1}*: The eastward component of the 10-meter wind speed lagged by 1 month.
- *u_{10_lag_2}*: The eastward component of the 10-meter wind speed lagged by 2 months.
- *u_{10_lag_3}*: The eastward component of the 10-meter wind speed lagged by 3 months.
- *v₁₀*: The northward component of the 10-meter wind speed.
- ...
- *t2m*: The 2-meter air temperature.
- ...
- *pev*: Potential evaporation.
- ...
- *ssr*: Surface solar radiation.
- ...
- *str*: Surface thermal radiation.
- ...
- *tp*: Total precipitation.
- ...
- *SPEI_n*: The Standardized Precipitation-Evapotranspiration Index (SPEI) for n months.
- *SPEI_n_lag_1*: The SPEI for n months lagged by 1 month.
- *SPEI_n_lag_2*: The SPEI for n months lagged by 2 months.

- *SPEI_n_lag_3*: The SPEI for n months lagged by 3 months.

where every feature, except month, latitude, and longitude, is lagged. The MIMO is a Multi-Output Regressor by Sklearn which uses the XGB Regressor by XGBoost. Multiple lagged features are passed into the model and the model outputs a prediction of the features ($u_{10}, t2m, SPEI_n, \dots$).

Lag Size

The optimal lag size had to be discovered by using several different lag sizes from 1 to 6, which mirrors a lag of one month to six months in the past. For this experiment, the 1-month SPEI has been chosen and the six different datasets were created containing the 1 to 6-month lagged features. The datasets were split into test and train for cross-validation and then the min, max, and mean difference between the actual and predicted 1-month SPEI were determined. The lag size of the model with the most values out of lowest min., max., mean difference, lowest MAE, and RMSE is chosen as the lag size utilized in the further experiments.

n-month SPEI

The identified optimal lag size from the previous experiment is used, to find out the most accurate models for the n-month SPEI. For that, the configuration mix approach has been utilized to find the most suitable configuration for the model. Several models with different numbers of estimators, learning rates, and max. depth was trained with the dataset containing the 6-month lagged features mentioned above including one of the n-month SPEI from the timescale 1, 3, 6, 9, 12, or 24. The MAE and RMSE were used as evaluation metrics.

Evaluation

Using the same evaluation methods as the mentioned methods for the Gradient Boosting Regressor in Section 4.4.1 because the Gradient Boosting Regressor and XGBoost are both decision tree methods that predict values and can be evaluated the same way.

4.4.3 Prophet

For the Prophet model by Meta (Taylor and Letham, 2018) the SPEI values for the coordinates latitude 53.6 and longitude 10.2 in 22145 Stapelfeld, Germany were taken for the period January 1980 to June 2024.

Implementation

Only the date and the 1-month SPEI were taken into account since the Prophet only accepts a combination of dates and values from the past for the forecast. While Prophet has a predefined model architecture the input data is variable while it must contain two columns: date and value. The SPEI values for the coordinates latitude 53.6 and longitude 10.2 in Germany were taken for the period January 1980 to June 2024 and the forecast has been calculated for January 1980 to September 2032.

Evaluation

The same evaluation methods as described in Section 4.4.1 which describes the MAE and RMSE for the GBR and XGBoost. Meta's framework itself has a function to calculate the MAE and RMSE after training the model on the supplied data.

4.4.4 SARIMA

SARIMA models were used as a benchmark for comparing the performance of machine learning models against traditional statistical methods. The parameters were optimized through grid search and the models were trained and tested on various periods from January 2000 to June 2024. For the forecast, the coordinates are latitude 53.6 and longitude 10.2 in 22145 Stapelfeld, Germany.

For this experiment the same features as for the best Gradient Boosting Regressor model were used: coordinates (lat, lon), lag (three previous month's SPEI values), and the day of the year. However, the usage of a lag is already implemented in the method by the configuration variable p which stands for the number of lag observations. For this reason, the lagged features are not directly passed to the models through the dataset. For the grid point in this experiment, the latitude and longitude values are (53.75, 10.25) in this case which is located in Northern Germany. See Section 3.7.4 for more information about the SARIMA method.

Several SARIMA models were created which had a combination of the following configuration settings:

- p : {0, 1}

- **d**: {0, 1}
- **q**: {0, 1}
- **P**: {0, 1}
- **D**: {0, 1}
- **Q**: {0, 1}
- **s**: {12}

The values for the non-seasonal parameters **p**, **d**, and **q** were chosen from the range {0, 1} to keep the initial models simple and computationally efficient. This allows for testing models with no or one autoregressive term (AR), no or one degree of differencing, and no or one moving average term (MA). This approach is used to identify the basic structure of the time series data without overfitting.

For the seasonal parameters **P**, **D**, and **Q**, the values were also chosen from the range {0, 1}. This decision was based on the assumption that the seasonal component of the data might be captured adequately with simple seasonal models. Specifically:

- **P** represents the seasonal autoregressive order, and testing values {0, 1} ensures that both the presence and absence of seasonal AR terms are considered.
- **D** represents the seasonal differencing order, with {0, 1} allowing for no differencing or first-order differencing, which is sufficient to achieve stationarity in seasonal data.
- **Q** represents the seasonal moving average order, and values {0, 1} allow testing models with and without seasonal MA terms.

These combinations provide a balance between model complexity and computational feasibility. The parameter **s** was set to 12. This parameter represents the length of the seasonal cycle, which in this case is 12 months. This value was chosen because the data being modeled is monthly and likely exhibits annual seasonality. Setting **s** to 12 allows the model to account for repeating patterns that occur each year, which is typical for climatic and environmental time series data such as the Standardized Precipitation-Evapotranspiration Index (SPEI).

Implementation

For the experiment, the training dataset always begins in 2000 and ends individually in January in 2005, 2007, 2010, 2012, 2014, 2015, 2016, 2017, 2018, and 2019. The distance between the years has been picked arbitrarily until 2014. After that, the distance between the previous year is only one year. The test dataset period's start depends on the training dataset and starts after the end of the training dataset. The end is always December 2020. For example: training January 2000 to January 2005, test: February 2005 to February 2020.

The process of selecting the optimal parameters for the SARIMA model involves systematic exploration and evaluation of different combinations of these parameters. The objective is to identify the parameter set that minimizes the error metrics, ensuring an accurate and reliable forecast.

First, the time series data needs to be extracted for a specific grid point. After that, the data is split into training and test sets to evaluate the model's performance on unseen data.

Now the values for each parameter (p, d, q, P, D, Q) are set. All possible combinations of (p, d, q) and (P, D, Q) were generated, using a Cartesian product, considering the seasonal period (s) as 12 months.

Evaluation

For each combination of parameters, the SARIMA model is fitted to the training data. After that, the forecast for the testing period is executed and the model is evaluated by the following metrics:

- **Akaike Information Criterion (AIC):** A measure of the relative quality of the statistical model for the given set of data.
- **Mean Squared Error (MSE):** The mean of the squares of the errors between the observed and forecasted values.
- **Mean Difference:** The mean absolute difference between the observed and forecasted values.

5 Results

5.1 SPEI Calculations

The SPEI values have been calculated using weather stations and remote sensing data. For each data source, multiple PET equations were used to compare the SPEI results of the PET equations with each other.

5.1.1 Weather Stations Data

The weather station data from the DWD's Climate Data Center (Deutscher Wetterdienst, 2024a) has been used to calculate the weather station SPEI.

Quantity Distribution

The German Weather Service's (DWD) weather station data from the Climate Data Center (CDC) (Deutscher Wetterdienst, 2024a) are used for the calculation of the results. FAO-56 Penman-Monteith's (FAO56PM), Thornthwaite's (TW), Priestley-Taylor's (PT), and Hargreaves' (HG) PET equation are utilized to calculate the SPEI. The SPEIbase (SPEI DB) (Beguería, 2010) is included in the chart to represent comparison values.

SPEI value distribution in percentage by PET equation methods and SPEI categories for 2022 in Germany

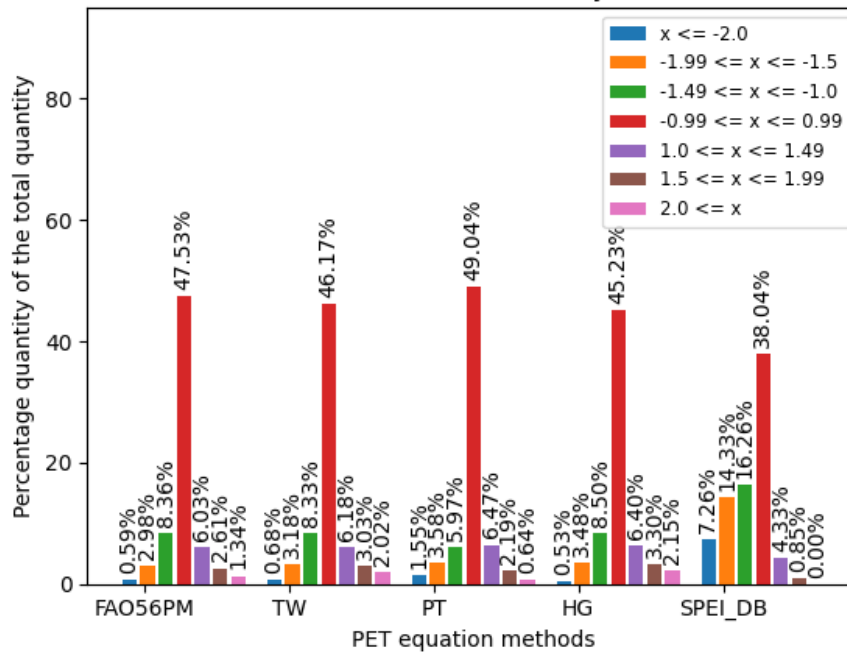


Figure 5.1: SPEI value distribution in percentage separated by PET equation for Germany represented as bars which mirror the SPEI categories from Extreme Wet ($2.0 \leq x$) to Extreme Drought ($x \leq -2.0$). Each bar shows the percentage quantity of the total quantity of the SPEI values. The values of the PET equations FAO-56 Penman-Monteith (FAO56PM), Thornthwaite (TW), Priestley-Taylor (PT), and Hargreaves (HG) are shown. The SPEIbase (SPEI DB) (Beguería, 2010) is included to have comparison values. The y-axis represents the percentage quantity of the total quantity by SPEI category and the x-axis shows the different PET equation methods.

In Figure 5.1 the SPEI value distribution can be seen in percentage for each data source mentioned before. The bars in the graph show the distribution of the SPEI value for the specific category from blue which is Extreme Drought ($x \leq -2.0$) to pink which is Extreme Wet ($2.0 \leq x$). Additionally, the percentages show to percentage quantity of the total quantity per data source. A different representation of the data can be found in Figure 5.2. In this figure, the x-axis shows the SPEI categories and the labels display the PET equation method used. A direct comparison between the PET equation methods per SPEI category can be followed visually in Figure 5.2.

In Table 5.1 the SPEI value range and the corresponding SPEI category label are displayed for a better understanding of the results.

| SPEI value | Condition |
|---------------------------|------------------|
| $x \leq -2.0$ | Extreme drought |
| $-1.99 \leq x \leq -1.50$ | Severe drought |
| $-1.49 \leq x \leq -1.0$ | Moderate drought |
| $-0.99 \leq x < 0.99$ | Normal |
| $1.0 \leq x \leq 1.49$ | Moderately Wet |
| $1.50 \leq x \leq 1.99$ | Severely wet |
| $2.0 \leq x$ | Extremely wet |

Table 5.1: SPEI value ranges and corresponding conditions from extreme drought (top) to extremely wet (bottom)

Beginning with the FAO-56 Penman-Monteith method (*FAO56PM*) shows that the majority of values, 47.53%, fall within the Normal category ($-0.99 \leq x \leq 0.99$)(*red*). This method also has 8.36% of its values in the Moderate Drought category ($-1.49 \leq x \leq -1.0$)(*green*) and 6.03% in the Moderate Wet category ($1.0 \leq x \leq 1.49$)(*violet*). The extreme categories have negligible values, with Extreme Drought at 0.59% (*blue*) and Extreme Wet at 1.34% (*pink*).

Additionally, the Thornthwaite method (*TW*) similarly shows a high percentage, 46.17%, in the Normal category. It has 8.33% in the Moderate Drought category and 6.18% in the Moderate Wet category. This method has 3.18% in the Severe Drought category and no values in the Extreme Wet category.

However the Priestley-Taylor method (*PT*) has the highest percentage of Normal values at 49.04%, which is the highest among all methods for this category. It also has 5.97% in the Moderate Drought category and 6.47% in the Moderate Wet category. The Extreme Drought category has 1.55% and the Extreme Drought category shows 0.64%.

The Hargreaves method (*HG*) shows 45.23% of its values in the Normal category, with 8.50% in the Moderate Drought category, which is the highest percentage for this category among all methods. It also has 6.40% in the Moderate Wet category and low values in the extreme categories with 0.53% for Extreme Drought and 2.15% for Extreme Wet.

The SPEI DB method is considered as a comparison value which has been developed by the founders of the SPEI Begueria et al. (Vicente-Serrano et al., 2010). It has a value of 38.04% in the Normal category, which is the lowest among all methods for this category. However, it has a significantly high percentage of Moderate Wet values at 16.26%, the highest for this category among all methods. It also shows a relatively high percentage of Severe Drought values at 14.33%. Surprisingly the Extreme Drought category has a percentage of 7.26% which is the highest value in this category as well as the lowest value among all methods of 0.00% for the Extreme Wet category.

Overall, the Normal category dominates across all methods, with the PT method having the highest percentage and the SPEI DB method having the lowest percentage for this category. The SPEI DB stands out with a high percentage in the Moderate Wet category, while the HG method has the highest percentage in the Moderate Drought category. The extreme categories are generally underrepresented across all methods except for SPEI DB where the Extreme Drought category exceeds the Moderately Wet, Severely Wet, and Extremely Wet categories combined.

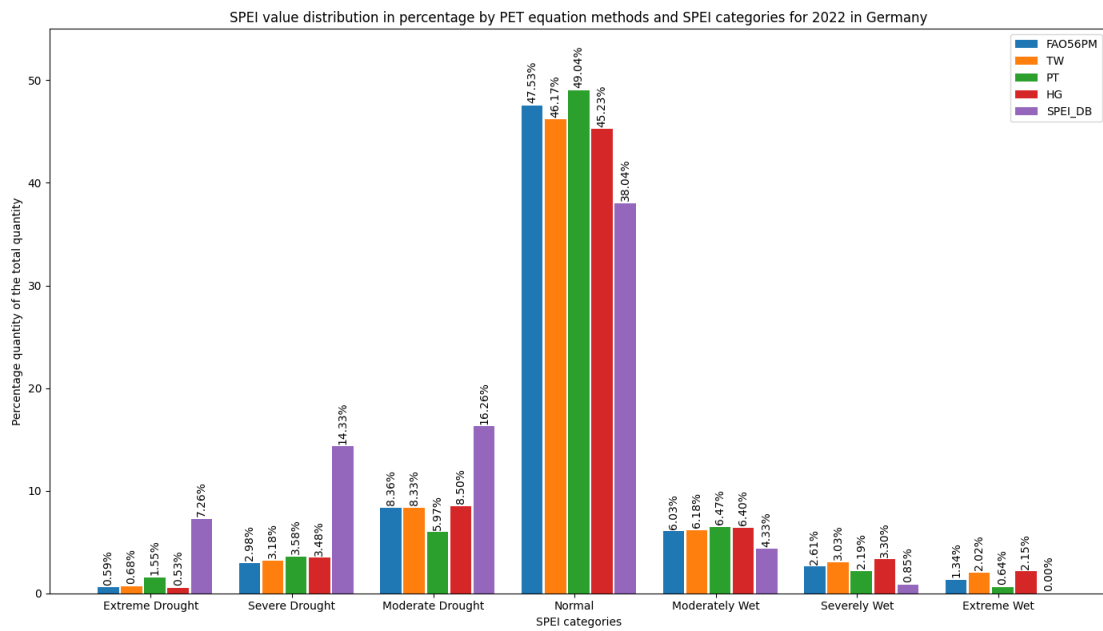


Figure 5.2: SPEI value distribution in percentage separated by SPEI categories for Germany represented as bars which mirror the SPEI categories' quantity of the specific SPEI equation from Extreme Drought (*left*) to Extreme Wet (*right*). Each bar shows the percentage quantity of the total quantity of the SPEI values of the specific PET equation used.

| Method | Ex. D. | Se. D. | Mo. D. | N. | Mo. W. | Se. W. | Ex. W. | σ Diff. |
|--------|--------|---------|---------|-------|--------|--------|--------|----------------|
| FAO | -6.67% | -11.35% | -7.9% | 9.49% | 1.07% | 1.76 | 1,34% | -12.26% |
| TW | -6.58% | -11.15% | -7.93% | 8.13% | 1.85 | 2.18% | 2,02% | -11.48% |
| PT | -5.71% | -10.75% | -10.29% | 11% | 2.14% | 1.34% | 0,64% | -11.63% |
| HG | -6.73% | -10.85% | -7.76% | 7.19% | 2.07% | 2.45% | 2,15% | -11.48% |

Table 5.2: Difference between the PET equation methods and the SPEI DB. Each PET equation method's total quantity per SPEI category is compared to the SPEI DB's total quantity and the difference is shown here. The right column shows the total difference between the specific PET equation method and the SPEI DB's total quantity percentage. The SPEI categories are abbreviated where D. means drought and W. means wet. For further information see Table 5.1.

In Table 5.2 the difference between the PET equation method's quantity percentage per SPEI category is compared to the SPEI DB's percentage. The FAO56PM method has the highest difference with -12.26% while the PT method has the second highest difference with -11.63%. Overall in total (*most right column*) the TW and HG methods show to have the least difference compared to the SPEI DB with -11.48%.

Maximum Comparison

In Figure 5.3, 5.4 and 5.5 the PET equation method's maximum, mean and minimum monthly 1-month SPEI values for the year 2022 in Germany are compared to the SPEI DB.

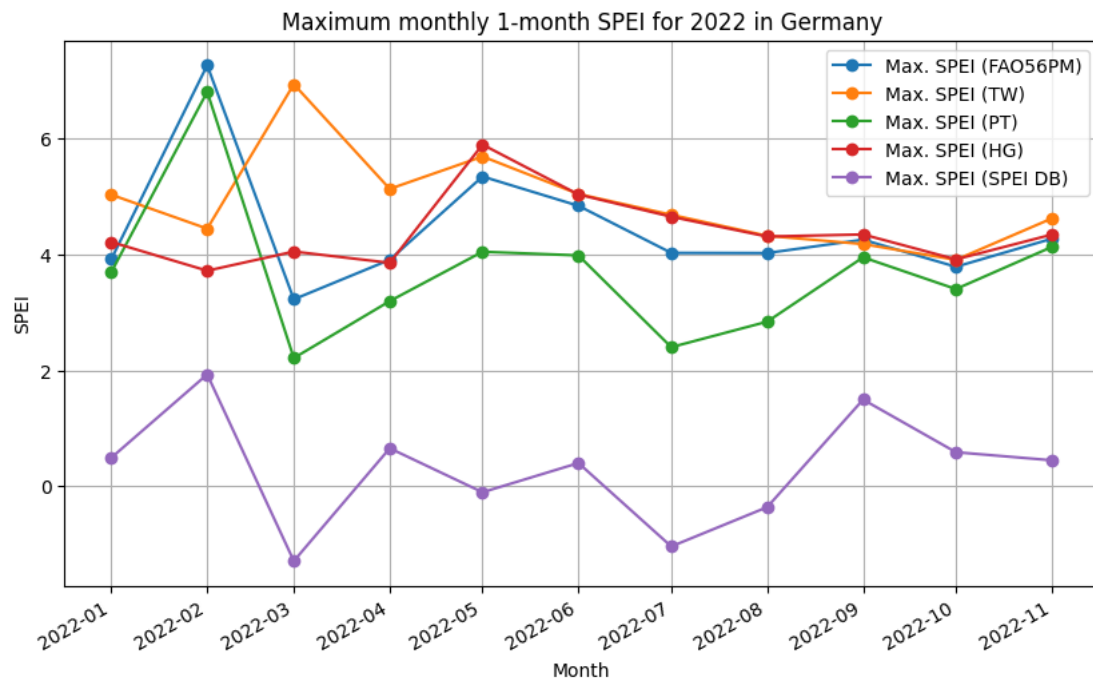


Figure 5.3: Comparison of the PET equation method's maximum monthly 1-month SPEI values using weather stations data for the year 2022 in Germany compared to the SPEI DB result (*purple*).

The method with the SPEI values calculated using the FAO56PM and the PT PET equations have similar trends, particularly because the PT PET equation is a simplification of the FAO56PM PET equation. Throughout the graph, the SPEI values for the PT method are generally lower than those of the FAO56PM method.

TW and HG have a kind of similar course from January to April 2022 except March 2022 where the TW method has a 3 higher maximum value. The TW's values align more closely with the FAO56PM and HG values in subsequent months starting from May 2022. The HG method remains relatively consistent and similar to the FAO56PM and PT methods from April 2022 onwards.

In comparison, the maximum SPEI values from the SPEI DB are lower, ranging between 0 and 3 throughout the year. This is consistently lower than the values derived from the four used methods, which range from around ≈ 4 to ≈ 7 . The values from the SPEI DB highlight a less extreme interpretation of wet conditions compared to the other methods.

Also, the maximum SPEI values from the SPEI DB are up to 2 lower than the lowest SPEI value of the four used methods. The values of the SPEI DB range from around -1.5 to 2. While the maximum SPEI values of the FAO56PM range from ≈ 3.2 to ≈ 7.2 , the PT method ranges from ≈ 2.2 to ≈ 6.8 , the TW method ranges from ≈ 3.9 to ≈ 5.8 and the HG method ranges from ≈ 3.7 to ≈ 5.9 .

Mean Comparison

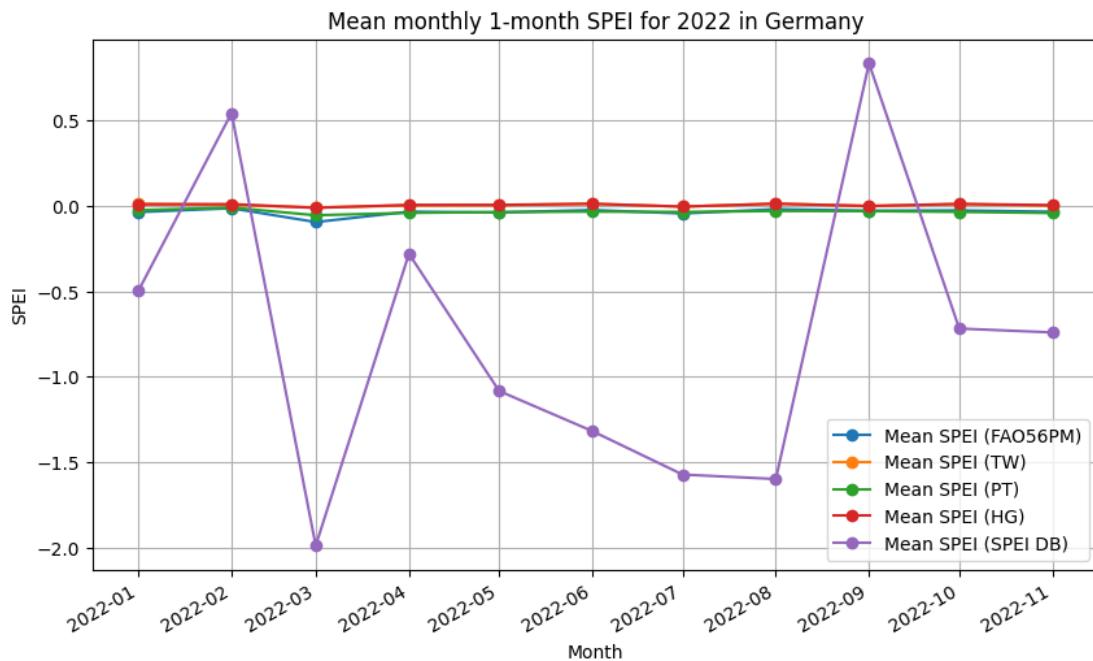


Figure 5.4: Comparison of the PET equation method's mean monthly 1-month SPEI values using only weather station data for the year 2022 in Germany compared to the SPEI DB result (*purple*). All calculated datasets have a mean 1-month SPEI of around 0 while the SPEI DB's values vary from -2.0 to 0.8.

The method with the SPEI values calculated using the FAO56PM, TW, PT, and HG PET equations shows consistent and stable behavior throughout the year 2022, with mean SPEI values hovering around 0. These methods exhibit minimal variances, indicating a relatively constant estimation of average drought and wet conditions.

In contrast, the SPEI DB values exhibit more variability, with notable drops in February, April, and from August to November 2022, reaching mean SPEI values as low as -2.0. This suggests that the SPEI DB indicates more severe drought conditions during these periods compared to the other methods.

For the mean difference the FAO-56 Penman-Monteith (*blue*) and SPEIbase (*purple*) were compared and the mean difference is ≈ 1.0973 .

Minimum Comparison

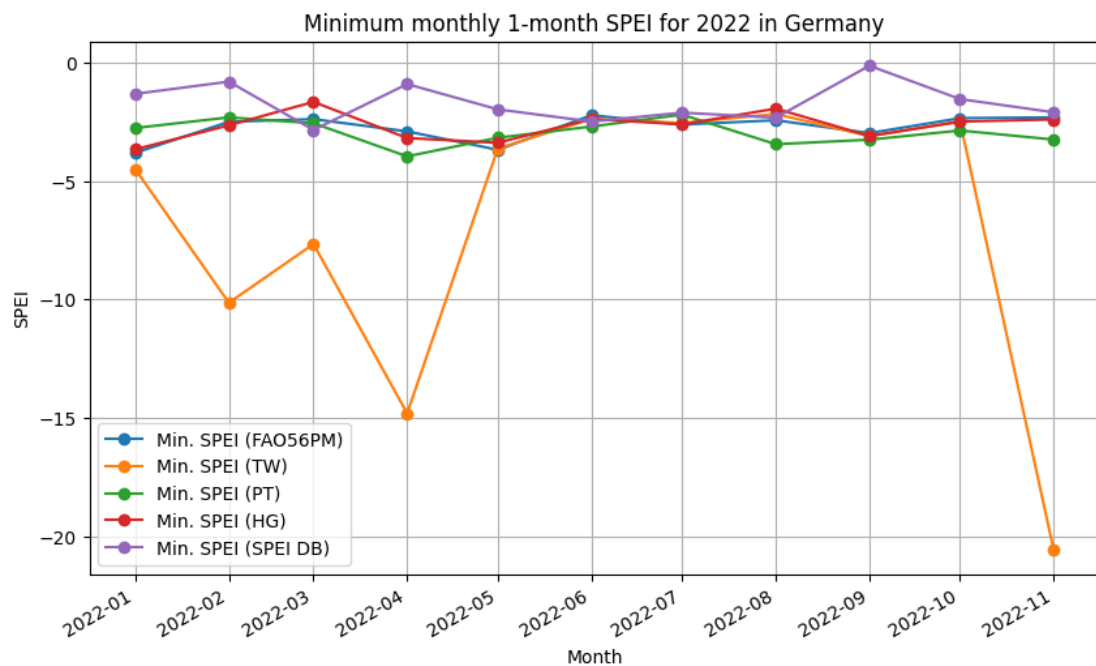


Figure 5.5: Comparison of the PET equation method's minimum monthly 1-month SPEI values using only weather station data for the year 2022 in Germany compared to the SPEI DB result (*violet*).

The methods with the minimum SPEI values calculated using the FAO56PM, PT, and HG PET equations show similar trends, generally maintaining values between ≈ -4 and ≈ 0 throughout 2022. These methods show consistent and stable behavior with minor variances.

In contrast, the TW PET equation displays significant variances, with notable drops in February, April, and November 2022, reaching extreme minimum values of around ≈ -15 and even below ≈ -20 in November. This suggests that the Thornthwaite method may be more sensitive to extreme conditions or could potentially overestimate drought severity during these months.

The SPEI DB values remain relatively higher and more stable compared to the Thornthwaite equation's extremes, aligning more closely with the FAO56PM, PT, and HG methods. This alignment suggests that the latter three methods may provide a more reliable and consistent measure of drought conditions, whereas the Thornthwaite method's variances indicate a higher degree of variability and potential overestimation.

Visual Comparison

Besides the comparison of the SPEI values between the PET equation methods, the visual comparison for understanding is important for the user, too. In Figure 5.6 the SPEI value map of Germany in January 2022 is shown for the PET equation methods TW (*upper left*), FAO56PM (*lower left*) and PT (*lower right*), as well as the comparison dataset SPEI DB (*upper right*). Due to the low resolution of the SPEI DB, it is hard to compare the maps directly but in the SPEI DB map the middle of Germany is around the SPEI value of 0.5 which is a normal condition while the rest of the map is below -0.5 which is a more dry condition.

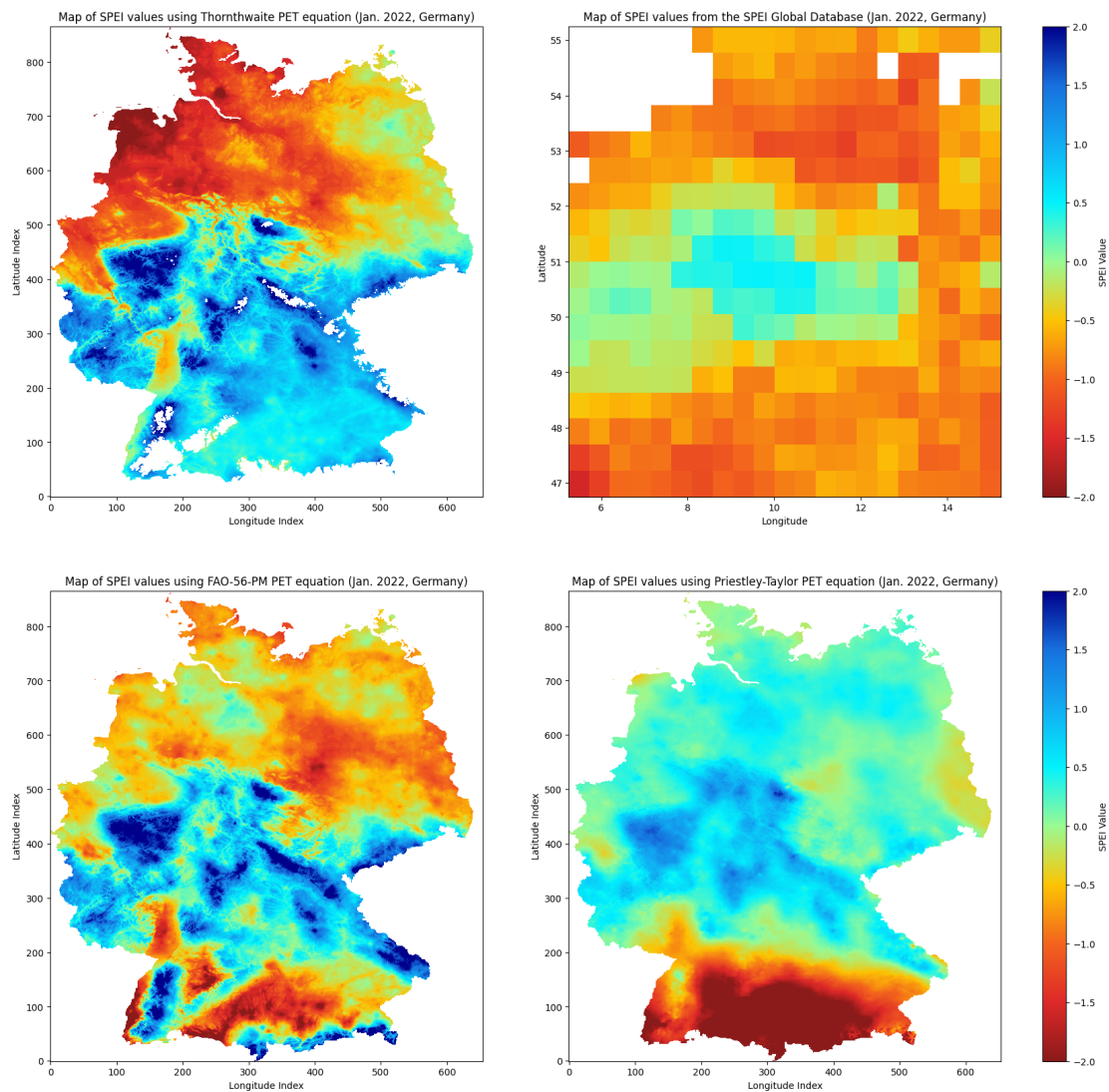


Figure 5.6: SPEI value maps of Germany in January 2022 calculated using data from German weather stations by Deutscher Wetterdienst (2024c). The Thornthwaite (upper left), FAO-56 Penman-Monteith (lower left) and Priestley-Taylor PET equation (lower right) are visually compared to the SPEI Global Databases values (upper right).

Looking at the three other SPEI maps, TW, FAO56PM and PT, all of them have normal to wet condition values from around 0 to 2.0 in the middle of Germany. First, the TW map shows extreme dry conditions in the North West of Germany which spreads to the North East. Southern Germany is affected by normal to wet conditions according to the map. Subsequently, the FAO56PM map shows some southern and middle eastern

parts which are affected by extreme drought while the rest of the map is covered by a severe drought condition. Lastly, the PT map shows the rest of the country in a normal condition except Southern Germany where there are dry conditions.

5.1.2 Remote Sensing Data

For the remote sensing calculation, the FAO-56 Penman-Monteith (FAO56PM) PET equation is used because the value progression for the weather station SPEI was relatively similar to the SPEI DB like in the Figures 5.3 and 5.5. Also the founders of the SPEI Vicente-Serrano et al. (2010) use the FAO56PM PET equation for their SPEIbase (Beguería, 2010). For these reasons, the Thornthwaite and Hargreaves PET equation was decided against, although it had the lowest difference to the SPEIbase in Figure 5.2.

Quantity Distribution

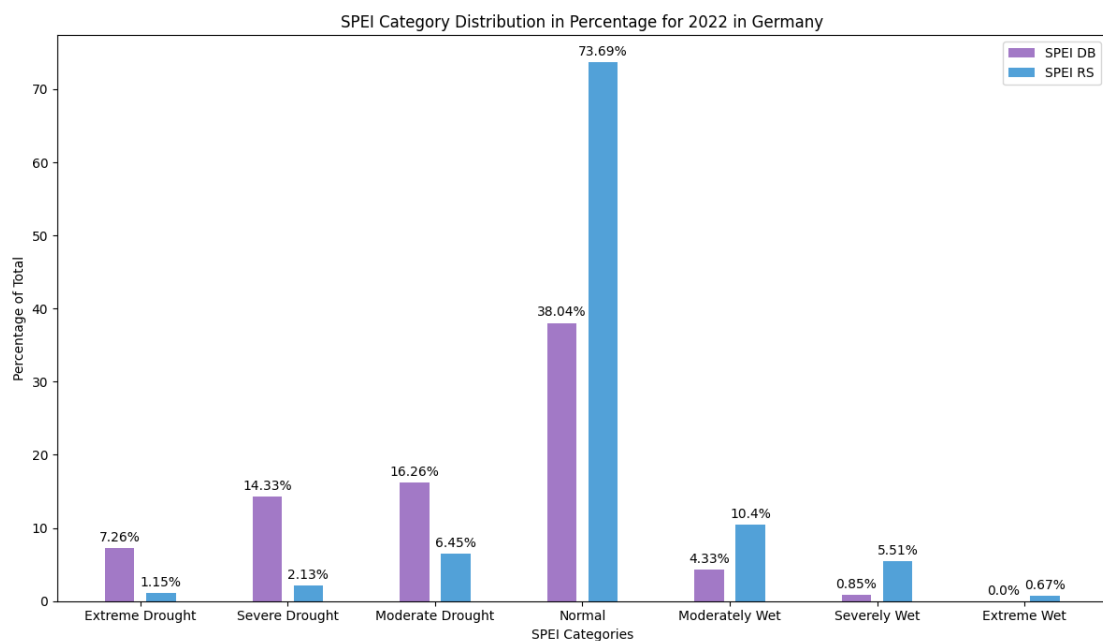


Figure 5.7: 1-month SPEI value distribution comparison in percentage between the SPEIbase (Beguería, 2010) (SPEI DB) and the remote sensing SPEI (SPEI RS) for the year 2022.

Figure 5.7 shows the SPEI value distribution in percentage for the year 2022 in Germany. The SPEIbase (Beguería, 2010) (SPEI DB) is compared to the SPEI calculated using remote sensing data (SPEI RS). The categories include extreme drought, severe drought, moderate drought, normal, moderately wet, severely wet, and extreme wet.

The most notable observation is the significant difference in the proportion of the Normal category between the two datasets. SPEI RS shows a higher percentage of normal conditions (73.69%) compared to SPEI DB (38.04%). Conversely, SPEI DB indicates a higher occurrence of drought conditions (extreme, severe, and moderate) compared to SPEI RS. The categories of moderately wet, severely wet, and extreme wet show relatively low percentages (4.33% to 0.00%) across the SPEI DB. The SPEI RS has more than two times the percentage for moderately wet (10.40%), more than six times the percentage for severely wet (5.51%), and an extreme wet value of 0.67%.

Overall the SPEI RS has a more equal distribution compared to the SPEI DB which indicates more drought areas.

Maximum Comparison

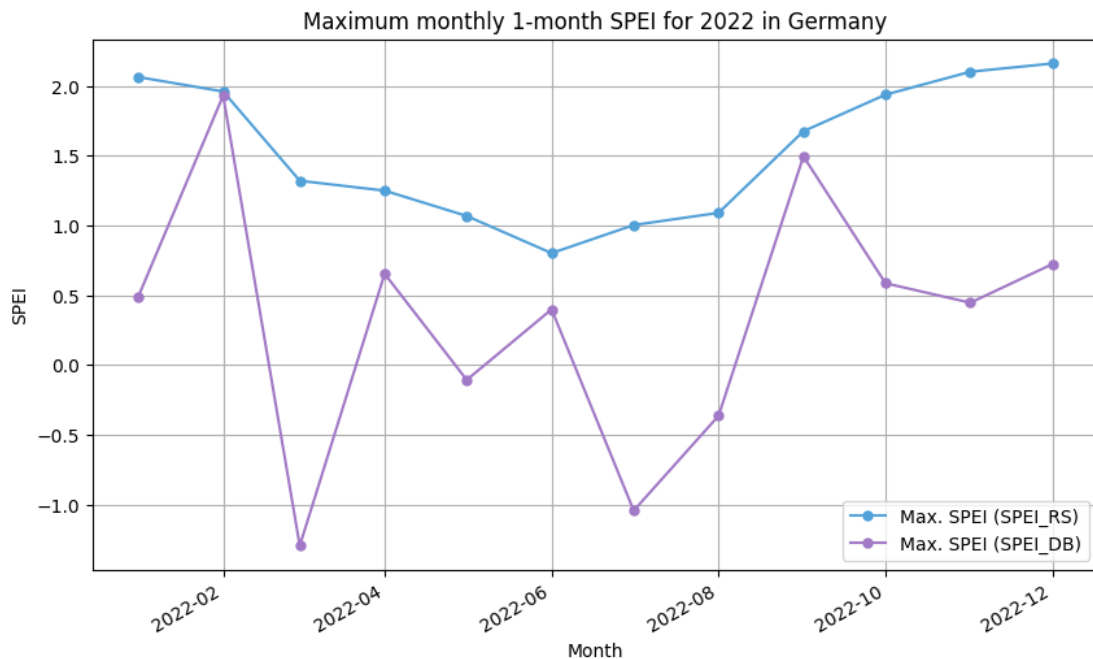


Figure 5.8: Comparison of the max. 1-month SPEI values using remote sensing data for the year 2022 in Germany compared to the SPEIbase (Beguería, 2010). The remote sensing SPEI (*blue*) starts in January 2022 at 2.1, falls month by month to 0.75 in June 2022, and then rises to 2.2 in December 2022. The values for the SPEIbase are not smooth and rise and fall from month to month having the maximum at 2.8 and the minimum at -1.3.

A comparison of the maximum monthly 1-month SPEI value for the year 2022 in Germany is shown in Figure 5.8. The dataset SPEI RS starts in January 2022 with above 2.0 and the SPEI DB starts with 0.5 which is a difference of around 1.5. The two months with the smallest difference are February and September. In March 2022 the biggest difference of 2.5 is measured. Overall the SPEI RS datasets show a smoother graph with a comprehensible reduction of the SPEI in the warmer spring and summer months while the SPEI DB values jump up and down from positive to negative which makes it less predictable.

Mean Comparison

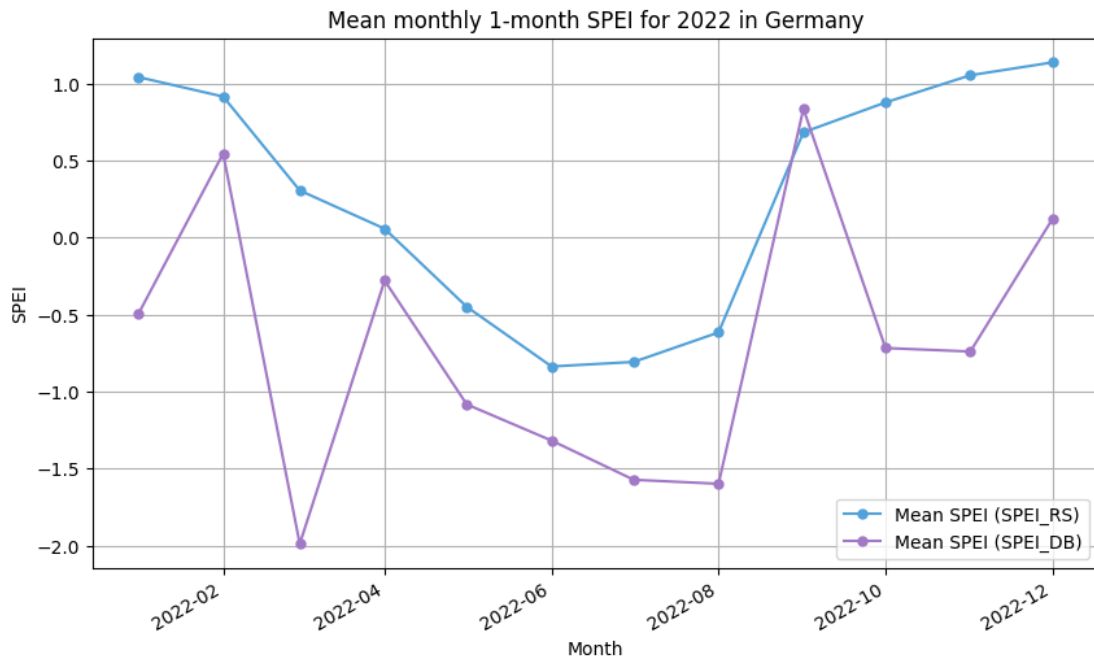


Figure 5.9: Comparison of the mean 1-month SPEI values using remote sensing data for the year 2022 in Germany compared to the SPEIbase (Beguería, 2010). The remote sensing SPEI (*blue*) starts in January 2022 at 1.1, drops to -0.7 in June 2022, and then rises to 1.25 in December 2022. On the other hand the values of the SPEIbase (*purple*) have no pattern as the values rise and fall except for April to August where the values are relatively close to the remote sensing SPEI. The mean difference between the values is ≈ 0.9058 .

Figure 5.9 shows the mean monthly 1-month SPEI values compared between the remote sensing SPEI and the SPEIbase(Beguera, 2010) for 2022 in Germany.

The SPEI RS graphs show a smooth graph when starting in January 2022 with above 1.0 and going into the warm summer months with -0.35 (June 2022). For the autumn and winter, the SPEI increases again to around 1.2. In comparison, the SPEI DB starts in January 2022 at -0.5 and jumps up and down from 0.5 to -2.0 between February 2022 and April 2022. Starting from April 2022 to September 2022 the slope is quite similar to the SPEI RS although the values differ between 0.5 to 1.0. The raising and lowering of SPEI values for the SPEI DB dataset continues from September 2022. On average the difference between both SPEI values is ≈ 0.9058 .

Overall the SPEI RS has a more comprehensible and smooth graph line while the SPEI DB values are rising and lowering expected for April 2022 to September 2022.

Minimum Comparison

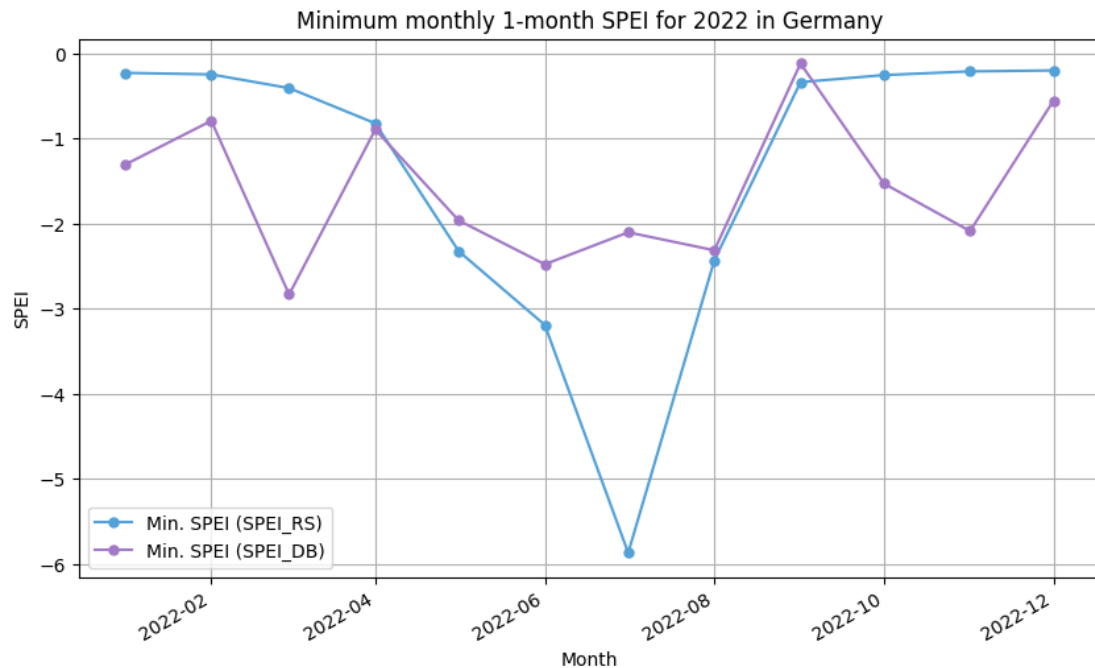


Figure 5.10: Comparison of the min. 1-month SPEI values using remote sensing data for the year 2022 in Germany compared to the SPEIbase (Beguería, 2010). The remote sensing SPEI (*blue*) has SPEI values from 0.2 to 0.9 in the autumn to spring months while in the summer the SPEI drops to -6. For the SPEIbase (*purple*) the SPEI values range between -2.9 and 0.1 and have no actual pattern.

Figure 5.10 compares the minimum monthly 1-month SPEI values derived from remote sensing data with those from the SPEIbase (Beguería, 2010).

In this graph, the SPEI values from the SPEIbase show fluctuations, with values oscillating from month to month, such as the period from February to April 2022. From April to September 2022, the values are quite similar with a maximum difference of 0.5, except for July 2022 where the remote sensing SPEI is approximately 5.8, contrasting sharply with the SPEIbase value of -2.1.

Overall the SPEI RS has a smooth graph again except for July 2022 where a considerable drop happened while the SPEI DB values were relatively stable in the summer months.

5.1.3 Result Comparison

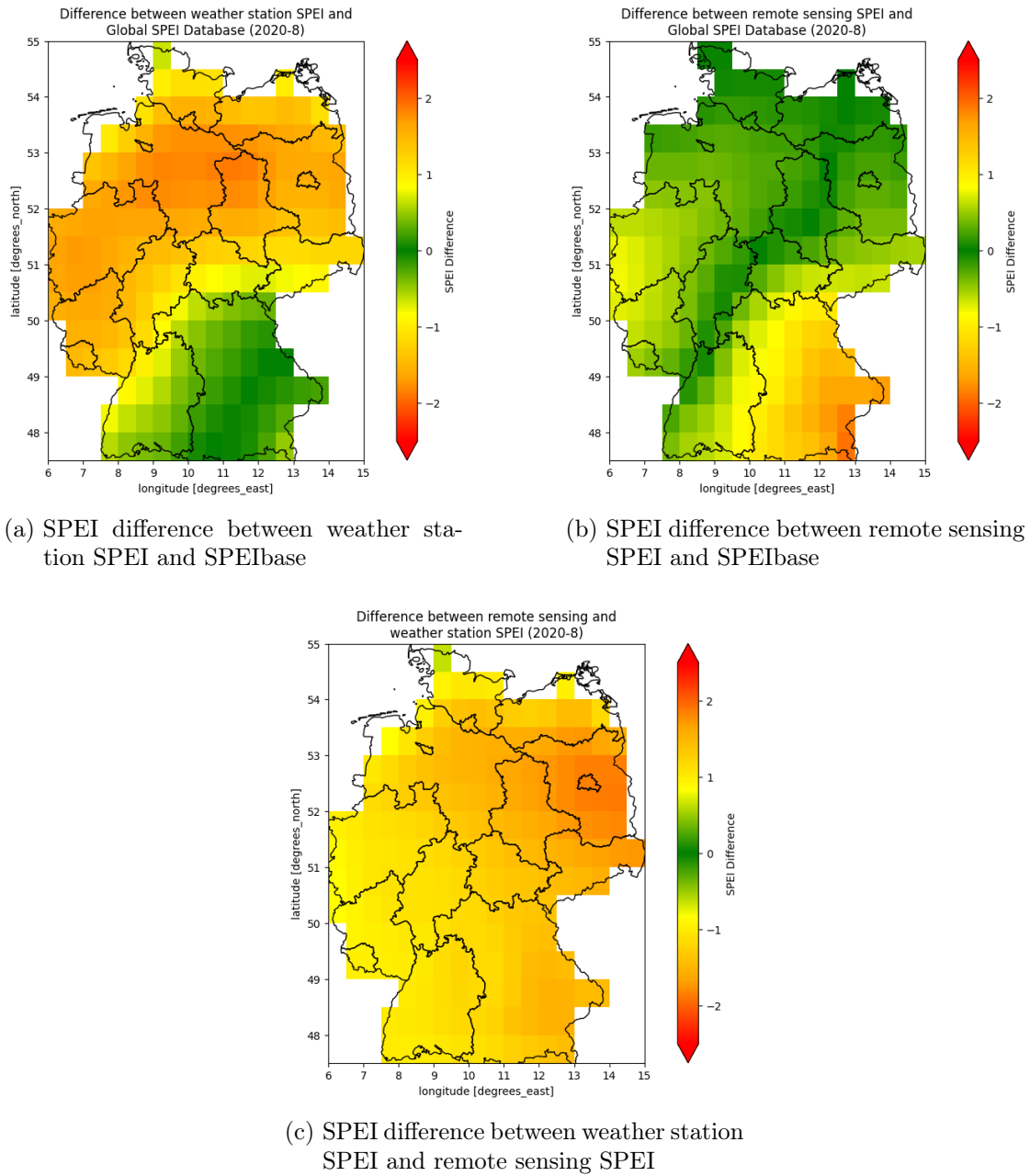


Figure 5.11: SPEI differences between the results of the weather station SPEI, the remote sensing SPEI, and the SPEIbase represented as maps for August 2020 in Germany. The difference between the remote sensing SPEI and SPEIbase is the least while the difference between the weather station and remote sensing SPEI is the most.

Figure 5.11 presents the differences between the SPEI results as map plots for visual comparison. The date was chosen randomly as several months compared show nearly the same results, which are detailed in the following sections.

The SPEI difference between the weather station SPEI and the SPEIbase in 5.11a shows a difference near ± 0 in Southern Germany which is less than a third of the land area of Germany. From the Middle West to the North East a SPEI difference from around ± 1.5 is spotted.

For 5.11b the SPEI difference between the remote sensing SPEI and the SPEIbase ranges in the greenish area (SPEI from 0.7 to -0.7) in 45.83% of the land area, primarily from South to North, with the most significant matching in the North West to North East regions. In the Middle West are yellow areas spotted which indicates a difference from around ± 1.0 . Also in the South Western part of Germany, the difference rises to approximately ± 1.2 .

The third image 5.11c shows the SPEI difference between the remote sensing SPEI and the weather station SPEI. The land area is nearly covered in at least a yellow color which shows a SPEI difference of ± 1.0 while parts in the Middle East around Berlin are orange which shows a SPEI difference of ± 1.5 .

In summary, the comparison of SPEI differences across various sources highlights significant regional variations in Germany, with minimal differences in Southern Germany and greater discrepancies from the Middle West to the North East. The weather station and SPEIbase show minimal differences in Southern Germany but greater discrepancies from the Middle West to the North East. The remote sensing SPEI aligns with the SPEI base in 20% of the land area, predominantly from South to North, with notable differences in the Middle West and South Western regions. The comparison between remote sensing and weather station SPEI reveals widespread differences, particularly around Berlin (North East).

5.2 Comparison with SMI

To validate the calculated SPEI values the SMI dataset for upper and total soil by the Helmholtz Zentrum für Umweltforschung (2024) has been consulted. Both indices have been compared to each other to identify a possible correlation using the Pearson and distance correlation formulae.

5.2.1 Upper soil

Correlation between the weather station, remote sensing, and SPEIbase SPEI and the SMI (upper soil).

Weather Station SPEI

Pearson Correlation

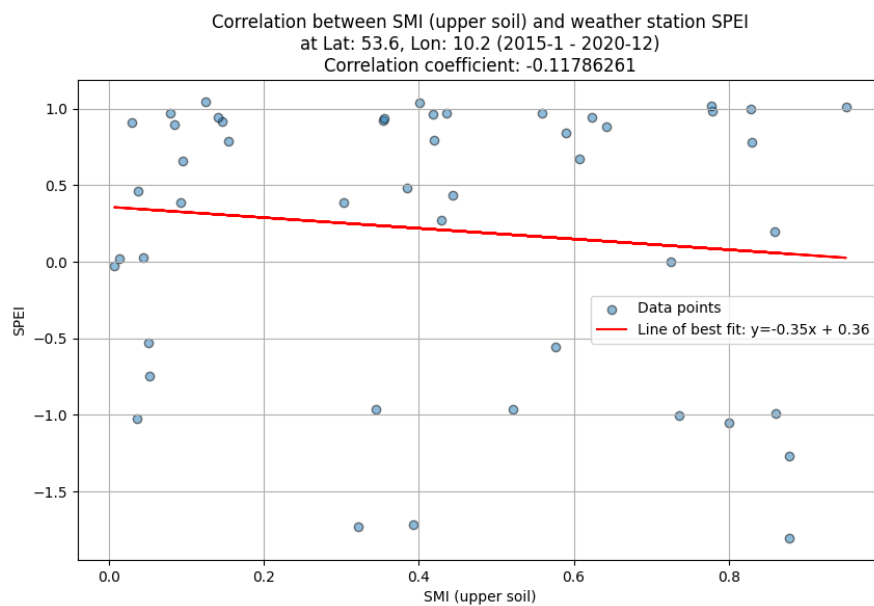


Figure 5.12: Pearson correlation between interpolated SMI of the upper soil (up to 25cm deep) and the 1-month SPEI in the date range 1st January 2015 to 31st December 2018 represented by a scatter plot. The Pearson correlation coefficient is ≈ -0.1179 .

Figure 5.12 shows a scatter plot that illustrates the Pearson correlation between the interpolated Soil Moisture Index (SMI) from the upper soil (up to 25cm deep) and the 1-month Standardized Precipitation-Evapotranspiration Index (SPEI) over the period from 1st January 2015 to 31st December 2018. Each point on the graph represents a paired observation of SMI and SPEI, with the x-axis representing SMI values and the y-axis representing SPEI values.

The data points are dispersed widely across the plot, suggesting variability in both indices. A regression line, depicted in red, is superimposed on the scatter plot to indicate the trend in the data. The equation of the regression line is given as $y = -0.31 + 0.34x$, where the slope (-0.31) indicates a very negative relationship between SMI (upper soil) and weather station 1-month SPEI, and the y-intercept (0.34) represents the expected value of SPEI when SMI is 0. The correlation coefficient between SMI and SPEI is calculated to be approximately -0.0983 .

Distance Correlation

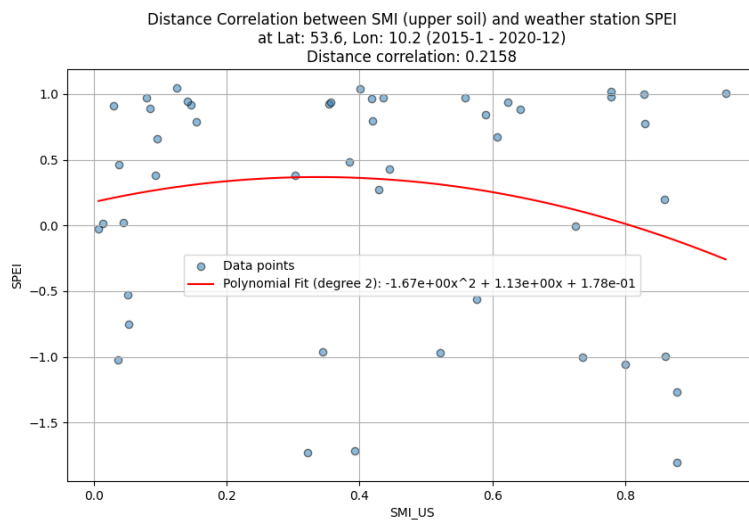


Figure 5.13: Distance correlation: 1-month Weather Station SPEI and SMI (upper soil) for the period January 2012 to December 2012 at latitude 53.6 and longitude 10.2 in Germany. The distance correlation coefficient is 0.2158.

The distance correlation between the 1-month weather station SPEI and the SMI of the upper soil is shown in Figure 5.13, which shows a distance correlation coefficient of

0.2068. The polynomial fit initially shows as SMI increases, SPEI also increases, reaching a peak at an SMI of ≈ 0.3 before declining as SMI continues to rise.

Time Series

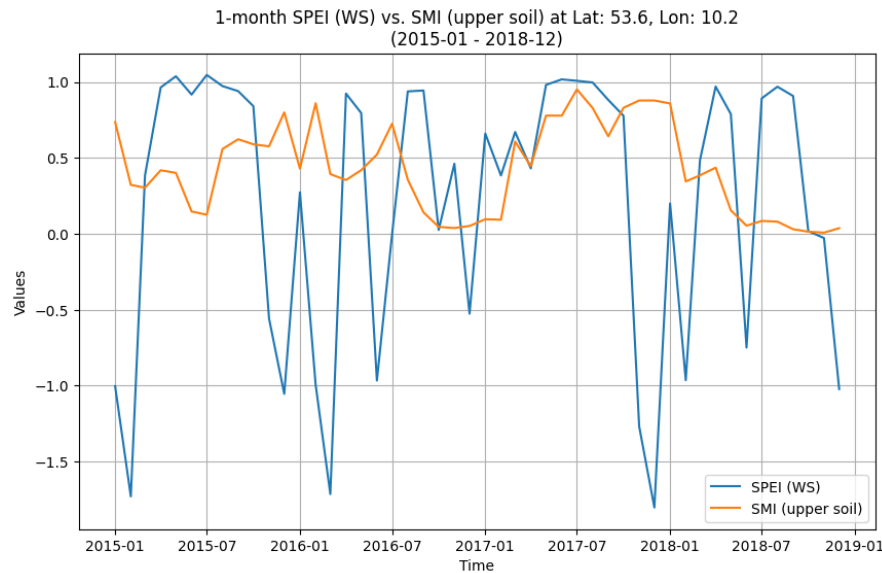


Figure 5.14: Time series of 1-month weather station SPEI (*blue*) and SMI (upper soil) (*orange*). The SMI of the upper soil ranges between 0 and 1.9 while the SPEI ranges from -1.4 to 1.1. Overall the graphs do not have a similar course except for the period March 2017 to July 2017.

Figure 5.14 represents a time series comparison of the 1-month weather station SPEI and the SMI for the upper soil at latitude 53.6 and longitude 10.2 from January 2015 to December 2018.

For the summer months around July, the SPEI WS shows the highest SPEI values of approximately 1.0 while the SMI is low in these months like in 2015, and also high like in 2017, so it does not show an actual pattern. The SPEI values change quickly from positive in one month going to negative in the other month, as shown for September 2015 to November 2015 where the SPEI changes from 0.85 to -1.05. Also visually one can identify no correlation between the 1-month weather station SPEI and the SMI of the upper soil.

Remote Sensing SPEI

Pearson Correlation

Plots showing the Pearson correlation between the interpolated SMI of the upper soil (up to 25cm deep) and n-month remote sensing SPEI in the date range 1st January 2015 to 31st December 2018 are presented in Figure 5.21.

The 1-, 3- and 9-month remote sensing SPEI have a positive near-null Pearson correlation coefficient of ≈ 0.0728 , ≈ 0.0209 and ≈ 0.0559 as well as a y-intercept of -0.01 , 0.10 and 0.23 . While the 6-, 12- and 24-month SPEI have a negative near-null Pearson correlation coefficient of ≈ -0.0336 , ≈ -0.0652 and ≈ -0.4359 . The y-intercepts for this SPEI's correlation with the SMI of the upper soil are 0.26 , 0.53 , and 0.76 .

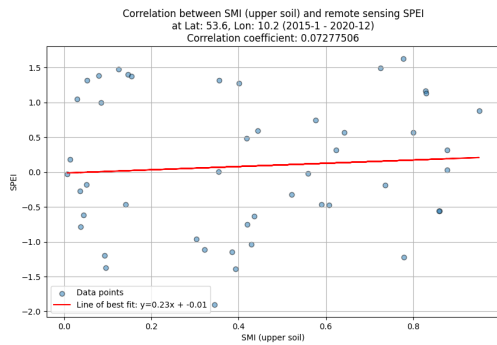


Figure 5.15: Pearson correlation between 1-month Remote Sensing SPEI and SMI (upper soil)

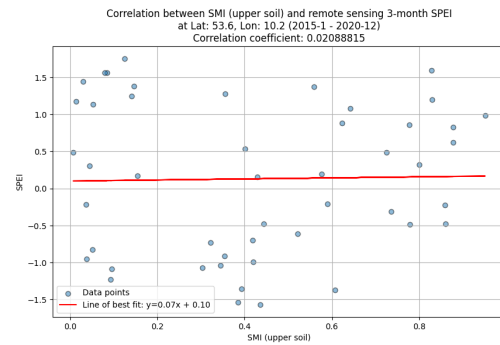


Figure 5.16: Pearson correlation between 3-month Remote Sensing SPEI and SMI (upper soil)

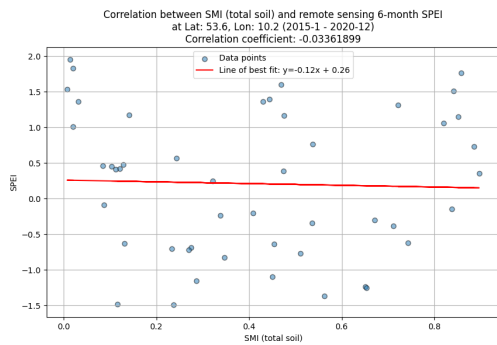


Figure 5.17: Pearson correlation between 6-month Remote Sensing SPEI and SMI (upper soil)

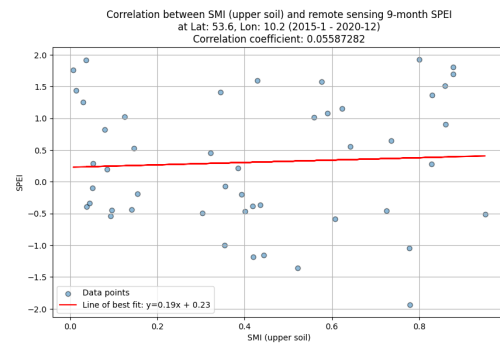


Figure 5.18: Pearson correlation between 9-month Remote Sensing SPEI and SMI (upper soil)

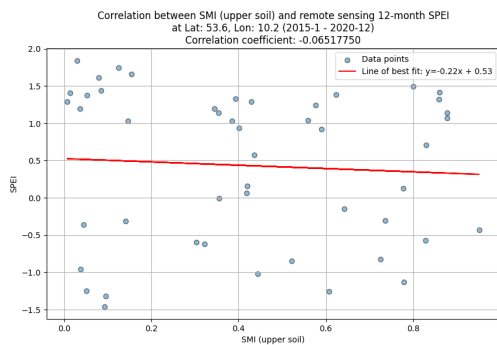


Figure 5.19: Pearson correlation between 12-month Remote Sensing SPEI and SMI (upper soil)

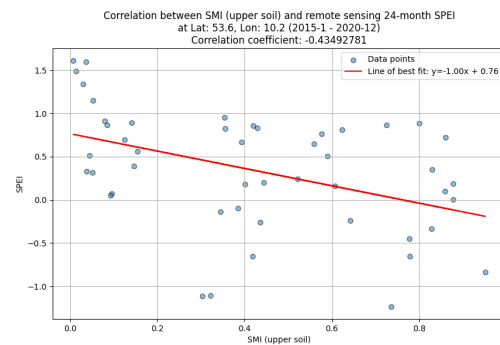


Figure 5.20: Pearson correlation between 24-month Remote Sensing SPEI and SMI (upper soil)

Figure 5.21: Pearson correlation analysis between the n-month Remote Sensing SPEI and the SMI for the upper soil at different time scales (1, 3, 6, 9, 12, 24) at the location with latitude 53.6 and longitude 10.2, from January 2015 to December 2018.

Distance Correlation

In Figure 5.28 the distance correlation between the n-month remote sensing SPEI and the SMI of the upper soil are shown for the time scales 1, 3, 6, 9, 12, and 24.

The 3- and 6-month have a distance correlation coefficient of 0.2919 and 0.3057 resulting in a similar polynomial fit of degree 2. Initially, the SPEI is at ≈ 0.67 to ≈ 0.82 when the SMI is 0. When the upper soil SMI rises to 0.4, the SPEI decreases to ≈ 0.35 . After that, the SMI rises while the SPEI does, too.

This behavior is also seen for the 1-, 9-, and 12-month remote sensing SPEI and the upper soil SMI, which have a distance correlation coefficient of 0.3057, 0.2582, and 0.1888, but with a flatter polynomial fit of degree with only a slight curve having a shallow dip around SMI of 0.4.

The polynomial fit curve of the 24-month remote sensing SPEI and the SMI (upper soil) differs from the other results, while the distance correlation coefficient is the highest of all with 0.4252. The SPEI is ≈ 0.9 when the SMI is 0 and the SPEI decreases to 0 when the SMI is at ≈ 0.76 . After that, the SPEI slightly rises again to below 0.1 when the SMI is at ≈ 0.92 .

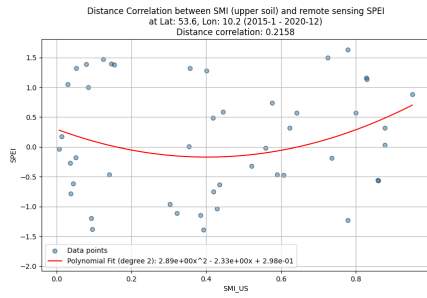


Figure 5.22: Distance correlation: 1-month Remote Sensing SPEI and SMI (upper soil)

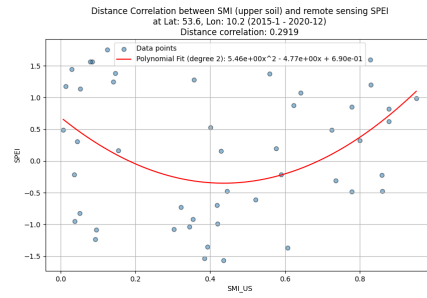


Figure 5.23: Distance correlation: 3-month Remote Sensing SPEI and SMI (upper soil)

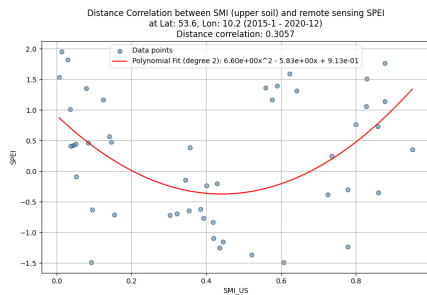


Figure 5.24: Distance correlation: 6-month Remote Sensing SPEI and SMI (upper soil)

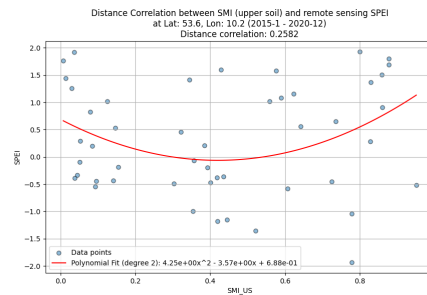


Figure 5.25: Distance correlation: 9-month Remote Sensing SPEI and SMI (upper soil)

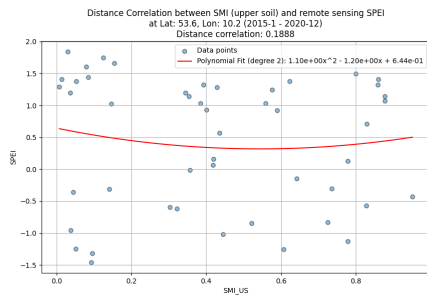


Figure 5.26: Distance correlation: 12-month Remote Sensing SPEI and SMI (upper soil)

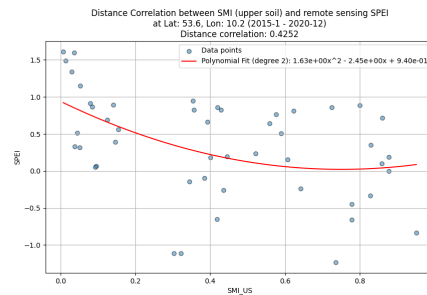


Figure 5.27: Distance correlation: 24-month Remote Sensing SPEI and SMI (upper soil)

Figure 5.28: Distance correlation analysis between the n-month Remote Sensing SPEI and the SMI for the upper soil at different time scales (1, 3, 6, 9, 12, 24) at the location with latitude 53.6 and longitude 10.2, from January 2015 to December 2018.

Time Series

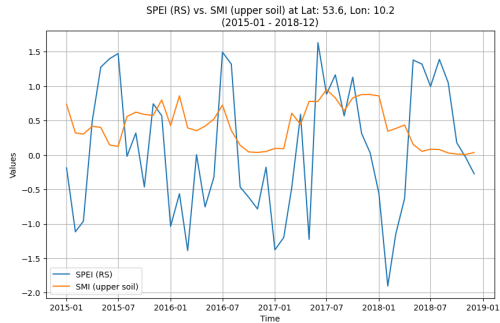


Figure 5.29: 1-month Remote Sensing SPEI vs. SMI (upper soil)

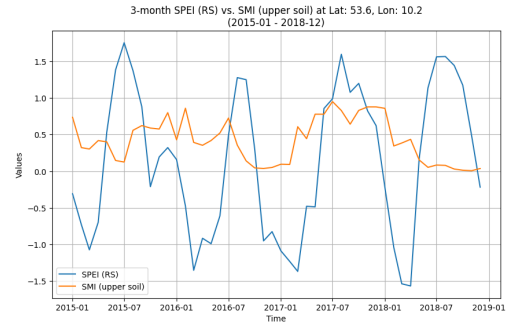


Figure 5.30: 3-month Remote Sensing SPEI vs. SMI (upper soil)

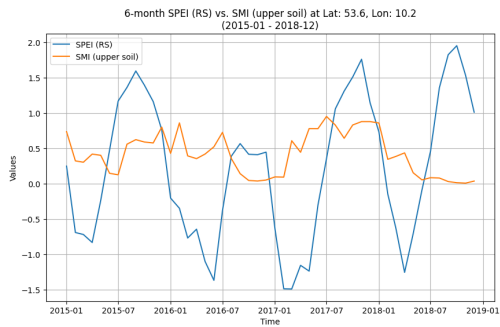


Figure 5.31: 6-month Remote Sensing SPEI vs. SMI (upper soil)

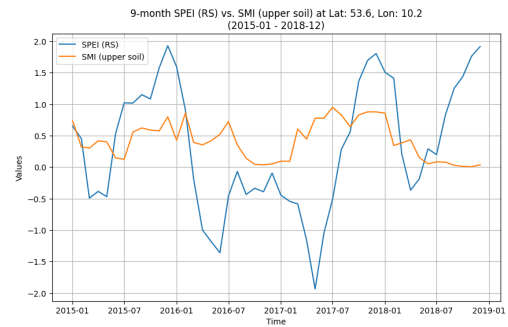


Figure 5.32: 9-month Remote Sensing SPEI vs. SMI (upper soil)

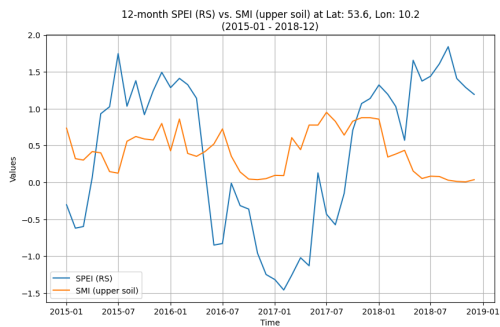


Figure 5.33: 12-month Remote Sensing SPEI vs. SMI (upper soil)

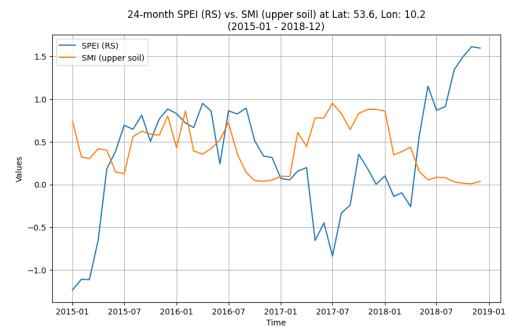


Figure 5.34: 24-month Remote Sensing SPEI vs. SMI (upper soil)

Figure 5.35: Visual comparison between the n-month remote sensing SPEI and the SMI for the upper soil at different time scales (1, 3, 6, 9, 12, 24) at the location with latitude 53.6 and longitude 10.2, from January 2015 to December 2018.

The 1-month to 24-month remote sensing SPEI is compared to the SMI of the upper soil for the period from January 2015 to December 2018 at the latitude 53.6 and longitude 10.2 in Figure 5.35.

The plots already show why the 24-month remote sensing SPEI has the highest distance correlation of 0.4252 because value development in the period between March 2015 and January 2017 is similar. However, the similar value development vanishes beginning from January 2017 to December 2018.

SPEIbase

Pearson Correlation

Figure 5.36 presents the Pearson correlation scatter plot between the monthly interpolated SMI of the upper soil and the 1-month SPEI from SPEIbase (Beguería, 2010) between January 2015 and December 2018. It shows that the correlation coefficient is 0.00244977 while the line of best fit shows a slight slope of 0.01.

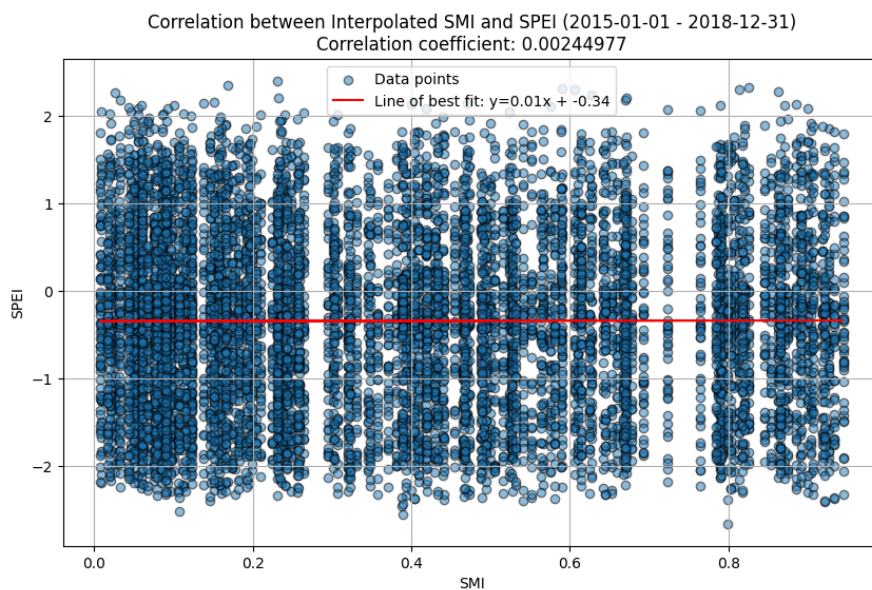


Figure 5.36: Pearson correlation between the monthly interpolated SMI (upper soil) and the 1-month SPEI from SPEIbase for the period from January 2015 to December 2018 with a correlation coefficient of 0.00244977

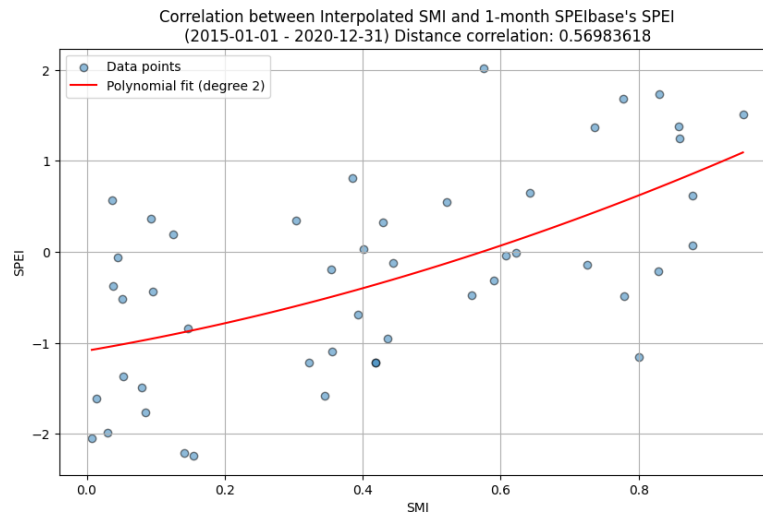
Distance Correlation

Figure 5.37: Distance correlation: 1-month SPEIbase SPEI and SMI (upper soil) from January 2015 to December 2018 at latitude 53.6 and longitude 10.2. The distance correlation coefficient is 0.56983618.

Comparing the 1-month SPEIbase SPEI and the upper soil SMI to calculate the distance correlation resulted in a distance correlation coefficient of ≈ 0.5698 , which is presented in Figure 5.37. The polynomial fit curve shows that the SPEI is at ≈ -1.05 when the SMI is 0. A near-linear curve follows showing that the SPEI rises when the SMI rises as well. At an SPEI of 0, the SMI has a value of 5.78.

Time Series

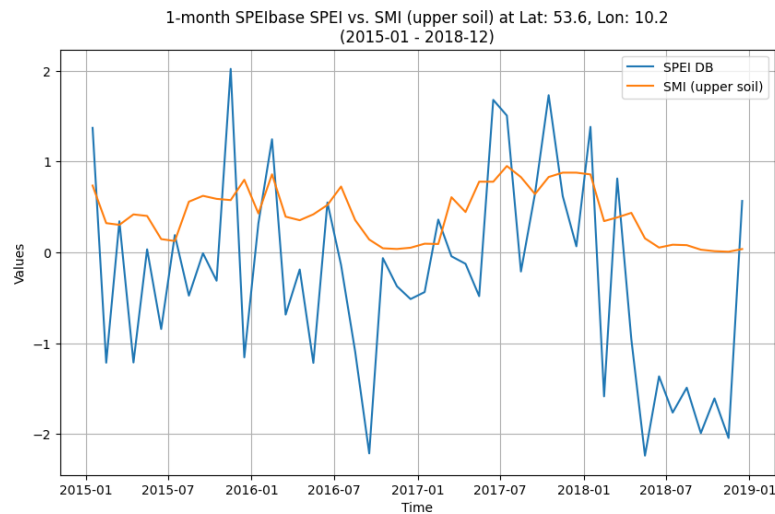


Figure 5.38: Time series of 1-month SPEIbase SPEI (*blue*) and SMI (upper soil) (*orange*) from January 2015 to December 2018 at latitude 53.6 and latitude 10.2.

In Figure 5.38 the time series of the 1-month SPEIbase SPEI and the upper soil SMI for the period of January 2015 to December 2023 at the latitude 53.6 and longitude 10.2 is shown. The graphs show that it is visually recognizable that there are some similar changes in values, such as between July 2016 and October 2016, where the SMI falls while the SPEI also falls. The opposite behavior can be seen for the period from February 2017 to July 2017.

5.2.2 Total soil

Correlation between the weather station, remote sensing, and SPEIbase SPEI and the SMI (total soil).

Weather Station SPEI

Pearson Correlation

Figure 5.39 shows the Pearson correlation between the interpolated SMI of the total soil and SPEI in the period January 2015 to December 2018. The value -0.31 is the slope of the line of best fit ($y = -0.31x + 0.34$) which represents a slight negative, but nearly no, relationship between the SMI (total soil) and the weather station 1-month SPEI.

The y-intercept 0.34 represents the expected value of SPEI when SMI is 0. A Pearson coefficient of ≈ -0.09829 has been calculated for the relationship of the two datasets.

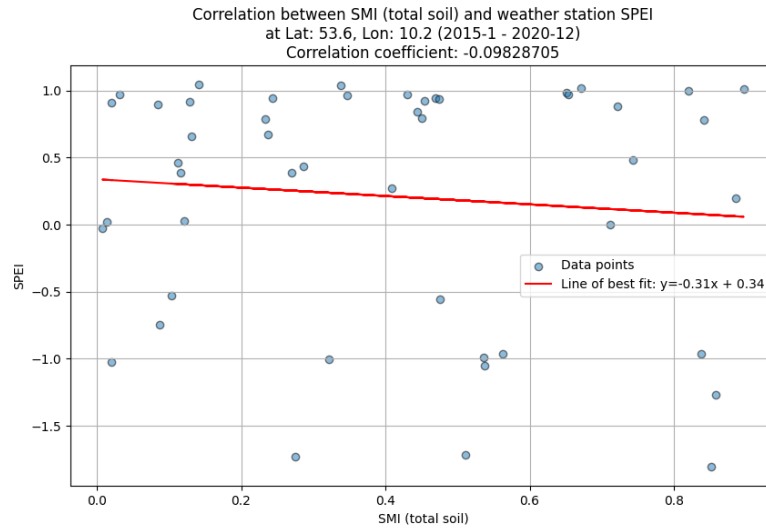


Figure 5.39: Pearson correlation: 1-month Weather Station SPEI and SMI (total soil) from January 2015 to December 2018 at latitude 53.6 and latitude 10.2. The Pearson correlation coefficient is -0.09828705 .

Distance Correlation

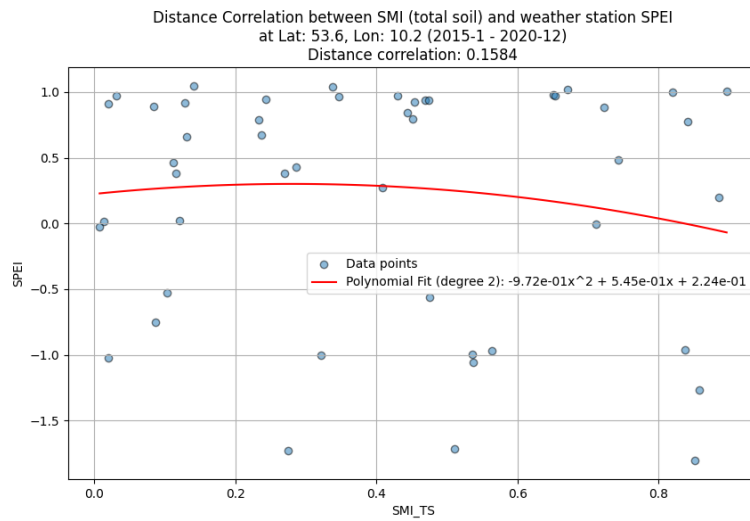


Figure 5.40: Distance correlation: 1-month Weather Station SPEI and SMI (total soil) from January 2015 to December 2018 at latitude 53.6 and longitude 10.2. The distance correlation is 0.1584.

A distance correlation coefficient of 0.1584 has been calculated for the 1-month weather station SPEI and the SMI of the total soil in Figure 5.40. The data ranges from January 2015 to December 2018 representing the location at latitude 53.6 and longitude 10.2. The curve of the polynomial fit has a small negative bulge, with the SPEI rising slightly up to the SMI of 0.3 and then falling more steeply than before. The SPEI ranges between ≈ -0.1 and 0.36.

Time Series

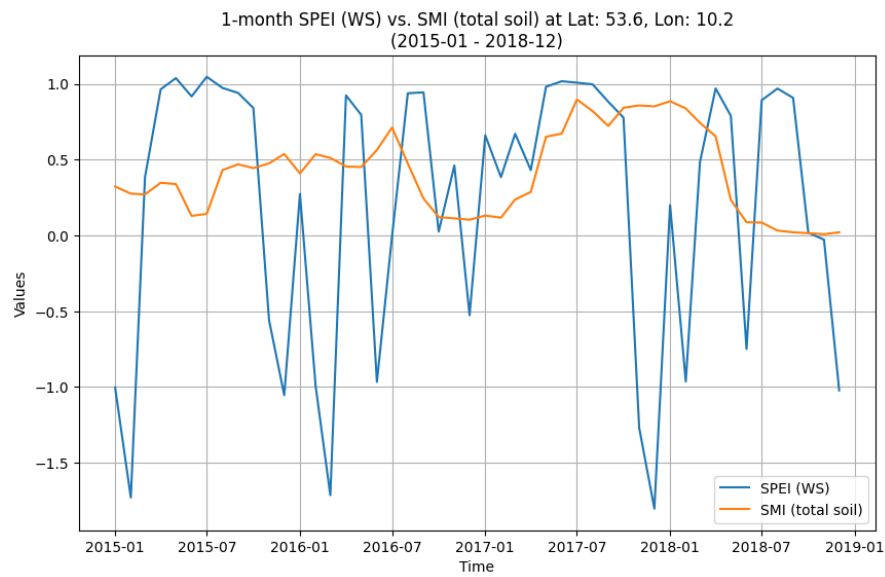


Figure 5.41: Comparison: 1-month Weather Station SPEI and SMI (total soil)

Also, the value comparison is shown in Figure 5.41 and it shows that the SPEI and SMI only have a partially negative reciprocal relationship with each other. In the period September 2015 to April 2016 for example the SPEI jumps from 0.85 down to -1.7 while the SMI remains around 0.5. However, it can also be observed that there is a phase, such as between August 2016 and March 2017, in which the SPEI and SMI fall, even if not synchronously.

Remote Sensing SPEI

Pearson Correlation

5 Results

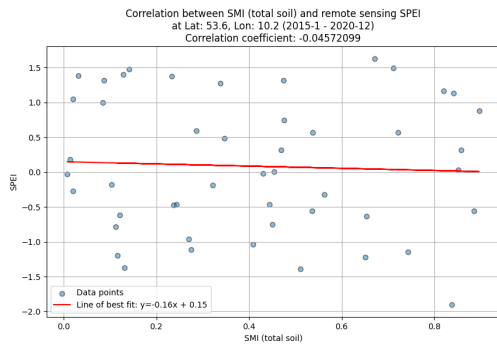


Figure 5.42: Pearson correlation between 1-month Remote Sensing SPEI and SMI (total soil)

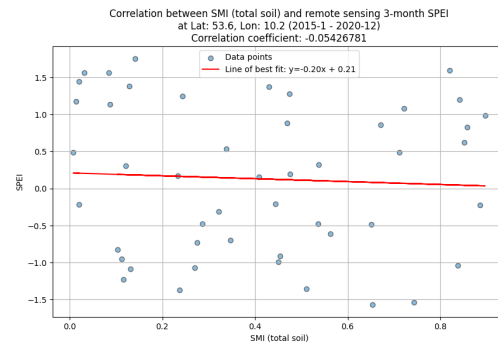


Figure 5.43: Pearson correlation between 3-month Remote Sensing SPEI and SMI (total soil)

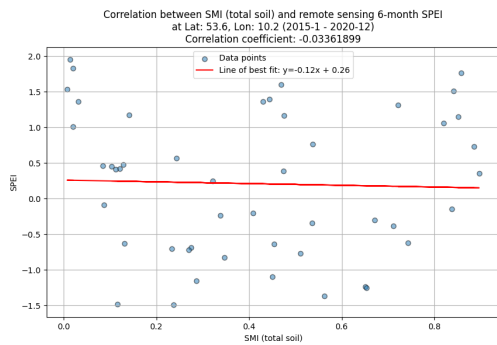


Figure 5.44: Pearson correlation between 6-month Remote Sensing SPEI and SMI (total soil)

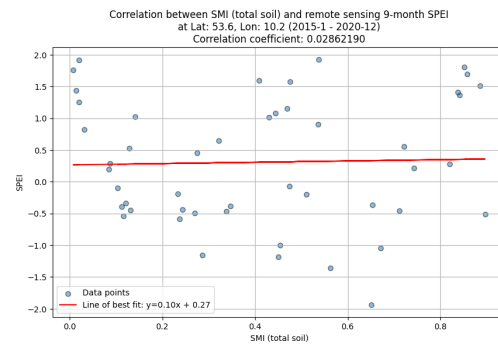


Figure 5.45: Pearson correlation between 9-month Remote Sensing SPEI and SMI (total soil)

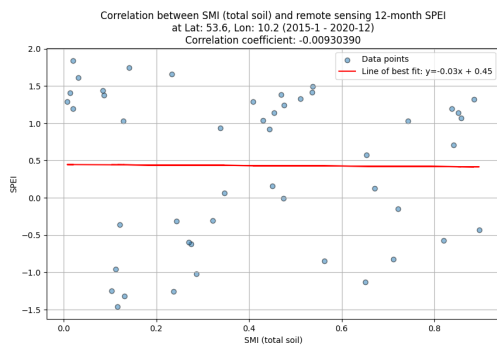


Figure 5.46: Pearson correlation between 12-month Remote Sensing SPEI and SMI (total soil)

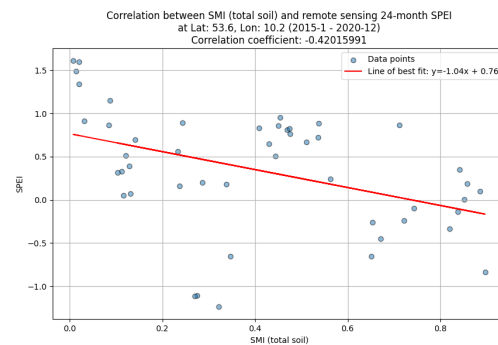


Figure 5.47: Pearson correlation between 24-month Remote Sensing SPEI and SMI (total soil)

Figure 5.48: Pearson correlation analysis between the n-month Remote Sensing SPEI and the SMI for the total soil at different time scales (1, 3, 6, 9, 12, 24) at the location with latitude 53.6 and longitude 10.2, from January 2015 to December 2018.

The Pearson correlation between the n-month Remote Sensing SPEI and the SMI for the total soil at different time scales (1, 3, 6, 9, 12, 24) for the period from January 2015 to December 2018 at the latitude 53.6 and longitude 10.2 is shown in Figure 5.48.

Only the 9-month remote sensing SPEI (Figure 5.45) has a slight positive correlation with a correlation coefficient of 0.0286, which is still near to no correlation, while the 1-, 3-, 6-, 12-, and 24-month remote sensing SPEI show a negative correlation near zero having the values ≈ -0.0457 , ≈ -0.0542 , ≈ -0.0336 and ≈ -0.009 . The most negative correlation is reached by the 24-month remote sensing SPEI in Figure 5.47 with a negative correlation coefficient of -0.4201 .

Distance Correlation

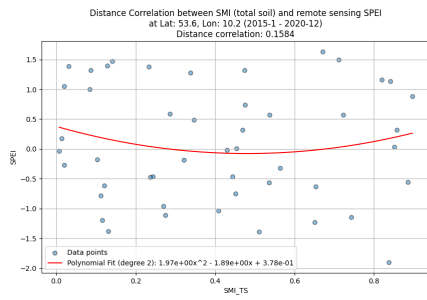


Figure 5.49: Distance correlation: 1-month Remote Sensing SPEI and SMI (upper soil)

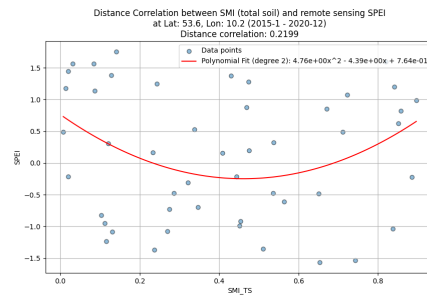


Figure 5.50: Distance correlation: 3-month Remote Sensing SPEI and SMI (upper soil)

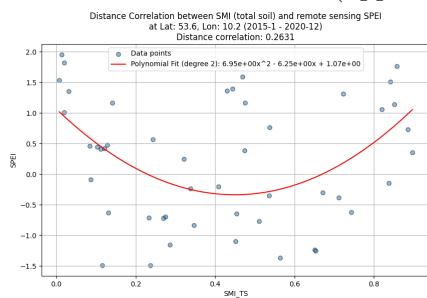


Figure 5.51: Distance correlation: 6-month Remote Sensing SPEI and SMI (upper soil)

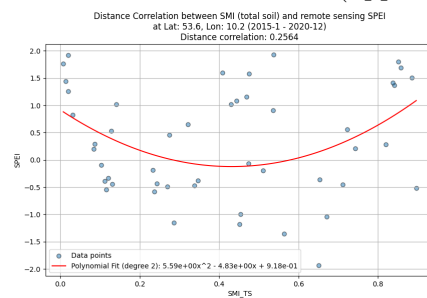


Figure 5.52: Distance correlation: 9-month Remote Sensing SPEI and SMI (upper soil)

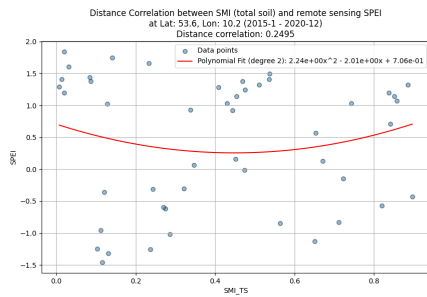


Figure 5.53: Distance correlation: 12-month Remote Sensing SPEI and SMI (upper soil)

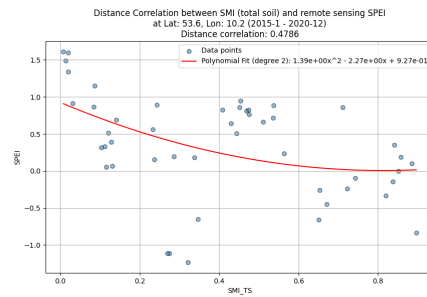


Figure 5.54: Distance correlation: 24-month Remote Sensing SPEI and SMI (upper soil)

Figure 5.55: Distance correlation analysis between the n-month Remote Sensing SPEI and the SMI for the upper soil at different time scales (1, 3, 6, 9, 12, 24) at the location with latitude 53.6 and longitude 10.2, from January 2015 to December 2018.

As shown in Figure 5.55 the distance correlation between the n-month Remote Sensing SPEI and the SMI for the upper soil at different time scales (1, 3, 6, 9, 12, 24) at the location with latitude 53.6 and longitude 10.2, from January 2015 to December 2018 is presented.

For the 1-month SPEI, the distance correlation is 0.1584. At 3 months, the correlation increases to 0.2199, and for 6 months, it further rises to 0.2631. The 9-month correlation slightly decreases to 0.2564, followed by a marginal drop to 0.2495 at the 12-month timescale. All polynomial fit curves show the typical curvature of a polynomial graph, whereby the 1-month SPEI and 12-month SPEI show a significantly weaker curvature, which is more in the direction of a linear graph.

However, at the 24-month timescale, the distance correlation significantly increases to 0.4786 while the polynomial fit curve starts at an SPEI of ≈ 0.82 when SMI is zero and decreases to an SPEI of 0 when the SMI is around 0.8.

Time Series

Figure 5.62 shows time series comparisons between n-month Remote Sensing SPEI and SMI for total soil at different time scales (1, 3, 6, 9, 12, 24) at the location with latitude 53.6 and longitude 10.2, from January 2015 to December 2018.

As with the remote sensing SPEI and the upper soil in Figure 5.35, it can be seen with the SPEI and the total soil in Figure 5.62 that the 24-month SPEI has the most aligning value development compared to the SMI of the total soil.

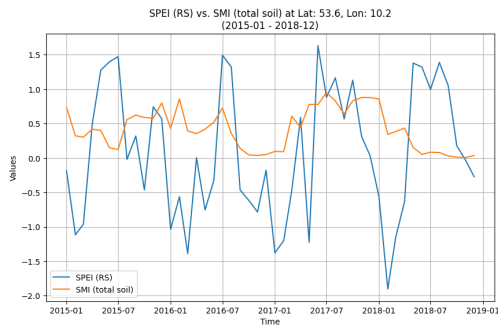


Figure 5.56: 1-month Remote Sensing SPEI vs. SMI (total soil)

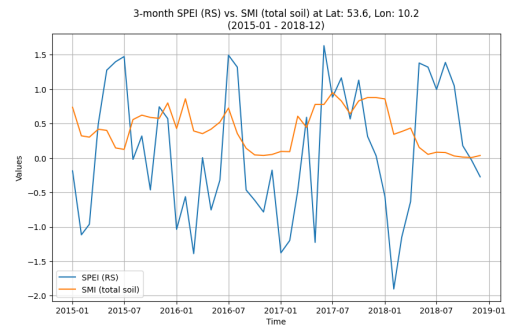


Figure 5.57: 3-month Remote Sensing SPEI vs. SMI (total soil)

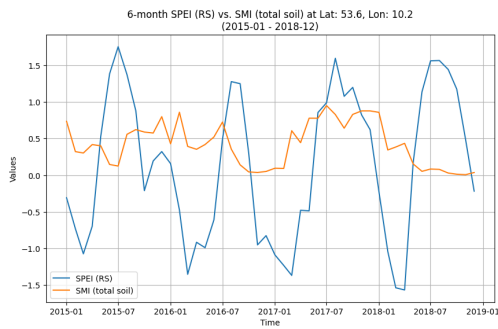


Figure 5.58: 6-month Remote Sensing SPEI vs. SMI (total soil)

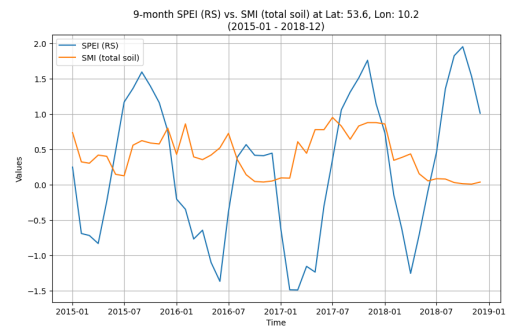


Figure 5.59: 9-month Remote Sensing SPEI vs. SMI (total soil)

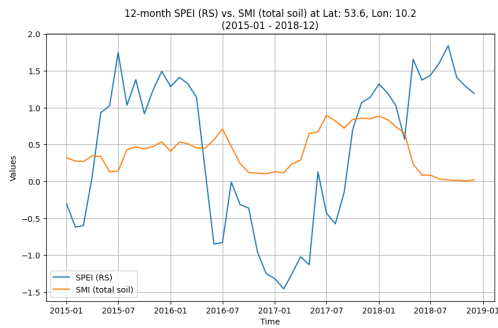


Figure 5.60: 12-month Remote Sensing SPEI vs. SMI (total soil)

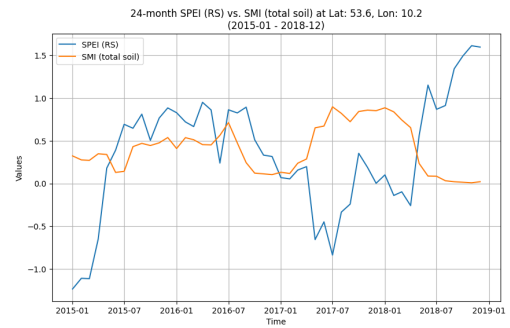


Figure 5.61: 24-month Remote Sensing SPEI vs. SMI (total soil)

Figure 5.62: Time series comparison between n-month Remote Sensing SPEI and SMI for total soil at different time scales (1, 3, 6, 9, 12, 24) at the location with latitude 53.6 and longitude 10.2, from January 2015 to December 2018.

SPEIbase

Pearson Correlation

The Pearson correlation plot between the monthly interpolated SMI of the total soil and the 1-month SPEI from SPEIbase (Beguería, 2010) for the period from January 2015 to December 2018 in Figure 5.63 shows a correlation coefficient of ≈ 0.0096 . When the SMI is 0, the SPEI is at -0.35 , which the line of best fit ($y = 0.04x + -0.45$) fit shows.

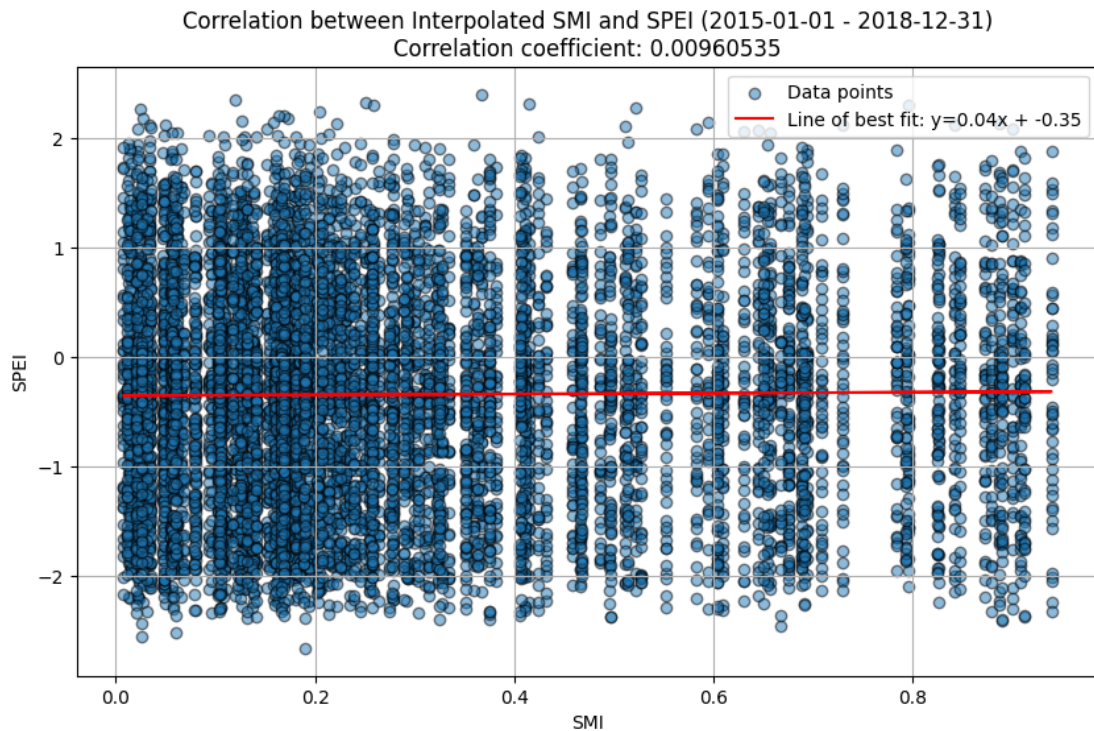


Figure 5.63: Pearson correlation between the monthly SMI (total soil) and the 1-month SPEI from SPEIbase for the period from January 2015 to December 2018 with a correlation coefficient of 0.00960535.

Distance Correlation

The polynomial fit curve for the 1-month SPEIbase SPEI and SMI (upper soil) for the period from January 2015 to December 2018 in Figure 5.64 resembles a linear graph rather than a polynomial graph, while the SPEI is at ≈ -1.06 when the SMI is 0 and the SPEI rises to ≈ 1.66 when the SMI is 0.7.

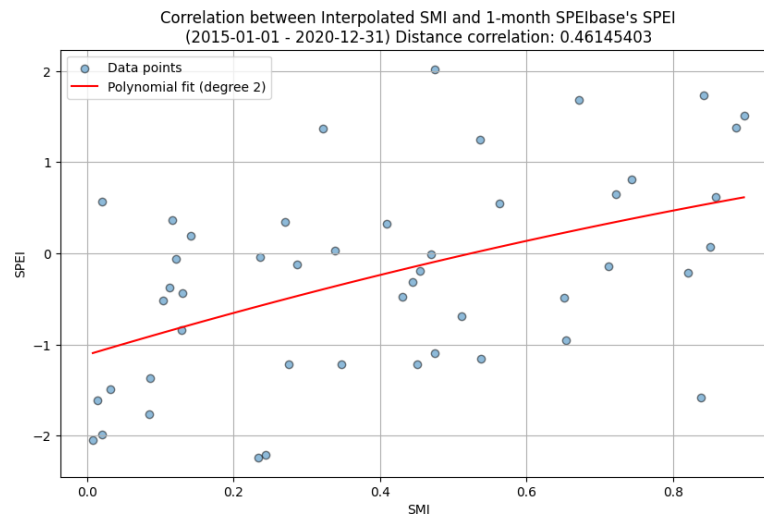


Figure 5.64: Distance correlation: 1-month SPEIbase SPEI and SMI (upper soil) for the period from January 2015 to December 2018 with a correlation coefficient of 0.46145403.

Time Series

In Figure 5.65 the time series of the 1-month SPEIbase SPEI and the total soil SMI for the period of January 2015 to December 2023 at the latitude 53.6 and longitude 10.2 is shown. A similar value development is discovered for example for the period from February 2017 to June 2018 where the SMI and SPEI both rise more or less with a curvature, with the SPEI sometimes fluctuating in value by more than 1.5 from one month to the next.

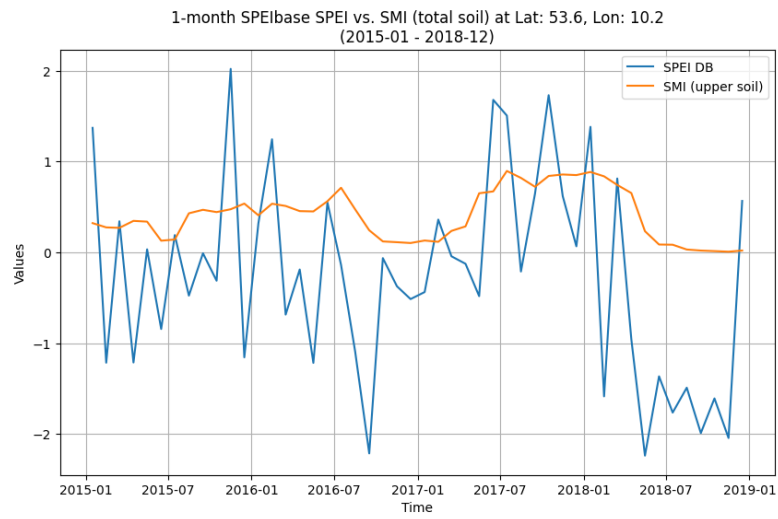


Figure 5.65: Time series of 1-month SPEIbase SPEI (*blue*) and SMI (total) (*orange*) from January 2015 to December 2018 at latitude 53.6 and latitude 10.2.

5.3 Prediction

This section is about the results of the prediction methods for wet and dry periods. As data input the remote sensing SPEI is used for training and testing the outputs of the prediction methods.

5.3.1 Gradient Boosting Regressor

For the prediction a Gradient Boosting Regressor is used, which has been previously explained in the Subsection 3.7.1.

Root Mean Squared Error

The performance of the Gradient Boosting Regressor was evaluated using Root Mean Squared Error (RMSE) as the metric because it represents the mean error in the units of the SPEI.

Initial models The RMSE values for these models with the configuration mentioned in Figure 4.4 are presented in Table 5.3.

| Model | RMSE |
|---------|--------|
| C+DOY | 1.0801 |
| C | 1.0787 |
| L+DOY | 0.3062 |
| L | 0.2963 |
| C+L+DOY | 0.2771 |

Table 5.3: Root Mean Squared Error (RMSE) of different GBR models sorted from highest (top) to lowest RMSE (bottom). The C+DOY model has the highest RMSE, whereas the C+L+DOY model has the lowest. This configuration is set to the same as in Figure 4.4.

The model using only geographical coordinates (C+DOY) has the highest RMSE of 1.0801. The model incorporating both geographical coordinates and the day of the year (C+DOY) has a lower RMSE of 1.0787, which is approximately 0.13% lower compared to the C+DOY model.

The L+DOY model achieved an RMSE of 0.3062 while the model with lag but without the day of the year (L) resulted in a slightly lower RMSE of 0.2963, which is less by about 3.23%. The combined model using geographical coordinates, SPEI values, and the day of the year (C+L+DOY) achieved the lowest RMSE of 0.2771, which is approximately 6.48% lower than the L model.

Configuration mix The data in Table 5.4 presents the top 5 Gradient Boosting Regressor models of the configuration mix with the lowest Root Mean Squared Error (RMSE) values. Each model variant, identified as C+L+DOY, incorporates geographical coordinates, the SPEI value of the last three months, and the day of the year. The models are configured with different combinations of estimators, learning rates, and max depths. The lowest RMSE achieved is 0.26234 with a configuration of 25 estimators, a learning rate of 0.30, and a max depth of 9.

| Estimators | Learning Rate | Max Depth | Model Variant | RMSE |
|------------|---------------|-----------|---------------|---------|
| 25 | 0.30 | 9 | C+L+DOY | 0.26234 |
| 100 | 0.05 | 12 | C+L+DOY | 0.26489 |
| 50 | 0.10 | 6 | C+L+DOY | 0.26495 |
| 0 | 0.10 | 6 | C+L+DOY | 0.26499 |
| 25 | 0.20 | 7 | C+L+DOY | 0.26500 |

Table 5.4: Top 5 lowest RMSE values from lowest (top) to highest (bottom). This table shows the numbers of estimators, learning rate, max depth, and model variants for the top 5 Gradient Boosting Regressor models with the lowest RMSE value. The model variant C+L+DOY, which expects the features of geographical coordinates, the SPEI value of the last three months, and the day of the year, is represented in all 5 places and achieves the lowest RMSE with 0.26234.

In contrast, Table 5.5 shows the top 5 Gradient Boosting Regressor models with the highest RMSE values. The model variant C+DOY, which includes geographical coordinates and the day of the year, is used in these configurations. The models vary in the number of estimators, learning rates, and max depths. The highest RMSE recorded is 1.234052, achieved with 50 estimators, a learning rate of 0.01, and a max depth of 5.

| Estimators | Learning Rate | Max Depth | Model Variant | RMSE |
|------------|---------------|-----------|---------------|----------|
| 50 | 0.01 | 5 | C+DOY | 1.234052 |
| 25 | 1.00 | 6 | C+DOY | 1.232895 |
| 25 | 1.00 | 7 | C+DOY | 1.232687 |
| 75 | 1.00 | 8 | C+DOY | 1.232676 |
| 25 | 1.00 | 9 | C+DOY | 1.232637 |

Table 5.5: Top 5 highest RMSE values from highest (top) to lowest (bottom). This table shows the numbers of estimators, learning rate, and max depth for the top 5 Gradient Boosting Regressor models with the highest RMSE value. The model variant C+DOY, which expects geographical coordinates and the day of the year, has achieved the highest RMSE value out of all model variants with an RMSE of 1.234052.

The models can be found in the GitHub repository under the directory `data_comparison/gbt_output` (Tran, 2024b). For further experiments, the C+L+DOY model with the lowest RMSE has been used, which has been mentioned in Table 5.4.

Value distribution

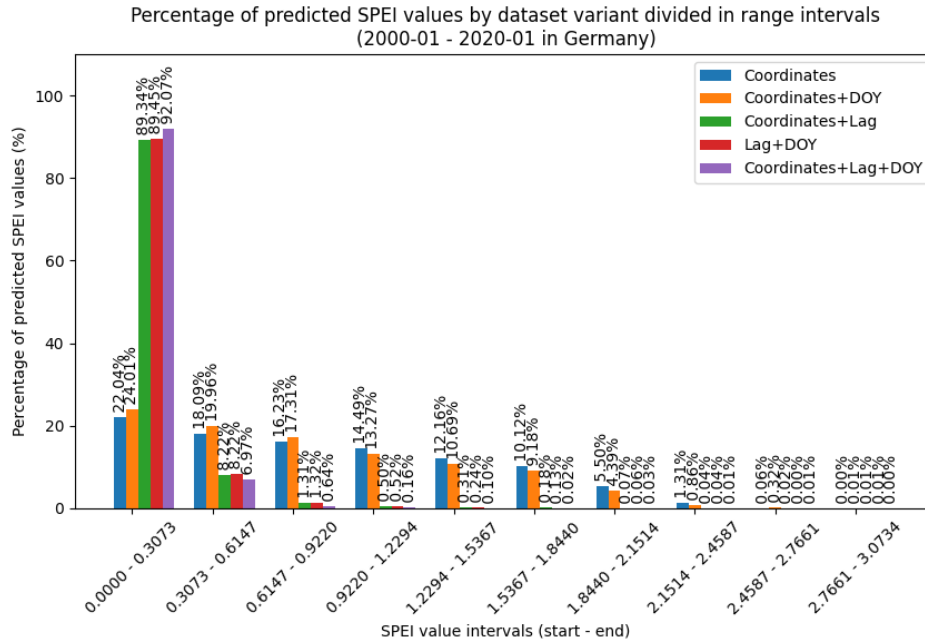


Figure 5.66: Percentage of predicted SPEI values by dataset variant using the Gradient Boosting Regressor. The variants include the features: coordinates, the day of the year (DOY), and a lag (SPEI values of three previous months). The models have been trained and tested with features from 2000-01 to 2015-01 for the region of Germany. After that, the values were predicted for the period 2015-02 to 2020-12.

The first interval, ranging from [0.0000, 0.3073], shows a significantly higher concentration of predictions, with the Coordinates+Lag, Lag+DOY, and Coordinates+Lag+DOY variants predicting around 89.34-92.07% of values in this range, compared to 22.04 and 24.01% for the Coordinates and Coordinates+DOY variant.

The interval [0.3073, 0.6147] has predictions distributed more evenly, with Coordinates predicting around 18.09%, Coordinates+DOY 19.96%, and the three remaining variants which had high percentages in the first interval have low values ranging from 6.97 to 8.22%.

In the following ranges the Coordinates and Coordinates+DOY percentages slightly with around 3-5% per step while the other variant's percentages from Coordinates+Lag, Lag+DOY, and Coordinates+Lag+DOY drop significantly around 7% from the second

to the third interval. The values stay under 0.52% in the remaining intervals for these three variants.

Overall, the chart highlights that the inclusion of lag and day-of-the-year features results in varied distributions of predicted values across different SPEI intervals, with specific intervals showing higher concentrations of predictions depending on the dataset variant used.

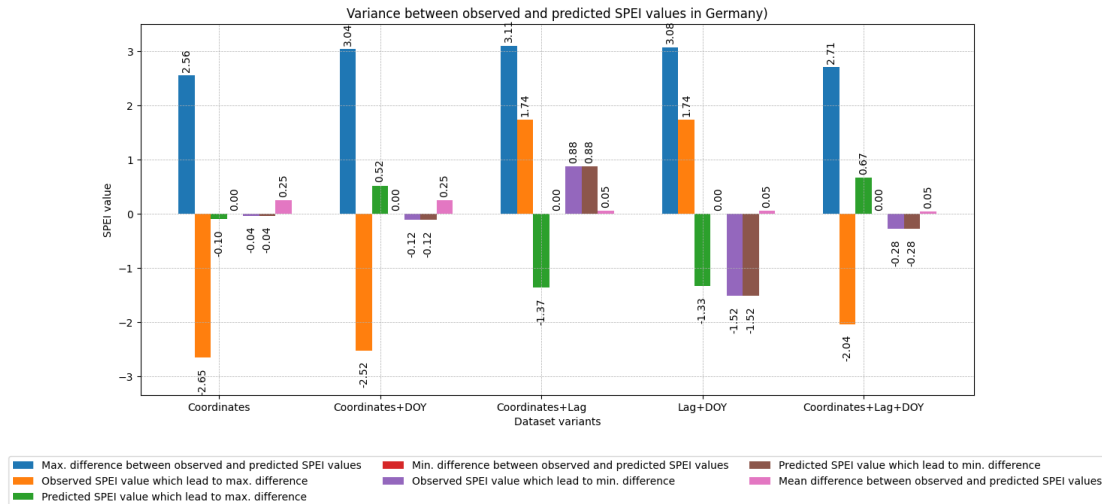


Figure 5.67: Variance between observed and predicted SPEI values from January 2015 to December 2020 in Germany. The maximum difference between the observed and predicted SPEI value is shown in blue, the observed SPEI value which leads to the maximum difference is shown in orange, and the predicted SPEI value which leads to the maximum difference is shown in green. Also, the minimum difference between the observed and predicted SPEI value is shown in red while the observed SPEI value which leads to the minimum difference is shown in violet, the predicted SPEI value which leads to the minimum difference is shown in brown, and last but not least the mean difference between the observed and predicted SPEI value is shown in pink. The models have been trained and tested with features from 2000-01 to 2015-01 for the region of Germany. After that, the values were predicted for the period 2015-02 to 2020-12.

The bar chart in Figure 5.67 presents the variance between observed and predicted SPEI values from January 2015 to December 2020 in Germany, across different dataset variants:

- Coordinates (Geographical Location),

- Coordinates+DOY (Day of Year),
- Coordinates+Lag (SPEI of the three previous months)
- Lag+DOY and
- Coordinates+Lag+DOY.

The y-axis represents the SPEI value, while the x-axis distinguishes between the dataset variants. For each variant, the chart shows the following:

- **Blue** - Maximum difference between the observed and predicted SPEI value.
- **Orange** - Observed SPEI value which led to the maximum difference.
- **Green** - Predicted SPEI value which led to the maximum difference.
- **Red** - Minimum difference between the observed and predicted SPEI value.
- **Violet** - Observed SPEI value which led to the minimum difference.
- **Brown** - Predicted SPEI value which led to the minimum difference.
- **Pink** - Mean difference between observed and predicted SPEI value

For the Coordinates variant, the maximum difference between the observed and predicted SPEI values is 2.56 which is the lowest value out of all model variants. The minimum difference between the observed and predicted SPEI values is 0.00 and this applies to all model variants mentioned in the following. Last but not least the mean difference has the value 0.25.

In the Coordinates + DOY variant, the maximum difference between the observed and predicted SPEI values is 3.04. Also here the mean difference is 0.25.

Regarding the Coordinates + Lag variant, the maximum difference between the observed and predicted SPEI values is 3.11 which is the highest max. difference out of all model variants. The mean difference is 0.20 smaller than for the previous models with a value of 0.05.

In the Lag + DOY variant, the maximum difference between the observed and predicted SPEI values is 3.08 which is the second highest max. difference out of all model variants. It is the same value for the difference here with 0.05.

For the last variant Coordinates + Lag + DOY, the maximum difference between observed and predicted SPEI values is 2.71 which is the second lowest value. The mean difference between the observed and predicted SPEI values is 0.05, too.

The analysis shows that different model variants impact the accuracy of SPEI predictions in Germany. Adding Lag (three previous SPEI values) lowers the mean difference by 0.20 for the model variants Coordinates+Lag, Lag+DOY, and Coordinates+Lag+DOY to 0.05 in comparison to the model variants Coordinates and Coordinates+DOY which both have a mean difference of 0.25. Overall the Coordinates had the lowest maximum difference between the observed and predicted SPEI values with 2.56 and all model variants had a minimum difference of 0.

If the best-performing model variant were to be selected, it would be the combination of Coordinates, Lag, and DOY. It only has the second lowest maximum difference but the lowest maximum difference within model variants that have a mean of 0.05.

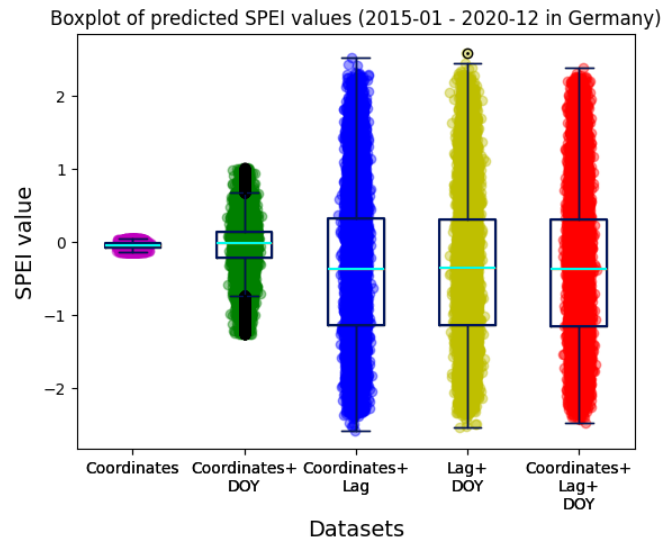
Boxplots

The first image A in Figure 5.68 reveals that the Coordinates dataset is showing a narrow distribution centered around -0.06, indicating low variability in predictions. The Coordinates + DOY dataset introduces slightly more variability but the distribution remains centered around 0 as well with a value of 0.02.

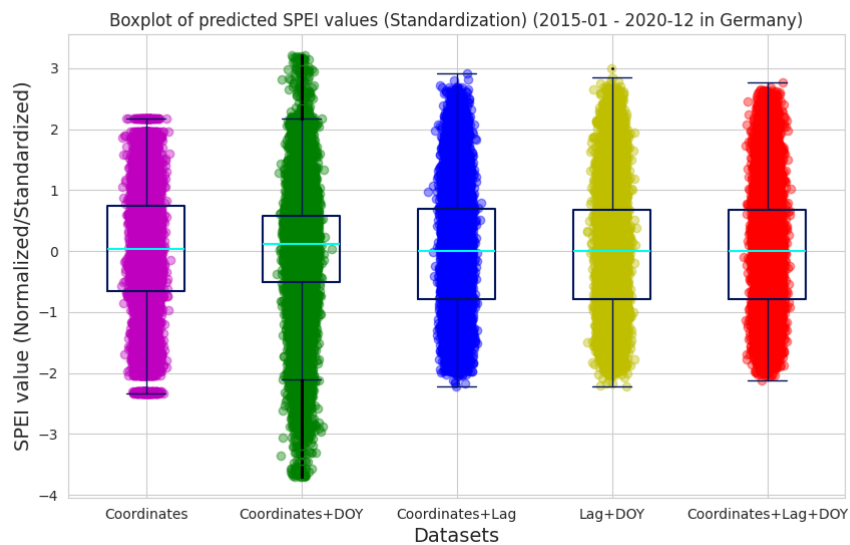
Adding lag to the datasets like in the Coordinates + Lag dataset results in a much broader distribution, highlighting the increased variability when using past SPEI values. The mean for this dataset settles around -0.375.

The Lag + DOY dataset displays a broad distribution similar to the Coordinates + Lag dataset, suggesting that both lag and day of the year contribute to prediction variability. The most right dataset Coordinates + Lag + DOY shows a distribution similar to the previous two, confirming the combined effect of these features on the variability of predicted SPEI values.

A standardized version of image A is presented as image B in Figure 5.68. The SPEI values are normalized and standardized, with the y-axis representing these standardized values ranging from -4 to +4. The x-axis lists the different datasets used for prediction, labeled as Coordinates, Coordinates + DOY, Coordinates + Lag, Lag + DOY, and Coordinates + Lag + DOY.



- (a) Box plot of predicted SPEI values by using four different datasets which have been trained within the time range from January 2000 to January 2015 while the predictions were made for the time range from February 2015 until December 2020. The Coordinates dataset has the feature parameters latitude and longitude. The x-axis contains the dataset names which relate to their feature parameters while Coordinates are the latitude and longitude, DOY is the day of the year and Lag is the SPEI value of the last three months. On the y-axis are the SPEI values.



- (b) Same boxplot like in Figure 5.68a but Standardization is applied to make it comparable by scaling them to the Standardization distribution.

Figure 5.68: Comparison of Gradient Boosting Regressor box plots of predicted SPEI value for the period 2015-01 to 2020-12 for the region Germany.

The plot indicates that the Coordinates dataset shows a narrow distribution centered around zero, indicating low variability in the predictions. The Coordinates + DOY dataset shows a wider distribution and its median is still centered around 0, indicating that the inclusion of DOY adds variability. The Coordinates + Lag dataset exhibits a broader distribution, highlighting increased variability in predictions due to the inclusion of lagged SPEI values. The Lag + DOY dataset shows a broad distribution similar to the Coordinates + Lag dataset, suggesting that both lag and DOY contribute significantly to prediction variability. Also the Coordinates + Lag + DOY dataset demonstrates a distribution similar to Coordinates + Lag and Lag + DOY, confirming the combined impact of these features on the variability of the predicted SPEI values. All last three mentioned dataset variants' median is settled around zero.

Overall, using only coordinates as input features provides results with a narrow distribution range while adding lag to the features increases the variability of the predicted SPEI values while the median remains around zero.

5.3.2 XGBoost

The results of the XGBoost models, which predict the SPEI values from January 1980 to June 2024 for the location Germany, are presented in this section.

SPEI Lag

The SPEI Lag (SL) model includes the lagged SPEI values of the three previous months.

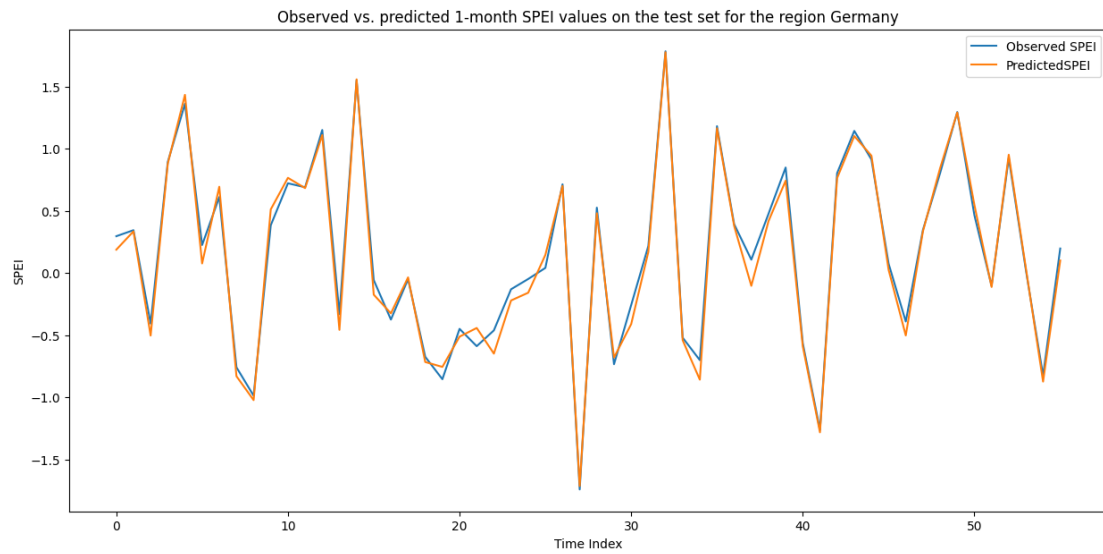


Figure 5.69: Observed (*blue*) and predicted 1-month SPEI values (*orange*) in comparison for Germany on the test dataset. The observed and predicted values share a common course with some expectations as around time index 20 to 25 and 34 to 39.

As a result, the model for the 1-month SPEI with a number of 300 estimators, a learning rate of 0.1, and a maximum depth of 12 reached the best metrics with an MSE of 0.01134 and an RMSE of 0.106524.

A prediction for the test set is shown in Figure 5.69. In this figure the predicted and observed 1-month SPEI have spots where there are some not equal values like around time index 25, but overall the values match and the model provides an accurate prediction.

Multi-in multi-out

The second model Multi-in multi-out (MIMO) an approach where multiple features and passed and the model outputs multiple predicted features, too.

Lag size

Figure 5.83 shows the comparison of the actual and the predicted SPEI values using different lag sizes from 1 to 6 for the coordinates latitude 53.6 and longitude 10.2 in Germany for the period from January 1980 to June 2024.

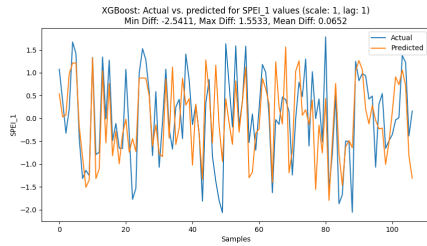


Figure 5.70: Actual vs. predicted 1-month (lag size: 1)

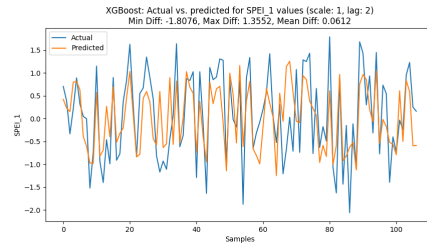


Figure 5.71: Actual vs. predicted 1-month (lag size: 2)

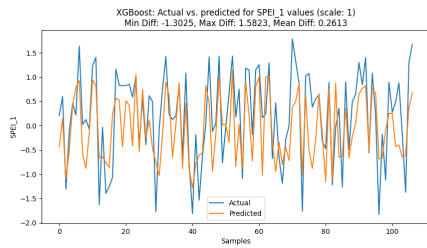


Figure 5.72: Actual vs. predicted 1-month (lag size: 3)

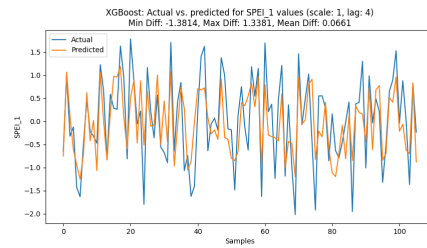


Figure 5.73: Actual vs. predicted 1-month (lag size: 4)

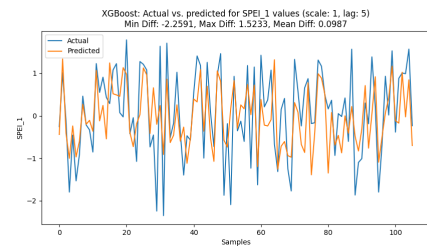


Figure 5.74: Actual vs. predicted 1-month (lag size: 5)

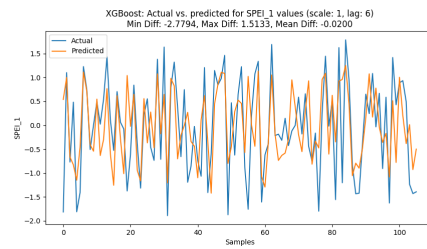


Figure 5.75: Actual vs. predicted 1-month (lag size: 6)

Figure 5.76: Comparison of the actual and predicted 1-month SPEI values for the lag sizes from 1 to 6 for the coordinates latitude 53.6 and longitude 10.2 in Germany for the period from January 1980 to June 2024. The lag size of 6 offers the lowest mean difference between the actual and predicted SPEI values, while the lowest minimum difference and the highest maximum difference are achieved by the lag size of 3.

The lag size with the lowest MAE is the lag size of 6, based on Table 5.6, because its occurrence is the highest three times. Looking at the RMSE, the lag size of 6 is also the most common with an occurrence of four times. Based on all other metrics min., max., and mean difference the lag size 6 occurs the most, too.

| Metric | Variable | Lag Size |
|---------------|-----------------------|-----------------|
| Min. Diff. | <i>SPEI_1</i> | 6 |
| Max. Diff. | <i>SPEI_1</i> | 4 |
| Mean Diff. | <i>SPEI_1</i> | 6 |
| MAE | <i>SPEI_1</i> | 4 |
| RMSE | <i>SPEI_1</i> | 4 |
| Min. Diff. | <i>pev</i> | 6 |
| Max. Diff. | <i>pev</i> | 2 |
| Mean Diff. | <i>pev</i> | 1 |
| MAE | <i>pev</i> | 3 |
| RMSE | <i>pev</i> | 4 |
| Min. Diff. | <i>ssr</i> | 4 |
| Max. Diff. | <i>ssr</i> | 6 |
| Mean Diff. | <i>ssr</i> | 3 |
| MAE | <i>ssr</i> | 3 |
| RMSE | <i>ssr</i> | 6 |
| Min. Diff. | <i>str</i> | 5 |
| Max. Diff. | <i>str</i> | 1 |
| Mean Diff. | <i>str</i> | 2 |
| MAE | <i>str</i> | 6 |
| RMSE | <i>str</i> | 1 |
| Min. Diff. | <i>t2m</i> | 5 |
| Max. Diff. | <i>t2m</i> | 5 |
| Mean Diff. | <i>t2m</i> | 5 |
| MAE | <i>t2m</i> | 2 |
| RMSE | <i>t2m</i> | 6 |
| Min. Diff. | <i>tp</i> | 4 |
| Max. Diff. | <i>tp</i> | 1 |
| Mean Diff. | <i>tp</i> | 1 |
| MAE | <i>tp</i> | 6 |
| RMSE | <i>tp</i> | 6 |
| Min. Diff. | <i>u₁₀</i> | 1 |
| Max. Diff. | <i>u₁₀</i> | 2 |
| Mean Diff. | <i>u₁₀</i> | 1 |
| MAE | <i>u₁₀</i> | 6 |
| RMSE | <i>u₁₀</i> | 6 |
| Min. Diff. | <i>v₁₀</i> | 5 |
| Max. Diff. | <i>v₁₀</i> | 5 |
| Mean Diff. | <i>v₁₀</i> | 5 |
| MAE | <i>v₁₀</i> | 2 |
| RMSE | <i>v₁₀</i> | 4 |

Table 5.6: Metric, variable, and lag size combinations with the lowest metric value for the metrics mentioned. The lag size of 6 appears three times for the MAE, four times for the RMSE, and the metrics min., max., and mean difference the lag size of 6 occurs the most, too.

Overall Figure 5.82 with a lag size of 6 shows the lowest mean difference with 0.02, while the lowest minimum difference and the highest maximum difference is achieved by the lag size of 3 shown in Figure 5.79.

n-month SPEI

From the analysis, it is evident that 6-month SPEI (SPEI_6) exhibits the lowest values for both MAE (0.241539) and RMSE (0.28719). This indicates that models using the 6-month SPEI have the highest predictive accuracy among the n-month SPEI variables. The metrics for 6-month SPEI, along with the best-performing metrics across other n-month SPEI variables, are summarized in the Tables 5.8 and 5.7. Also for the max. the difference the 6-month SPEI has the lowest value (see Table 5.9) while the 1-month SPEI has the lowest values for the min. and mean difference.

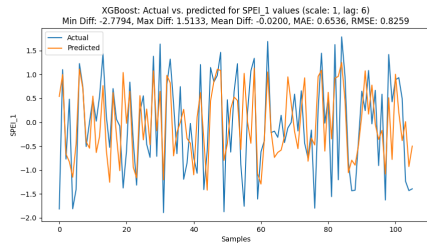


Figure 5.77: 1-month SPEI

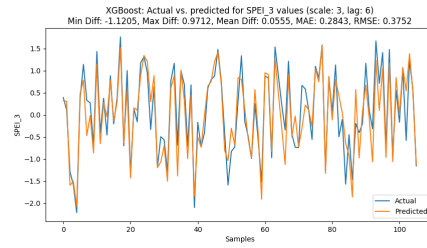


Figure 5.78: 3-month SPEI

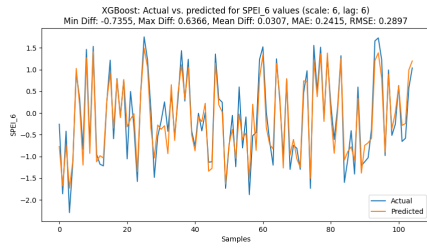


Figure 5.79: 6-month SPEI

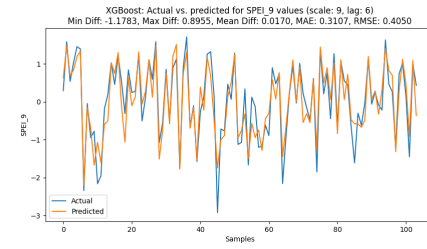


Figure 5.80: 9-month SPEI

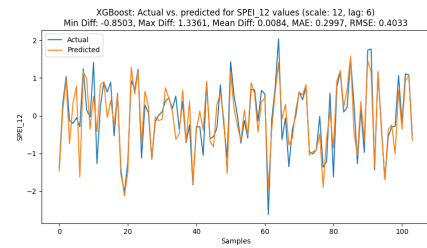


Figure 5.81: 12-month SPEI

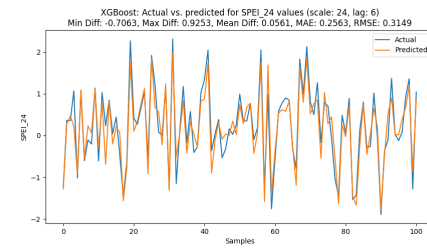


Figure 5.82: 24-month SPEI

Figure 5.83: Comparison between actual and predicted n -month SPEI values where n is 1, 3, 6, 9, 12 or 24. The train and test dataset contains SPEI values for the period January 1980 to June 2024 for the coordinates latitude 53.6 and longitude 10.2 in Germany. The model with the lowest MAE and RMSE is shown per n -month SPEI.

The 24-month SPEI had the second lowest MAE and RMSE values, with an MAE of 0.256250 and a RMSE of 0.314867. The third lowest MAE and RMSE values are achieved for the 3-month SPEI prediction with an MAE of 0.284332 and a RMSE of 0.375156. Followed by the 12-month and 9-month SPEI while the 1-month SPEI prediction has the highest MAE and RMSE of all n -month SPEI predictions.

Looking at the hyperparameters `n_estimators`, `learning_rate`, and `max_depth`, the combination 50, 0.1 occurs three times in the top 6 table on 1st, 2nd and 6th place. The

| Variable | MAE | n_estimators | learning_rate | max_depth |
|----------|----------|--------------|---------------|-----------|
| SPEI_6 | 0.241539 | 50 | 0.1 | 3 |
| SPEI_24 | 0.256250 | 50 | 0.1 | 3 |
| SPEI_3 | 0.284332 | 50 | 0.2 | 3 |
| SPEI_12 | 0.299697 | 50 | 0.2 | 3 |
| SPEI_9 | 0.310704 | 200 | 0.2 | 3 |
| SPEI_1 | 0.653570 | 50 | 0.1 | 3 |

Table 5.7: Top 6 Lowest MAE for SPEI_n. SPEI_6 has achieved the lowest MAE with 0.241539 whereas the SPEI_1 reached the highest MAE with 0.653570.

| Variable | RMSE | n_estimators | learning_rate | max_depth |
|----------|----------|--------------|---------------|-----------|
| SPEI_6 | 0.289719 | 50 | 0.1 | 3 |
| SPEI_24 | 0.314867 | 50 | 0.1 | 3 |
| SPEI_3 | 0.375156 | 50 | 0.2 | 3 |
| SPEI_12 | 0.403282 | 50 | 0.2 | 3 |
| SPEI_9 | 0.405004 | 200 | 0.2 | 3 |
| SPEI_1 | 0.825903 | 50 | 0.1 | 3 |

Table 5.8: Top 6 Lowest RMSE for SPEI_n. SPEI_6 has achieved the lowest RMSE with 0.289719 whereas the SPEI_1 reached the highest MAE with 0.825903.

| Metric | Variable | Value | n_estimators | learning_rate | max_depth |
|-------------------|----------|-----------|--------------|---------------|-----------|
| Min. Diff. | SPEI_1 | -2.779440 | 50 | 0.1 | 3 |
| Max. Diff. | SPEI_6 | 0.636556 | 50 | 0.1 | 3 |
| Mean Diff. | SPEI_1 | -0.020037 | 50 | 0.1 | 3 |
| MAE | SPEI_6 | 0.241539 | 50 | 0.1 | 3 |
| RMSE | SPEI_6 | 0.289719 | 50 | 0.1 | 3 |

Table 5.9: Lowest Metric Values for SPEI_n. The lowest min. and mean difference is achieved by SPEI_1 and the lowest max. the difference, MAE, and RMSE by the SPEI_6.

combination 50, 0.2, and 3 occurs the second most with two times in 3rd and 5th place. These hyperparameter combinations provide the combination needed for an accurate prediction model.

In summary, the evaluation metrics show that 6-month SPEI provides the most reliable and accurate predictions regarding the MAE and RMSE. The low values for MAE and RMSE signify that the predictive models for 6-month SPEI are better at minimizing errors, thereby offering more robust performance for drought index predictions. The

consistent performance across different metrics highlights the suitability of 6-month SPEI for such analyses.

Other Features

| Variable | MAE | n_estimators | learning_rate | max_depth |
|-----------------------|---------------|--------------|---------------|-----------|
| <i>pev</i> | 0.000612 | 50 | 0.2 | 3 |
| <i>ssr</i> | 951181.233446 | 50 | 0.1 | 3 |
| <i>str</i> | 494823.112767 | 50 | 0.1 | 3 |
| <i>t2m</i> | 1.431370 | 50 | 0.2 | 3 |
| <i>tp</i> | 0.000713 | 50 | 0.1 | 3 |
| <i>u₁₀</i> | 0.761888 | 50 | 0.1 | 3 |
| <i>v₁₀</i> | 0.519835 | 50 | 0.2 | 3 |

Table 5.10: Lowest MAE for the predicted variables *pev*, *ssr*, *str*, *t2m*, *tp*, *u₁₀* and *v₁₀* (lowest value at the top, then ascending downwards). The two occurring combinations of hyperparameters for the number of estimators, learning rate, and max depth are 50, 0.1 or 0.2, 3.

| Variable | RMSE | n_estimators | learning_rate | max_depth |
|-----------------------|-----------|--------------|---------------|-----------|
| <i>pev</i> | 0.000831 | 200 | 0.2 | 3 |
| <i>ssr</i> | 1283492.0 | 50 | 0.1 | 3 |
| <i>str</i> | 628517.3 | 50 | 0.1 | 3 |
| <i>t2m</i> | 1.817388 | 50 | 0.2 | 3 |
| <i>tp</i> | 0.000935 | 50 | 0.1 | 3 |
| <i>u₁₀</i> | 0.957871 | 50 | 0.1 | 3 |
| <i>v₁₀</i> | 0.647676 | 50 | 0.2 | 3 |

Table 5.11: Lowest RMSE for the predicted variables *pev*, *ssr*, *str*, *t2m*, *tp*, *u₁₀* and *v₁₀* (lowest value at the top, then ascending downwards). The two occurring combinations of hyperparameters for the number of estimators, learning rate, and max depth are 50 or 200, 0.1 or 0.2, 3.

For the remaining features *pev*, *ssr*, *str*, *t2m*, *tp*, *u₁₀* and *v₁₀* the lowest MAE, RMSE and best hyperparameter combinations are shown in the Tables 5.10 and 5.11.

The hyperparameter combination 50, 0.1, 3 consisting of the n_estimators, learning_rate and max_depth appears four times in Table 5.10 while the combination 50, 0.2, 3 appears three times. Also in Table 5.11 the hyperparameter combination 50, 0.1, 3 is shown four times, and the combination 50, 0.2, 3 appears three times.

The high MAE and RMSE values for the *ssr* and *str* variables occur because the values are in the millions due to their unit J/m^2 . This suggests that while the models perform well in terms of predictive accuracy for some variables, others, particularly those with high-magnitude units, present more significant challenges.

The analysis highlights that for most variables, the hyperparameter combinations of 50 `n_estimators`, 0.1 or 0.2 `learning_rate`, and 3 `max_depth` provide the best performance in terms of minimizing MAE and RMSE. The consistent appearance of these combinations suggests their robustness across different predicted variables. However, variables such as *ssr* and *str* require further optimization due to their inherently high values and prediction errors.

5.3.3 Prophet

Forecast Trend

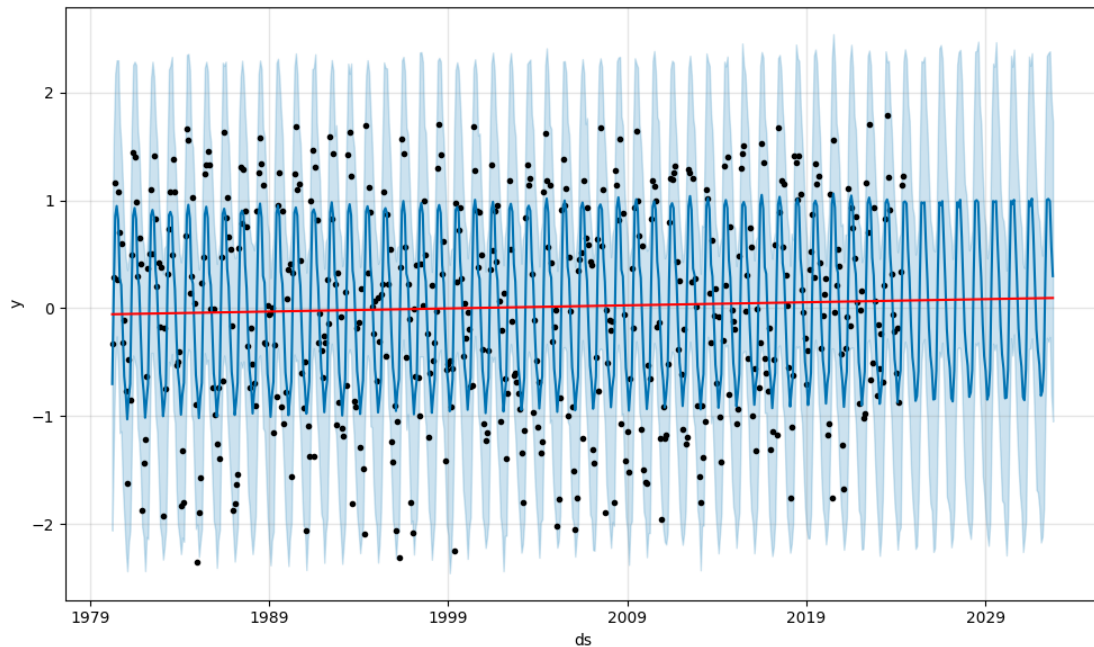


Figure 5.84: Prophet’s 1-month SPEI forecast graph (blue) from January 1980 to September 2032 for the coordinates latitude 53.6 and longitude 10.2 (Northern Germany). The black markers show the actual monthly 1-month SPEI values and the red line shows the rising trend which goes from -0.06 (1980) to 0.1 (2032). The blue graph shows the forecast which tends to have a seasonal pattern.

The forecast which is shown in Figure 5.84 shows the 1-month SPEI forecast by the Prophet model from January 1980 to September 2032 for the coordinates latitude 53.6 and longitude 10.2 (Northern Germany). The blue graph shows the forecast which tends to have a seasonal pattern and the red line shows the trend which rises from -0.06 (1980) to 0.1 (2032). Black markers show the actual monthly 1-month SPEI values.

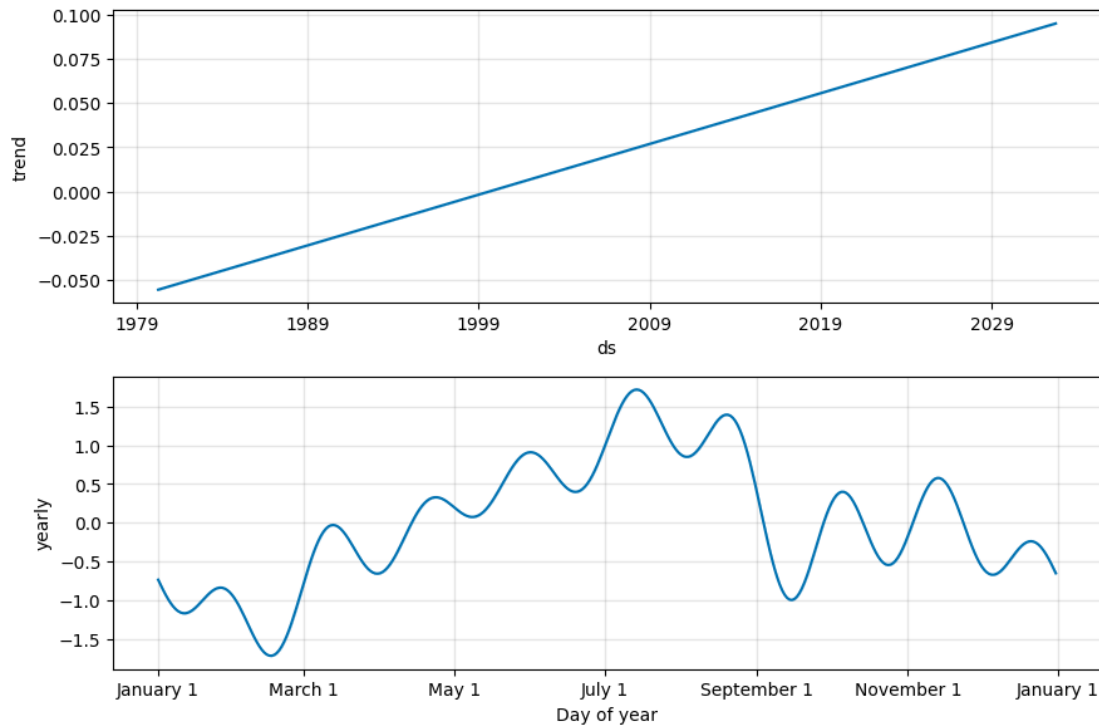
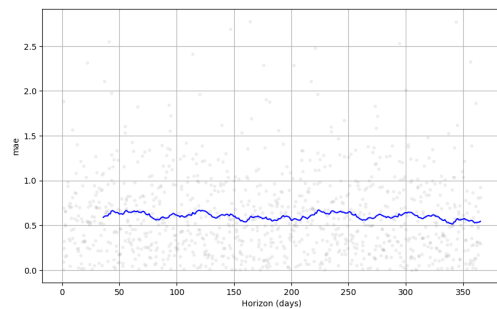


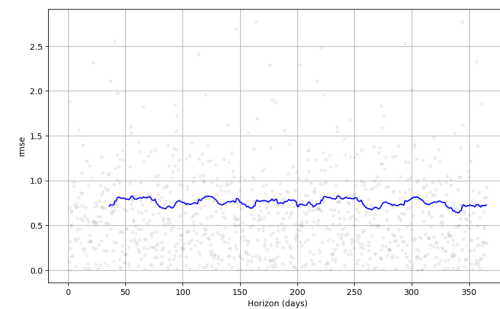
Figure 5.85: Trend and yearly pattern of the Prophet forecast for the period from January 1980 to September 2032 for the coordinates latitude 53.6 and longitude 10.2 (Northern Germany. The top figure shows the trend which will rise from 1980 to 2030 from around -0.06 to 0.1. Below the yearly pattern of the SPEI is shown which rises in the summer months and falls in autumn to spring.

In a more detailed view in Figure 5.85 the trend line is shown which which raises from -0.06 (1980) to 0.1 (2032) as well as the yearly 1-month SPEI pattern. The lowest SPEI is in the middle of February with around -1.7 and the highest SPEI is in the first third of July with 1.7. In the summer months, the SPEI rises, while the SPEI falls again in the fall to spring months.

Evaluation



(a) Prophet's Mean Absolute Error (MAE) for the forecast from January 1980 to September 2032 for the coordinates latitude 53.6 and longitude 10.2 (Northern Germany).



(b) Prophet's Root Mean Squared Error (RMSE) for the forecast from January 1980 to September 2032 for the coordinates latitude 53.6 and longitude 10.2 (Northern Germany).

Figure 5.86: Performance metrics MAE and RMSE of Prophet model which forecasts the 1-month SPEI for the period from January 1980 to September 2032 for the coordinates latitude 53.6 and longitude 10.2 (Northern Germany).

Figures 5.86a and 5.86b show the performance metrics of the Prophet model in predicting the 1-month SPEI from January 1980 to September 2032.

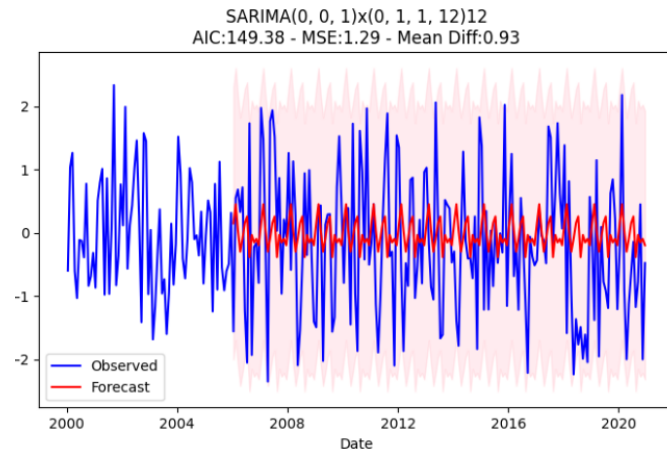
In Figure 5.86a, the MAE is plotted against the forecast horizon in days. The MAE measures the average magnitude of errors in the predictions, without considering their direction (plus or minus). The MAE values are generally around 0.6 on average while the values consistently fluctuate from 0.51 to 0.71 over time indicating a consistent prediction accuracy.

In Figure 5.86b, the RMSE is plotted against the forecast horizon in days. The RMSE is more sensitive to larger errors, as it squares the prediction errors before averaging them. The RMSE values hover around 0.7, while the model's predictions deviate by about 0.65 to 0.8 SPEI. Similar to the MAE, the RMSE remains stable across the forecast horizon, indicating no significant increase in error for longer-term forecasts.

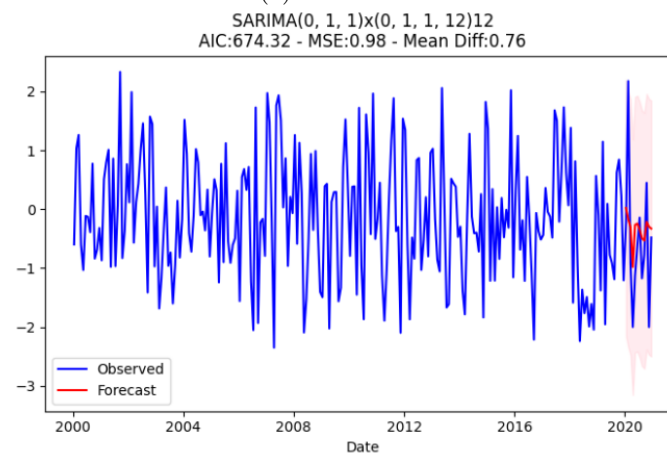
The Prophet model's performance metrics, as shown in these figures, demonstrate a relatively consistent error margin across different forecast horizons. The stability in both MAE and RMSE suggests that the model maintains its prediction accuracy over time, which is a positive indicator for its reliability in forecasting the 1-month SPEI.

5.3.4 SARIMA

Figure 5.87 shows results as time series of two different SARIMA models which have the lowest AIC (Figure 5.87a) and the lowest RMSE plus the lowest mean difference between the observed and forecasted SPEI values (Figure 5.87b).



(a) Lowest AIC



(b) Lowest Mean RMSE + Diff

Figure 5.87: Comparison of the best performing SARIMA models based on AIC, RMSE, and mean difference between the observed and forecasted 1-month SPEI values. The models have been tested with various training and forecast periods for the location (53.75, 10.25) which is located in Bargteheide/Elmenhorst in Germany.

The model with the lowest AIC of 149.38 in Figure 5.87a has been trained with SPEI values from January 2000 to January 2007 and the 1-month SPEI values are forecasted for the period February 2007 to December 2022.

Next, the model from Figure 5.87b with the lowest RMSE of 0.98 and the lowest mean difference between the observed and forecasted SPEI values of 0.76 has been trained for the period January 2000 to January 2020 and the forecast has been applied to the period February 2020 to December 2022.

The findings highlight the trade-offs between different model selection criteria. While the model with the lowest AIC is beneficial for its overall fit and complexity balance, the model with the lowest RMSE and mean difference excels in predictive accuracy.

For applications where accurate forecasts are crucial, the model with the lowest RMSE and mean difference is preferable. Conversely, if the goal is to have a model that generalizes well without overfitting, the model with the lowest AIC may be more suitable.

6 Discussion

6.1 Interpretation of Results

The results are discussed in terms of the causes of the results and what conclusions can be drawn from them.

6.1.1 SPEI Calculation

In this thesis, the Standardized Precipitation-Evapotranspiration Index (SPEI) calculations for Germany were recreated using different types of potential evapotranspiration (PET) equations: FAO-56 Penman-Monteith, Thornthwaite, Priestley-Taylor, and Hargreaves. Despite using the same weather station dataset from the German Weather Service (Deutscher Wetterdienst, 2024c), the resulting SPEI value distributions varied significantly across the different PET equations. The Thornthwaite and Hargreaves PET equations showed the smallest difference of -11.48% compared to the SPEIbase (Beguería, 2010). However, all calculated results showed discrepancies from the official SPEIbase values. The mean difference between the 1-month weather station SPEI using the FAO-56 Penman-Monteith PET equation and the 1-month SPEI of the SPEIbase is ≈ 1.0973 , which means that the requirement having an SPEI accuracy of lower than 0.3 (see Section 4.1 for all requirements) is not reached for the weather station data.

For remote sensing-based SPEI calculations, the ERA5-Land Reanalysis (Hersbach et al., 2020) with the FAO-56 Penman-Monteith PET equation has been used. This approach was chosen because the SPEIbase uses this equation, and it demonstrated a relatively similar value progression to the SPEIbase when using weather station data. In direct comparison, the remote sensing SPEI exhibited a smoother value distribution and a more understandable pattern of seasonal variations, with drops in summer due to heat and rises during the wetter seasons from autumn to spring. When comparing the 1-month remote sensing SPEI using the FAO-56 Penman-Monteith PET equation with the 1-month SPEI

of the SPEIbase, a difference of ≈ 0.9058 has been discovered. Also for the remote sensing data, the SPEI accuracy requirements could not be fulfilled.

It could not be predicted that the use of remote sensing data instead of weather station data improves prediction accuracy, as the SPEIbase dataset provided unreproducible results with the datasets used in this thesis.

This thesis confirms the sensitivity of SPEI to different PET equations, underlining the necessity of careful selection based on the application context. The use of the FAO-56 Penman-Monteith equation in the remote sensing calculations reflects the recommendation by Vicente-Serrano et al. (2010), as it is considered a superior method. Using the SPEIbase (Beguería, 2010) as a comparison dataset was not ideal, as the values were not comprehensible because the SPEI values fluctuated greatly, and in some cases, the SPEI fell from 0.5 to -1.98 from one month to the next. Unfortunately, there was no other comparison dataset for the SPEI available. Related work did not use a comparison dataset and relied on their results.

6.1.2 Correlation with SMI

The Pearson correlation between the SPEI and the SMI was examined in Section 5.2. For the coordinates latitude 53.6 and longitude 10.2, during the period from January 2015 to December 2018, there was no Pearson correlation between the 1-month SPEI calculated from weather station data and the SMI of both the upper and total soil layers. However, a negligible small positive Pearson correlation coefficient of below -0.1 , which is no correlation, was found between the 1-month SPEI from remote sensing data and the SMI of the upper soil (*Figure 5.21*).

Negligible positive Pearson correlation coefficients were also observed between the 3-month and 9-month SPEI from remote sensing data and the SMI of the upper soil (*Figure ??*). A slight negligible positive Pearson correlation coefficient below 0.056 was also noted between the 9-month SPEI and the SMI of the total soil, but not for other n-month SPEIs (*Figure 5.48*). However, the positive correlation was so weak and near zero that no meaningful linear correlation could be found.

Also for the comparison dataset SPEIbase and the SMI, a correlation coefficient has been calculated, whereby the 1-month SPEI had a negligible slight positive Pearson correlation coefficient of below 0.0097 with both the upper and total soil.

Likewise, the distance correlation between the SPEI and the SMI has been calculated in Section 5.2. The results here were different: the 24-month remote sensing SPEI had the highest distance correlation coefficients of above 0.42 with the upper soil SMI and above 0.47 with the total soil SMI. All other weather stations and remote sensing n-month SPEI compared to SMI variants had a distance correlation coefficient of less than 0.25. Only the 1-month SPEIbase SPEI could prove a distance correlation coefficient above 0.57 for the upper soil SMI.

It was not possible to prove that the self-calculated SPEI and the SMI have a significant Pearson or distance correlation due to weak to no correlations. Only the 1-month SPEIbase SPEI with the upper soil SMI did surpass the correlation coefficient threshold of 0.5, stated in the second requirement (see Section 4.1 for the requirements). This could be an indication of different data sources used, incorrect calculations of the SPEI or SMI, or that there is no correlation between the two indices. Since Samaniego et al. (2013) highlighted the importance of soil moisture data in drought assessments the last statement is rather unlikely. However, it should be emphasized that the 24-month remote sensing SPEI was close to the 0.5 threshold with both the upper and total soil SMI.

6.1.3 Gradient Boosting Regressor (GBR)

The GBR method, which has been detailed in the earlier sections, was evaluated using the Root Mean Squared Error (RMSE) metric. The performance of the GBR models with varying feature sets using the initial configuration described in Section 4.4.1, is summarized in Table 5.3.

- The model using geographical coordinates and day of the year (C+DOY) had the highest RMSE of 1.0801.
- Incorporating lagged SPEI values and the day of the year (L+DOY) significantly reduced the RMSE to 0.3062.
- The best performance was achieved by the model incorporating geographical coordinates, lagged SPEI values, and the day of the year (C+L+DOY) with an RMSE of 0.2771.

Various configurations of GBR were tested to optimize the model parameters. Table 5.4 and Table 5.5 present the top 5 lowest and highest RMSE values, respectively. The

optimal configuration, with 25 estimators, a learning rate of 0.30, and a max depth of 9, achieved an RMSE of 0.26234. With this model and configuration, an RMSE of 0.2771 has been achieved and so the third requirement is that the maximum RMSE should be lower than 0.3.

Figures 5.66 and 5.67 illustrate the distribution and variance of predicted SPEI values across different model variants, highlighting the impact of feature selection on model performance.

These results indicate that the inclusion of lagged SPEI values is valuable for improving the accuracy of SPEI predictions using the GBR. The models that included lagged values consistently outperformed those that did not, as seen in the significant reduction in RMSE. This suggests that past SPEI values have a strong predictive power for future conditions, likely due to the persistence of wet and dry spells in climatic conditions.

6.1.4 XGBoost

XGBoost models were trained on SPEI data from January 1980 to June 2024. Two approaches were used: the SPEI Lag (SL) model and the Multi-in multi-out (MIMO) model.

- **SL Model:** The SL model uses lagged SPEI values along with other meteorological features. The optimal configuration achieved a Mean Squared Error (MSE) of 0.01134 and an RMSE of 0.106524.
- **MIMO Model:** The MIMO model predicts multiple features simultaneously. A 6-month lag size was determined to be optimal. Using 50 estimators, a learning rate of 0.1 or 0.2 and a max depth of 3 provide the best performance in terms of minimizing MAE and RMSE for the predicted features. For the 6-month SPEI, the lowest RMSE of the model variants has been achieved with an RMSE of 0.2897.

Tables 5.10 and 5.11 present the lowest MAE and RMSE values for other predicted variables, indicating the robustness of specific hyperparameter combinations across different features. With an RMSE of 0.106524, the third requirement of prediction accuracy is fulfilled because it is lower than the maximum allowed RMSE of 0.3.

To sum up, the results underscore the importance of selecting appropriate lag sizes and feature combinations for enhancing model performance. The consistent performance of

the 6-month lagged model across various metrics suggests that it captures the essential temporal dependencies in the SPEI data. Moreover, the ability of the MIMO model to predict multiple features simultaneously presents a comprehensive approach to understanding and predicting climatic variations.

6.1.5 Prophet

The Prophet model by Meta was used to forecast the 1-month SPEI values for the coordinates latitude 53.6 and longitude 10.2 in Northern Germany.

- The forecast trend, as shown in Figure 5.84, indicates a seasonal pattern with a rising trend from -0.06 in 1980 to 0.1 in 2032.
- The yearly pattern reveals a cyclical behavior with peaks in summer and troughs in winter (Figure 5.85).

Performance metrics for the Prophet model, including MAE and RMSE, are presented in Figures 5.86a and 5.86b. The MAE values hover around 0.6, while the RMSE values are around 0.7, indicating a stable prediction accuracy over time. However, an RMSE of 0.7 exceeds the desired RMSE maximum of 0.3 mentioned in the third requirement.

Overall the Prophet model results highlight its capability to capture long-term trends and seasonal patterns effectively. The rising trend in SPEI values suggests an overall increase in wet conditions over the forecast period. This observation confirms the statement by Dukat et al. (2022) that they observed an increase in the severity of droughts. The consistent performance metrics indicate that Prophet is reliable for medium to long-term forecasts, particularly for data with pronounced seasonal cycles.

6.1.6 SARIMA

SARIMA models were evaluated for their ability to forecast the 1-month SPEI values using seasonal patterns.

- The model with the lowest AIC (Figure 5.87a) was trained on data from January 2000 to January 2007 and forecasted for the period February 2007 to December 2022.

- The model with the lowest RMSE of 0.98 and mean difference (Figure 5.87b) of 0.76 was trained on data from January 2000 to January 2020 and forecasted for the period February 2020 to December 2022.

The comparison highlights the trade-offs between model selection criteria, with the lowest AIC model being more suitable for generalization and the lowest RMSE model providing higher predictive accuracy. With an RMSE of 0.98 also the SARIMA model did not fulfill the third requirement (see all requirements in Section 4.1).

In conclusion, the SARIMA results emphasize the model's effectiveness in capturing seasonal variations. The lowest AIC model is advantageous for its balance between fit and complexity, while the lowest RMSE model excels in accuracy. This dual approach allows for flexible model selection based on specific forecasting needs, whether prioritizing generalization or precision.

6.2 Forecasts

The evaluation of the hypothesis that applying machine learning algorithms improves the accuracy of indicating wet and dry phases compared to traditional statistical methods reveals findings in this study. The Gradient Boosting Regressor (GBR) and XGBoost models demonstrated notable accuracy in forecasting the 1-month SPEI values. Specifically, the GBR model incorporating geographical coordinates lagged SPEI values, and the day of the year (C+L+DOY) achieved the lowest RMSE of 0.26234, indicating high predictive accuracy. Likewise, the XGBoost model, optimized with 50 estimators, a learning rate of 0.1, and a max depth of 3, showed the lowest MAE of 0.241539 and RMSE of 0.289719 for the 6-month SPEI, underscoring the efficacy of machine learning algorithms.

In comparison, the traditional statistical method represented by the SARIMA model provided reasonable accuracy but was generally outperformed by the machine learning models. The SARIMA model with the lowest RMSE and mean difference had an RMSE of 0.98 and a mean difference of 0.76, higher than those achieved by the GBR and XGBoost models. Although the SARIMA model's lowest AIC value of 1.11 suggests a good fit, it does not necessarily translate to superior predictive accuracy. It showed that the SPEI trend goes positive while other related work ((Vicente-Serrano et al., 2022),

(Philip et al., 2020)), say that the severity and occurrences of drought increased, which would contradict the idea that the SPEI will change into the more positive.

Another traditional statistical method, the Prophet model, displayed stable performance with MAE values around 0.6 and RMSE values around 1 for the forecast horizon. While adequate, this performance is less accurate than the results from the machine learning models.

6.3 Implications for Drought Monitoring

The results of this study have significant implications for real-world drought monitoring, forecasting, and management. The high predictive accuracy of the Gradient Boosting Regressor and XGBoost models, particularly with the inclusion of lagged SPEI values and seasonal features, indicates that these models can be effectively used for early warning systems. Accurate forecasting of wet and dry periods allows for better preparation and resource allocation in agriculture, water resource management, and disaster mitigation.

Furthermore, the Prophet model's ability to capture long-term trends and seasonal patterns provides valuable insights for policymakers and planners. The rising trend in SPEI values suggests changing climatic conditions, which can inform long-term strategies for water conservation and infrastructure development.

The SARIMA model's balance between fit and complexity highlights its utility in operational settings where both accuracy and generalizability are important. This model can be used to complement other forecasting methods, providing a robust cooperative tool for drought monitoring and forecasting.

6.4 Limitations

Several limitations were encountered during this research, which could impact the generalizability and applicability of the results:

- **Evaluation Data:** Vicente-Serrano et al. (2010) release the SPEIbase (Beguería, 2010) which only had the 1-month SPEI and presented incomprehensible SPEI values compared to temperature and precipitation values for Germany. Likewise, the spatial resolution of 0.5° was too high to be reasonably compared with the

high-resolution data of the study with a spatial resolution of 0.01° for the weather station data and 0.25° for the remote sensing data.

- **Mimicking SPEI calculation:** The mimicking of the SPEI calculation, which has been described in Vicente-Serrano et al. (2010), it turned out that the implementation of the calculations using Python was more complicated than expected. This may also have to do with the data sources. However, the authors claimed that the calculation was simple. been found to
- **Data Availability:** The format, quality, and availability of remote sensing SPEI data varied from data source to data source, which may affect the model's performance. The choice of which data source to use was difficult. Also, the different PET equations required different data, and it was difficult to find a data source that contained all the required data. Conversely, some data were self-calculated or estimated as accurately as possible using formulas. Additionally, the SPEIbase dataset only contained SPEI values until December 2022.
- **Comparison Dataset:** For the calculation of the SPEI the SPEIbase Beguería (2010) is the only SPEI dataset available but the SPEI values could not be reproduced and the values fluctuate a lot going from negative to positive from month to the other.
- **Complexity of Nature:** Drought forecasting is a complex process due to the multifaceted nature of droughts, which are influenced by various climatic, hydrological, and environmental factors. A prediction that has been made could be incorrect after a short time, as is sometimes the case with weather forecasts.
- **Temporal Limitations:** The models were trained on data up to June 2024, which limits the ability to predict far-future scenarios. Additionally, the models might not fully capture long-term climatic shifts or anomalies that could occur beyond the training period.
- **Generalization Across Regions:** While the models were tested for a specific region (Germany), their performance might differ in other regions with distinct climatic patterns. Further validation across diverse geographic areas is necessary.
- **Accuracy:** The forecasting models had a high accuracy but were off at peaks and valleys. But looking at weather forecasts the accuracy is around 90% for 1-5 days in the future, while the accuracy drops to 80% for 6-7 days in the future.

From 7 days on the accuracy drops even more to around 50% (National Oceanic and Atmospheric Administration, 2024). Under these circumstances, a deviation is justifiable but could be improved.

6.5 Recommendations for Future Research

Based on the findings and limitations of this study, several recommendations for future research can be made to improve SPEI calculations and predictive models.

- **More Comparison Datasets:** Additional comparative data sets would have helped to better validate the calculated results. Authors of related work could make their datasets available when contacting them.
- **SPEI Calculation Library:** The R library called SPEI is intended to be used with the datasets of the Climatic Research Unit and NCAS (2024) to calculate the SPEI. For future studies, it is recommended to either transform the datasets so that they are compatible with the library or to directly use the datasets of Climatic Research Unit and NCAS (2024) and the SPEI library.
- **Enhanced Data Integration:** Future studies should explore the integration of additional data sources, such as soil moisture, vegetation indices, and socio-economic data, to improve the accuracy of SPEI calculations and drought forecasts.
- **Updatable Machine-Learning Models:** Newly released meteorological and remote sensing data can be passed to machine learning models that train and update their models to have the latest data for more accurate forecasting.
- **Regional Adaptation:** Conduct region-specific studies to validate and adapt the models to different climatic conditions and geographic areas, ensuring their generalizability and applicability.
- **Long-term Forecasting:** Extend the forecast horizon by incorporating long-term climatic models and scenario analysis to better understand the potential impacts of climate change on drought patterns.
- **Interdisciplinary Approaches:** Foster interdisciplinary collaborations that combine expertise from meteorology, hydrology, agriculture, and socio-economics to create holistic drought management strategies.

- **User-friendly Tools:** Develop user-friendly tools and interfaces that allow practitioners and decision-makers to easily implement and interpret the forecasting models, facilitating their integration into operational drought monitoring systems. This has already been tried with the Satellite Hub from Section 3.1.

By addressing these recommendations, future research can build on the foundation laid by this study, advancing the state-of-the-art in drought prediction, monitoring, and management.

7 Conclusion

7.1 Summary of Key Findings

This research has explored the calculation, comparison, and prediction of the Standardized Precipitation-Evapotranspiration Index (SPEI) using different data sources and methods as well as the correlation with the Soil Moisture Index (SMI). The key findings are summarized below.

7.1.1 SPEI Calculations

For the weather station SPEI weather data by the Deutscher Wetterdienst (2024c) was utilized to calculate the SPEI using various PET equations: FAO-56 Penman-Monteith (FAO56PM), Thornthwaite (TW), Priestley-Taylor (PT), and Hargreaves (HG). The SPEIbase (SPEI DB) (Beguería, 2010) was included for comparison. The Normal category dominated across all methods, with the PT method having the highest percentage. The SPEI DB stood out with higher percentages in the Moderate Wet and Severe Drought categories. FAO56PM and PT methods showed similar trends, while TW and HG displayed higher variability.

For the remote sensing data, the FAO56PM PET equation was used for SPEI calculations. The comparison with the SPEIbase (SPEI DB) revealed that the remote sensing SPEI (SPEI RS) showed a more balanced distribution, with a higher percentage of normal conditions. Maximum, mean, and minimum comparisons highlighted that remote sensing data provided smoother trends compared to the SPEI DB.

7.1.2 SMI Correlation

The investigation into the correlation between the SPEI and the SMI revealed several key insights. The Pearson correlation between the 1-month SPEI and SMI, both from weather station data and remote sensing data, was found to be negligible. For instance, at specific coordinates (latitude 53.6 and longitude 10.2) from January 2015 to December 2018, the Pearson correlation coefficient was below 0.1, indicating an almost non-existent linear relationship between these indices. This weak correlation persisted across different time scales, such as the 3-month and 9-month SPEI.

However, when employing distance correlation, which can capture both linear and non-linear associations, some stronger correlations emerged. Notably, the 24-month remote sensing SPEI exhibited a higher distance correlation with SMI, reaching coefficients above 0.42 for the upper soil layer and above 0.47 for the total soil moisture. These values suggest that while traditional linear correlations (as measured by Pearson's coefficient) are weak, more complex relationships between SPEI and SMI may exist over longer periods and in specific soil layers.

These findings underscore the complexity of drought assessment and the challenges in using SPEI as a standalone indicator for soil moisture levels. While SPEI is effective for capturing precipitation deficits relative to potential evapotranspiration, it does not always directly correlate with soil moisture levels, particularly in the short term. This divergence may be attributed to various factors, such as the temporal lag between precipitation events and their impact on soil moisture, or differences in how each index responds to environmental conditions.

7.1.3 Prediction Methods

For the Gradient Boosting Regressor (GBR) (Prettenhofer and Louppe, 2014), different models incorporating geographical coordinates, lagged SPEI values and day of the year were tested. The model combining all three features (Coordinates+Lag+DOY) achieved the lowest RMSE. Boxplots and variance analysis indicated that adding lag increased the variability of predictions, although the median remained around zero.

The XGBoost (Chen and Guestrin, 2016) models showed that a lag size of 6 provided the best performance in terms of MAE and RMSE for predicting the 1-month SPEI. Experimenting with the lag size of 6 the 6-month SPEI was found to be the most reliable for

predicting, showing the lowest MAE and RMSE values. This finding confirms the results of Mehr et al. (2022) who had higher accuracy with 3- and 6-month SPEI predictions using a Hybrid Random Forest Model.

Using the Prophet model by Taylor and Letham (2018), the 1-month SPEI was predicted for the coordinates latitude 53.6 and longitude 10.2 in Germany from January 1980 to September 2032. The model indicated a rising trend from -0.06 (1980) to 0.1 (2032), with a seasonal pattern. Performance metrics, including MAE and RMSE, showed stable values across the prediction horizon, indicating consistent prediction accuracy.

For the SARIMA models, various configurations were tested. The model with the lowest AIC had an AIC of 1.11 and was trained from January 2000 to January 2007, forecasting from February 2007 to December 2022. Another model, with the lowest RMSE (0.98) and the lowest mean difference (0.76) between observed and forecasted SPEI values, was trained from January 2000 to January 2020, forecasting from February 2020 to December 2022. The findings highlighted the trade-offs between different model selection criteria, with the model having the lowest RMSE and mean difference being preferable for accurate forecasts, while the model with the lowest AIC was better for generalization without overfitting.

From these observations, it is evident that the application of machine learning algorithms enhances the accuracy of wet and dry phase indications compared to traditional statistical methods. Machine learning models, particularly GBR and XGBoost, achieved lower MAE and RMSE values, indicating higher predictive accuracy in predicting SPEI values. Although traditional statistical methods provide reasonable accuracy, they are generally outperformed by machine learning approaches. Thus, the application of machine learning algorithms indeed improves the accuracy of indicating wet and dry phases, affirming the hypothesis. This enhancement can be attributed to the machine learning models' ability to capture complex patterns and relationships in the data that traditional statistical methods might overlook.

7.1.4 Requirements

See refereed requirements in Section 4.1:

1. In fulfilling the requirements (see Section 4.1), there was the requirement of a maximum average deviation between the calculated SPEI using remote sensing

and weather station data in comparison to the SPEIbase should be lower than 0.3 which could not be fulfilled for both data.

2. The correlation of the SMI has been desired to be above 0.5 to have a meaningful positive correlation, but likewise here the requirement could not be fulfilled using the remote sensing or weather station SPEI. The 24-month remote sensing SPEI barely missed the requirement with a 0.03 difference in distance correlation for upper and total soil SMI and the 1-month SPEIbase SPEI had a distance correlation of over 0.5 for the upper soil SMI. However, the requirements only applied to the self-calculated SPEI values, which were not met.
3. Only the third requirement that a SPEI prediction model should have an RMSE of a maximum of 0.3 has been achieved by the GBR and the XGBoost models with an optimal configuration which has been found out during this thesis.

7.2 Final Remarks

The forecast results demonstrate the efficiency of different machine learning and time series models in predicting wet and dry periods using SPEI data. The GBR and XGBoost models showed high predictive accuracy, particularly with the inclusion of lagged SPEI values and seasonal features. The Prophet model provided insights into long-term trends and seasonal patterns, while the SARIMA models balanced complexity and accuracy.

This research has demonstrated the effectiveness of using various data sources and methods for calculating, comparing, and forecasting SPEI. The results indicate that remote sensing data can provide smoother and more balanced SPEI trends compared to traditional weather station data.

Regarding the correlation between the self-calculated SPEI and the Soil Moisture Index (SMI), the analysis revealed that there was no significant correlation. This was observed across both weather station and remote sensing data, as well as in comparison with the official SPEIbase dataset. The weak correlation suggests that while SPEI is useful for capturing precipitation and evapotranspiration dynamics, it does not directly align with soil moisture levels, particularly in the short term. This finding highlights the complexity of drought assessment and the need for careful consideration when using SPEI as a proxy for soil moisture conditions.

Additionally, incorporating lagged SPEI values and day of the year features can enhance the accuracy of forecasting models. Among the forecasting methods, the GBR and XGBoost models showed promising results, with the 6-month SPEI being particularly reliable. The Prophet model provided consistent prediction accuracy over time, and the SARIMA models highlighted the importance of balancing accuracy and generalization.

Future work can focus on refining these models, exploring additional features, and extending the forecast horizon to enhance the reliability of predictions. The integration of these models into a comprehensive forecasting framework can significantly improve the management and mitigation of droughts and wet periods. Future research could focus on exploring additional data sources and refining the forecasting models to further improve accuracy and reliability. The insights gained from this study can contribute to better understanding and managing drought conditions, ultimately aiding in more effective climate adaptation and mitigation strategies.

Bibliography

- Alfieri, L., Pappenberger, F., Wetterhall, F., Haiden, T., Richardson, D., and Salamon, P. (2014). Evaluation of ensemble streamflow predictions in europe. *Journal of Hydrology*, 517:913–922. <https://doi.org/10.1016/j.jhydrol.2014.06.035> (12/08/2024, 1:45 PM).
- Allen, R. G. (1998). *Crop evapotranspiration - Guidelines for computing crop water requirements - FAO Irrigation and drainage paper 56*. FAO. <https://www.fao.org/3/X0490E/x0490e00.htm> (13/03/2024, 12:18 PM).
- Aschonitis, V., Touloumidis, D., ten Veldhuis, M.-C., and Coenders-Gerrits, M. (2022). Correcting thornthwaite potential evapotranspiration using a global grid of local coefficients to support temperature-based estimations of reference evapotranspiration and aridity indices. *Earth System Science Data*, 14(1):163–177. <https://doi.org/10.5194/essd-14-163-2022> (12/06/2024, 11:24 PM).
- Ault, T. R. (2020). On the essentials of drought in a changing climate. *Science*, 368(6488):256–260. <https://doi.org/10.1126/science.aaz5492> (05/07/2024, 4:05 PM).
- Balsamo, G., Viterbo, P., Beljaars, A., van den Hurk, B., Betts, A., and Scipal, K. (2009). A revised hydrology for the ecmwf model: Verification from field site to water storage and impact in the integrated forecast system. *Journal of Hydrometeorology*, 10(3):623–643. <https://doi.org/10.1175/2008JHM1068.1> (18/08/2024, 2:55 PM).
- Beguera, S. (2010). A multiscalar global drought dataset: The speibase: A new gridded product for the analysis of drought variability and impacts. *Bulletin of the American Meteorological Society*, 91(10):1351–1354. <http://www.jstor.org/stable/26233020> (26/03/2024, 12:07 PM).

- Blyth, S. (1994). Karl pearson and the correlation curve. *International Statistical Review / Revue Internationale de Statistique*, 62(3):393–403.
- BmfBuF (2022). Drought in Germany: research, solutions, adaptation. *Bundesministerium für Bildung und Forschung*. <https://www.bmbf.de/bmbf/shareddocs/kurzmeldungen/de/2022/08/duerre-und-trockenheit-in-deutschland.html> (18/08/2024, 12:40 PM).
- Chen, T. and Guestrin, C. (2016). Xgboost: A scalable tree boosting system. *Association for Computing Machinery*, page 785–794. <https://doi.org/10.1145/2939672.2939785> (05/07/2024, 1:30 PM).
- Climatic Research Unit and NCAS (2024). High-resolution gridded datasets. <https://crudata.uea.ac.uk/cru/data/hrg/> (26/06/2024, 1:30 PM).
- CoMelissant (2024). Web Frameworks for Python. <https://wiki.python.org/moin/WebFrameworks> (24/05/2024, 1:43 PM).
- Copernicus (2024a). Copernicus Browser. <https://browser.dataspace.copernicus.eu/> (26/06/2024, 12:41 AM).
- Copernicus (2024b). ERA5-Land hourly data from 1950 to present. <https://cds.climate.copernicus.eu/cdsapp#!/dataset/reanalysis-era5-land?tab=overview> (26/06/2024, 1:30 PM).
- Dabral, P. P. and Murry, M. Z. (2017). Modelling and forecasting of rainfall time series using sarima. *Environmental Processes*, 4(2):399–419. <https://doi.org/10.1007/s40710-017-0226-y> (06/08/2024, 6:22 PM).
- Deutscher Wetterdienst (2020). DWD - Climate Data Center - Read Me Intro. https://opendata.dwd.de/climate_environment/CDC/Liesmich_intro_CDC-FTP.pdf (24/05/2024, 2:20 PM).
- Deutscher Wetterdienst (2024a). CDC - Index of /climate_environment/CDC. https://opendata.dwd.de/climate_environment/CDC/ (26/06/2024, 10:53 AM).
- Deutscher Wetterdienst (2024b). Datengewinnung im Deutschen Wetterdienst (DWD). https://www.dwd.de/DE/derdwd/messnetz/dg_im_dwd.pdf?__blob=publicationFile&v=3 (01/08/2024, 3:01 PM).

- Deutscher Wetterdienst (2024c). Deutscher Wetterdienst - CDC (Climate Data Center). https://www.dwd.de/DE/klimaumwelt/cdc/cdc_node.html (12/03/2024, 12:23 AM).
- Deutscher Wetterdienst (2024d). Weather and climate - Deutscher Wetterdienst - Map with agrarmet. stations and additional information. https://www.dwd.de/DE/fachnutzer/landwirtschaft/appl/stationskarte/_node.html (12/06/2024, 9:03 AM).
- Deutscher Wetterdienst (2024e). Wetter und Klima - Deutscher Wetterdienst - Informationstechnik - Datenmanagement. https://www.dwd.de/DE/derdwd/it/_functions/Teasergroup/datenmanagement_bf.html?nn=20256 (01/08/2024, 3:07 PM).
- Deutscher Wetterdienst (2024f). Wetter und Klima - Deutscher Wetterdienst - Informationstechnik - Datenverarbeitung, DMRZ. https://www.dwd.de/DE/derdwd/it/_functions/Teasergroup/datenverarbeitung.html (01/08/2024, 2:55 PM).
- Deutscher Wetterdienst (2024g). Wetter und Klima - Deutscher Wetterdienst - Informationstechnik - Datenverteilung. https://www.dwd.de/DE/derdwd/it/_functions/Teasergroup/datenverteilung.html?nn=20256 (01/08/2024, 3:05 PM).
- Deutscher Wetterdienst (2024h). Wetter und Klima - Deutscher Wetterdienst - Informationstechnik - Meteorologische Anwendungen. https://www.dwd.de/DE/derdwd/it/_functions/Teasergroup/met_anwendungen_bf.html?nn=20256 (01/08/2024, 3:10 PM).
- Dikshit, A., Pradhan, B., and Santosh, M. (2022). Artificial neural networks in drought prediction in the 21st century—a scientometric analysis. *Applied Soft Computing*, 114:108080. <https://doi.org/10.1016/j.asoc.2021.108080> (12/08/2024, 2:01 PM).
- Dukat, P., Bednorz, E., Ziemblińska, K., and Urbaniak, M. (2022). Trends in drought occurrence and severity at mid-latitude european stations (1951–2015) estimated using standardized precipitation (spi) and precipitation and evapotranspiration (spei) indices. *Meteorology and Atmospheric Physics*, 134(1):20. <https://doi.org/10.1007/s00703-022-00858-w> (23/03/2024, 2:12 PM).

- En-Nagre, K., Aqnouy, M., Ouarka, A., Ali Asad Naqvi, S., Bouizrou, I., Eddine Stitou El Messari, J., Tariq, A., Soufan, W., Li, W., and El-Askary, H. (2024). Assessment and prediction of meteorological drought using machine learning algorithms and climate data. *Climate Risk Management*, 45:100630. <https://doi.org/10.1016/j.crm.2024.100630> (12/08/2024, 5:19 PM).
- European Centre for Medium-Range Weather Forecasts (2023a). How AI models are transforming weather forecasting. <https://www.ecmwf.int/en/about/media-centre/news/2023/how-ai-models-are-transforming-weather-forecasting-showcase-data> (27/07/2024, 10:45 AM).
- European Centre for Medium-Range Weather Forecasts (2023b). Integrated forecasting system (ifs). <https://www.ecmwf.int/en/research/modelling-and-prediction> (18/08/2024, 3:12 PM).
- European Centre for Medium-Range Weather Forecasts (2024). Era5: data documentation. <https://confluence.ecmwf.int/display/CKB/ERA5%3A+data+documentation> (18/08/2024, 2:23 PM).
- Gupta, P. and Bagchi, A. (2024). Essentials of Python for Artificial Intelligence and Machine Learning. https://link.springer.com/chapter/10.1007/978-3-031-43725-0_5 (01/08/2024, 3:23 PM).
- Gyaneshwar, A., Mishra, A., Chadha, U., Raj Vincent, P. M. D., Rajinikanth, V., Pattukandan Ganapathy, G., and Srinivasan, K. (2023). A contemporary review on deep learning models for drought prediction. *Sustainability*, 15(7). <https://doi.org/10.3390/su15076160> (12/08/2024, 3:18 PM).
- Hao, Z., Agha Kouchak, A., Nakhjiri, N., and Farahmand, A. (2014). Global integrated drought monitoring and prediction system. *Scientific Data*, 1(1):140001. <https://doi.org/10.1038/sdata.2014.1> (12/08/2024, 12:25 PM).
- Hao, Z., Singh, V. P., and Xia, Y. (2018). Seasonal drought prediction: Advances, challenges, and future prospects. *Reviews of Geophysics*, 56(1):108–141. <https://doi.org/https://doi.org/10.1002/2016RG000549> (12/06/2024, 9:23 AM).
- Hao et al. (2018). Seasonal Drought Prediction: Advances, Challenges, and Future Prospects. *Reviews of Geophysics*, pages 125–130. <https://doi.org/10.1002/2016RG000549> (12/08/2024, 12:01 PM).

- Hargreaves, G. H. and Allen, R. G. (2003). History and evaluation of hargreaves evapotranspiration equation. *Journal of Irrigation and Drainage Engineering*, 129(1):53–63. [https://doi.org/10.1061/\(ASCE\)0733-9437\(2003\)129:1\(53\)](https://doi.org/10.1061/(ASCE)0733-9437(2003)129:1(53)) (19/08/2024, 15:15 PM).
- Helmholtz Zentrum für Umweltforschung (2024). Dürremonitor Deutschland - Helmholtz-Zentrum für Umweltforschung UFZ. <https://www.ufz.de/index.php?de=37937> (23/06/2024, 10:56 AM).
- Hersbach, H., Bell, B., Berrisford, P., Hirahara, S., Horányi, A., Muñoz-Sabater, J., Nicolas, J., Peubey, C., Radu, R., Schepers, D., Simmons, A., Soci, C., Abdalla, S., Abellan, X., Balsamo, G., Bechtold, P., Biavati, G., Bidlot, J., Bonavita, M., De Chiara, G., Dahlgren, P., Dee, D., Diamantakis, M., Dragani, R., Flemming, J., Forbes, R., Fuentes, M., Geer, A., Haimberger, L., Healy, S., Hogan, R. J., Hólm, E., Janisková, M., Keeley, S., Laloyaux, P., Lopez, P., Lupu, C., Radnoti, G., de Rosnay, P., Rozum, I., Vamborg, F., Villaume, S., and Thépaut, J.-N. (2020). The era5 global reanalysis. *Quarterly Journal of the Royal Meteorological Society*, 146(730):1999–2049. <https://doi.org/10.1002/qj.3803> (10/02/2024, 5:32 PM).
- Hunt, E. D., Hubbard, K. G., Wilhite, D. A., Arkebauer, T. J., and Dutcher, A. L. (2009). The development and evaluation of a soil moisture index. *International Journal of Climatology*, 29(5):747–759. <https://doi.org/10.1002/joc.1749> (04/07/2024, 2:42 PM).
- Künzel, A., Münzel, S., Böttcher, F., and Spengler, D. (2021). Analysis of weather-related growth differences in winter wheat in a three-year field trial in north-east germany. *Agronomy*, 11(9). <https://doi.org/10.3390/agronomy11091854> (04/08/2024, 4:13 PM).
- Li, J., Zhang, S., Huang, L., Zhang, T., and Feng, P. (2020). Drought prediction models driven by meteorological and remote sensing data in Guanzhong Area, China. *Hydrology Research*, 51(5):942–958. <https://doi.org/10.2166/nh.2020.184> (13/06/2024, 10:15 AM).
- Mehr et al. (2022). A New Evolutionary Hybrid Random Forest Model for SPEI Forecasting. *Water*, 14(5). <https://doi.org/10.3390/w14050755> (13/06/2024, 9:55 AM).

BIBLIOGRAPHY

- Mishra, A. K. and Desai, V. R. (2005). Drought forecasting using stochastic models. *Stochastic Environmental Research and Risk Assessment*, 19(5):326–339. <https://doi.org/10.1007/s00477-005-0238-4> (12/08/2024, 2:01 PM).
- Mitra, A. K. (2023). *Use of Remote Sensing in Weather and Climate Forecasts*, pages 77–96. Springer Nature Singapore, Singapore. https://doi.org/10.1007/978-981-19-6929-4_5 (07/08/2024, 1:21 PM).
- Muñoz Sabater, J., Dutra, E., Agustí-Panareda, A., Albergel, C., Arduini, G., Balsamo, G., Boussetta, S., Choulga, M., Harrigan, S., Hersbach, H., Martens, B., Miralles, D. G., Piles, M., Rodríguez-Fernández, N. J., Zsoter, E., Buontempo, C., and Thépaut, J.-N. (2021). Era5-land: a state-of-the-art global reanalysis dataset for land applications. *Earth System Science Data*, 13(9):4349–4383. <https://doi.org/10.5194/essd-13-4349-2021> (18/08/2024, 2:05 PM).
- Nandgude, N., Singh, T. P., Nandgude, S., and Tiwari, M. (2023). Drought prediction: A comprehensive review of different drought prediction models and adopted technologies. *Sustainability*, 15(15). <https://doi.org/10.3390/su151511684> (12/06/2024, 9:39 AM).
- National Oceanic and Atmospheric Administration (2024). How Reliable Are Weather Forecasts? <https://scijinks.gov/forecast-reliability/> (05/07/2024, 5:42 PM).
- Ndulue, E. and Ranjan, R. S. (2021). Performance of the fao penman-monteith equation under limiting conditions and fourteen reference evapotranspiration models in southern manitoba. *Theoretical and Applied Climatology*, 143(3):1285–1298. <https://doi.org/10.1007/s00704-020-03505-9> (01/08/2024, 3:50 PM).
- Oberhäuser, N. (2018). Climate change already affecting German farms. <https://www.dw.com/en/climate-change-already-affecting-german-farmers/a-44768594> (02/08/2024, 9:16 AM).
- Philip, S. Y., Kew, S. F., van der Wiel, K., Wanders, N., and van Oldenborgh, G. J. (2020). Regional differentiation in climate change induced drought trends in the netherlands. *Environmental Research Letters*, 15(9):094081. <https://dx.doi.org/10.1088/1748-9326/ab97ca> (12/08/2024, 8:34 PM).
- PostGIS PSC/OSGeo (2023). PostGIS. <https://postgis.net/> (24/05/2024, 1:20 PM).

- Prettenhofer, P. and Louppe, G. (2014). Gradient boosted regression trees in scikit-learn. *PyData*. <https://hdl.handle.net/2268/163521> (06/08/2024, 6:40 PM).
- Priestley, C. H. B. and Taylor, R. J. (1972). On the assessment of surface heat flux and evaporation using large-scale parameters. *Monthly Weather Review*, 100(2):81 – 92. [https://doi.org/10.1175/1520-0493\(1972\)100<0081:OTAOSH>2.3.CO;2](https://doi.org/10.1175/1520-0493(1972)100<0081:OTAOSH>2.3.CO;2) (13/03/2024, 6:51 PM).
- QGIS (2024). QGIS - A Free and Open Source Geographic Information System. <https://qgis.org/de/site/> (24/05/2024, 1:23 PM).
- Robinson, A. C., MacEachren, A., and Bacastow, T. (2024). Overview of Programming Languages for GIS. *GeoG 583*. <https://www.e-education.psu.edu/geog583/node/67> (24/05/2024, 4:23 PM).
- Samaniego, L., Kumar, R., and Attinger, S. (2010). Multiscale parameter regionalization of a grid-based hydrologic model at the mesoscale. *Water Resources Research*, 46(5). <https://doi.org/10.1029/2008WR007327> (23/03/2024, 4:32 PM).
- Samaniego, L., Kumar, R., and Zink, M. (2013). Implications of parameter uncertainty on soil moisture drought analysis in germany. *Journal of Hydrometeorology*, 14(1):47 – 68. <https://doi.org/10.1175/JHM-D-12-075.1> (23/03/2024, 4:51 PM).
- Shang, J., Zhao, B., Hua, H., Wei, J., Qin, G., and Chen, G. (2023). Application of informer model based on spei for drought forecasting. *Atmosphere*, 14(6). <https://doi.org/10.3390/atmos14060951> (09/07/2024, 9:55 AM).
- Sinergise Solutions d.o.o. (2024). Sentinel Hub API. <https://www.sentinel-hub.com/develop/api/> (26/06/2024, 12:43 AM).
- Székel, G. J., Rizzo, M. L., and Bakirov, N. K. (2007). Measuring and testing dependence by correlation of distances. *The Annals of Statistics*, 35(6):2769 – 2794.
- Taylor, S. J. and Letham, B. (2018). Forecasting at scale. *The American Statistician*, 72(1):37–45. <https://doi.org/10.7287/peerj.preprints.3190v2> (19/08/2024, 11:13 AM).
- Thorntwaite, C. W. (1948). An approach toward a rational classification of climate. *Geographical Review*, 38(1):55–94. <http://www.jstor.org/stable/210739> (12/06/2024, 10:41 PM).

- Tran, J. (2024a). GitHub: JustinTrvz/dews-datahub. <https://github.com/JustinTrvz/dews-datahub> (24/05/2024, 11:34 AM).
- Tran, J. (2024b). GitHub: JustinTrvz/drought-detector. <https://github.com/JustinTrvz/drought-detector> (04/07/2024, 4:25 PM).
- Vicente-Serrano, S. M., Beguería, S., and López-Moreno, J. I. (2010). A multiscalar drought index sensitive to global warming: The standardized precipitation evapotranspiration index. *Journal of Climate*, 23(7):1696 – 1718. <https://doi.org/10.1175/2009JCLI2909.1> (22/03/2024, 6:25 PM).
- Vicente-Serrano, S. M., Beguería, S., and López-Moreno, J. I. (2024). SPEI Global Drought Monitor. <https://spei.csic.es/map/maps.html> (26/06/2024, 12:40 AM).
- Vicente-Serrano, S. M., Peña-Angulo, D., Beguería, S., Domínguez-Castro, F., Tomás-Burguera, M., Noguera, I., Gimeno-Sotelo, L., and El Kenawy, A. (2022). Global drought trends and future projections. *Philosophical Transactions of the Royal Society A: Mathematical, Physical and Engineering Sciences*, 380(2238):20210285. <https://doi.org/10.1098/rsta.2021.0285> (12/08/2024, 7:19 PM).
- World Meteorological Organization (2022). State of Global Water Resources 2021. *WMO- No. 1308*. <https://library.wmo.int/records/item/58262-state-of-global-water-resources-2021#.ZFzKHOTPlas> (23/03/2024, 4:45 PM).
- Xu, D., Zhang, Q., Ding, Y., and Zhang, D. (2022). Application of a hybrid arima-lstm model based on the spei for drought forecasting. *Environmental Science and Pollution Research*, 29(3):4128–4144. <https://doi.org/10.1007/s11356-021-15325-z> (05/07/2024, 1:30 PM).

Erklärung zur selbstständigen Bearbeitung

Hiermit versichere ich, dass ich die vorliegende Arbeit ohne fremde Hilfe selbständig verfasst und nur die angegebenen Hilfsmittel benutzt habe. Wörtlich oder dem Sinn nach aus anderen Werken entnommene Stellen sind unter Angabe der Quellen kenntlich gemacht.

Ort

Datum

Unterschrift im Original